INFORMATION TO USERS

This dissertation was produced from a microfilm copy of the original document. While the most advanced technological means to photograph and reproduce this document have been used, the quality is heavily dependent upon the quality of the original submitted.

The following explanation of techniques is provided to help you understand markings or patterns which may appear on this reproduction.

1. The sign or "target" for pages apparently lacking from the document photographed is "Missing Page(s)". If it was possible to obtain the missing page(s) or section, they are spliced into the film along with adjacent pages. This may have necessitated cutting thru an image and duplicating adjacent pages to insure you complete continuity.

2. When an image on the film is obliterated with a large round black mark, it is an indication that the photographer suspected that the copy may have moved during exposure and thus cause a blurred image. You will find a good image of the page in the adjacent frame.

3. When a map, drawing or chart, etc., was part of the material being photographed the photographer followed a definite method in "sectioning" the material. It is customary to begin photoing at the upper left hand corner of a large sheet and to continue photoing from left to right in equal sections with a small overlap. If necessary, sectioning is continued again — beginning below the first row and continuing on until complete.

4. The majority of users indicate that the textual content is of greatest value, however, a somewhat higher quality reproduction could be made from "photographs" if essential to the understanding of the dissertation. Silver prints of "photographs" may be ordered at additional charge by writing the Order Department, giving the catalog number, title, author and specific pages you wish reproduced.

University Microfilms

300 North Zeeb Road
Ann Arbor, Michigan 48106

A Xerox Education Company

73-11,192

LUXON, Jr., James Laurence, 1942-
A PRECISION MEASUREMENT OF THE MAGNETIC MOMENT OF THE PROTON IN NUCLEAR MAGNETONS AND THE MASS DIFFERENCE OF THE DOUBLET H_2^+-D^+.

The University of Michigan, Ph.D., 1972
Physics, atomic

University Microfilms, A XEROX Company, Ann Arbor, Michigan

THIS DISSERTATION HAS BEEN MICROFILMED EXACTLY AS RECEIVED.

A PRECISION MEASUREMENT OF THE MAGNETIC MOMENT OF THE PROTON IN NUCLEAR MAGNETONS AND THE MASS DIFFERENCE OF THE DOUBLET H_2^+–D^+

by
James Laurence Luxon, Jr.

A dissertation submitted in partial fulfillment
of the requirements for the degree of
Doctor of Philosophy
(Physics)
in The University of Michigan
1972

Doctoral Committee:

Associate Professor Arthur Rich, Chairman
Professor H. Richard Crane
Professor Peter A. Franken
Professor W. Albert Hiltner
Professor C. Wilbur Peters

PLEASE NOTE:

Some pages may have

indistinct print.

Filmed as received.

University Microfilms, A Xerox Education Company

DEDICATION

To my parents,

who made this possible,

and to my wife

who helped me finish it.

PREFACE

This thesis reports the preliminary results of a new technique for measuring the cyclotron frequency of ions, and the application of this technique to the measurement of the magnetic moment of the proton in nuclear magnetons and the mass difference of the doublet $H_2^+ - D^+$. This technique was suggested in 1967 by Professor Rich as a logical combination of the "trapping" techniques of the Michigan g-factor group and conventional cyclotron resonance techniques.

Since a description of the apparatus and the theory of the operation has not been published elsewhere, it is presented here in detail. The casual reader may only want to read part or all of Chapter I and Sections 5.3 and 5.4. A less detailed discussion of the experiment is given in a forthcoming Physical Review Letter by Professor Rich and myself.

I would like to sincerely thank Professor Rich for suggesting the experiment and devoting much time and patience to its completion. I would also like to thank my committee for their suggestions and advice. Dr. J. Wesley deserves special thanks for educating me in the laboratory techniques of the g-factor group and for generously sharing part of the equipment originally designed for his electron g-factor experiment with me. Professor G. W. Ford provided several comments on the theoretical aspects of the experiment and especially on the understanding of the spin motion for the experiment proposed at the end of this work.

The completion of this work would not have been possible without the resources of the g-factor group and the departmental staff. Mr. D. Hartman constructed part of the equipment, and Mr. O. Haas has been a constant source of technical information. Mr. G. Edict provided much counseling in electronics. Particular thanks must be given to a number of adept undergraduate assistants, in particular Messrs. T. Tesar, W. Wood, D. Pope, and D. Wilson. Finally, it has been a pleasure to work with the secretarial, shop, and stores staffs of the Physics Department.

The Michigan A.E.C. High Energy Computing Center generously provided computing time and assistance in the analysis of data. The Monsanto Corporation and in particular Messrs. E. J. Boek and G. D. Fowler generously provided the Monsanto 3100 A frequency synthesizer. Messrs. J. Carrico, M. Johnson, and T. Foote of the Bendix Corporation provided assistance in building the strip multiplier.

I would like to thank Mrs. Wanita Rasey for her patience in typing and editing the final copy, and Mr. L. Thurston for his thoughtfulness and skill in completing all of the figures.

The construction of the apparatus was generously funded by the U. S. Atomic Energy Commission, and by the National Bureau of Standards through a Precision Measurements Grant.

TABLE OF CONTENTS

	Page
CHAPTER I. INTRODUCTION	1
1.1 Background	1
1.2 Measurement Technique	9
1.3 The Present Apparatus	19
CHAPTER II. MEASUREMENT THEORY	24
2.1 Orbital Motion of the Trapped Ions	24
2.2 Averaging Over the Motion in the Well	31
2.3 RF Resonance and Lineshape Theory	35
2.4 The Effect of a Change in Radius on the Time-Average Field	60
2.5 Comparison of Various Techniques for Observing Resonance	64
2.6 Determination of Ion Mass Ratios	68
2.7 Determination of μ'_p/μ_n	
CHAPTER III. APPARATUS	73
3.1 The Solenoid	73
3.2 Power Supply, and Cooling, and Field Regulation	76
3.3 Field Mapping System	79
3.4 The Ion Source and Beam System	82
3.5 The Main Vacuum System	98
3.6 Trapping and RF Assembly	99
3.7 Electronic Equipment--Trapping and Cyclotron Resonance	104
3.8 Detection System	111
3.9 Data Acquisition	117
CHAPTER IV. EXPERIMENTAL PROCEDURE	119
4.1 The dc Beam in the Trapping Region	119
4.2 Ion Trapping	120
4.3 Data Collection	120
4.4 Axial Motion of the Ions in the Well	125
4.5 Cyclotron Resonance	127
4.6 Determination of μ_p/μ_n	129
4.7 Measurements of Mass Differences	133

	Page
CHAPTER V. ERRORS, RESULTS, AND CONCLUSIONS	135
5.1 Systematic Study of the Resonance Lines and the Error in $[\tilde{\omega}_c]$	135
5.2 Errors in $[\omega_s(\tilde{z}_1)]$	144
5.3 Results μ'_p/μ_n	154
5.4 Results $H_2^+-D^+$	160
5.5 A New Apparatus	163
APPENDIX I. THE DC ELECTRIC FIELD OF THE C's	179
APPENDIX II. THE GARREN WELL	183
APPENDIX III. SUMMARY OF ION ORBIT DRIFTS	186
APPENDIX IV. MEAN VALUES	193
APPENDIX V. DATA SHEET	196
BIBLIOGRAPHY	200

LIST OF TABLES

Table		Page
I	Procedure for Determining $[\tilde{\omega}_s]$.	132
II	Summary of Data Runs.	156
III	Summary of Errors.	157
IV	Summary of the Parameters of the Present and Proposed Apparatus.	164

LIST OF ILLUSTRATIONS

Figure		Page
1	Summary of the Data for μ_p/μ_n.	5
2	Schematic Representation of the Resonance Process.	11
3	Three Apparatuses used to Measure μ_p/μ_n.	16
4	The Present Apparatus.	20
5	A Magnetic Well.	26
6	Schematic Representation of Injection and Ejection.	30
7	The Density Function.	34
8	Cyclotron Motion within the C's.	36
9	The Resonant Radius Vector.	41
10	The Resonant Change in Radius.	43
11	Ion Motion near Resonance.	45
12	Inward and Outward Resonance.	47
13	Removal Resonance.	51
14	Expected Lineshape.	53
15	RF Amplitude Required to Maintain a Constant Resonant Change in Radius vs. Harmonic Order.	56
16	An Ion Moving in Phase with the RF Field at the Third Harmonic.	58
17	The Main Apparatus.	74
18	The Solenoid and the Auxiliary Magnetic Coils.	75
19	NMR Field Regulator.	78
20	NMR Mapper Probe Assembly.	80
21	Ion Source System.	83

Figure		Page
22	Energy Distributions for Several Ions Leaving the Source Simultaneously.	86
23	Focusing by an Einzel Lens.	88
24	Deflection Plate Voltage Supply.	91
25	Trapping Region.	101
26	Electronics for Trapping Ions and Observing Cyclotron Resonance.	105
27	Electrical Signals Appearing on Various Electrodes.	106
28	Zero Offset RF Driver.	110
29	Detector.	113
30	Detector Gain vs. Dynode Voltage.	115
31	The Magnetic Field in the Trapping Region.	130
32	A Typical Population and Magnetic Well.	132
33	Inward and Outward Resonances.	137
34	Removal Resonances.	142
35	Extrapolation to Zero Mass.	155
36	Spin Rotation in the Field of a Wire.	175
37	The Electric Field of the C's.	180
38	The Fit of a Garren Well to the Magnetic Well Below the Flag.	184
39	The Function $G(z_1)$.	189

CHAPTER I. INTRODUCTION

This work concerns itself with the precision measurement of the magnetic moment of the proton in nuclear magnetons and atomic mass differences, in particular the difference of the doublet H_2^+–D^+. If these measurements are to be useful it will not be for the values of the numbers given but because of the relationship of these quantities to others which can be experimentally measured or theoretically calculated.

1.1 Background

The Magnetic Moment of the Proton in Nuclear Magnetons, μ_p/μ_n.

The magnetic moment of the proton μ_p in a magnetic field B is given by $\mu_p = \hbar\omega_s/2B$ where ω_s is the precession frequency of μ_p about B. The nuclear magneton μ_n for a proton with charge e and mass M_p is defined as $\mu_n = e\hbar/2M_pc$.

Thus if we form the ratio of μ_p to μ_n, we have

$$\frac{\mu_p}{\mu_n} = \frac{\omega_s}{\frac{eB}{M_pc}} = \frac{\omega_s}{\omega_o} , \qquad (1.1)$$

where $\omega_o = eB/M_pc$ is the cyclotron frequency. Thus, we see that μ_p/μ_n may be measured by measuring the ratio of ω_s to ω_o in the same magnetic field (Alvarez and Block, 1940).

μ_p/μ_n is usefully related to a number of other physical constants. Its relationship to the Faraday F and hence Avogadro's number N (F = Ne) is currently of interest. The Faraday is the net charge of a mole of singly ionized atoms. The relationship between the Faraday and μ_p/μ_n is given by

$$\frac{\mu_p}{\mu_n} = \frac{\gamma_p}{F} M_p(\text{amu}) \quad , \tag{1.2}$$

where the gyromagnetic ratio of the proton $\gamma_p = \omega_s/B$ is the spin frequency measured in field units. Since B is often calculated in current units, γ_p is then related to an absolute current standard. The value of M_p in amu (atomic mass units: ^{12}C = 12 u exactly) is known very precisely from the techniques of mass spectroscopy as will be discussed later. The least accurate quantity on the right-hand side of Eq. (1.2) is the Faraday. This quantity is normally measured by chemical techniques and can be measured to an accuracy of about 10 ppm.

Another significant relationship is given by

$$\frac{\mu_p}{\mu_n} = \frac{\mu_p/\mu_B}{\mu_B/\mu_n} = \frac{\mu_p}{\mu_B} \frac{M_p}{M_e} \quad , \tag{1.3}$$

where M_e is the electron mass and μ_B is the Bohr magneton (the electron equivalent of the nuclear magneton). Since μ_p/μ_B can be measured very precisely by several methods, Eq. 1.3 allows a very precise measurement of the proton to electron mass ratio using μ_p/μ_n.

One final relationship is given in terms of the fine structure constant α which requires interpretation of the experimental measurements by quantum electrodynamics (QED). This relationship is

$$\frac{\mu_p}{\mu_n} = \frac{\alpha^3}{e^2 N}\left\{\frac{M_p(\text{amu})}{\mu_o R_\infty}\cdot\frac{\mu_p}{\mu_B}\right\}, \qquad (1.4)$$

where R_∞ is the Rydberg for infinite mass, and μ_o is the permeability of free space. The quantities within the braces have negligible error when compared to the others.

From the preceding relations we can see that μ_p/μ_n is related to quantities which are typically measured in widely separated areas of physics and physical chemistry. Our understanding of these quantities and their interrelationship represents our understanding of physics. An example of this is provided by μ_p/μ_n. At the time of

the last least-squares adjustment of the values of the fundamental constants by Taylor, Parker, and Langenberg (1969) there were six reasonably accurate measurements of μ_p/μ_n (see Fig. 1). Taylor et al., along with other authors of the day had concluded that the error assignments on the measurement of Sommer et al. (1951) should be reduced from 22 ppm to 11 ppm to conform to the accepted error assignments of one standard deviation. These new error assignments are indicated by the small arrows in the figure. Thus it may be seen that the available data fell into two groups: a high set containing the measurements of Mamyrin and Frantsuzov (1965) and Boyne and Franken (1961), and a low set containing the others. The values indicated by these two groups differ by about 30 ppm. The lower of these values was also in agreement with the value indicated by a single measurement of the Faraday with an assigned accuracy of 6.8 ppm (Craig et al., 1960). This results in a determination of μ_p/μ_n using Eq.(1.3)with an accuracy of about 10 ppm when the errors in the other terms are included. Thus Taylor et al., chose to drop the measurements of the high group and their final recommended value is shown in Fig. 1.

The discrepancy still existed,however, and encouraged much effort at several laboratories including ours. As a result of this effort, the discrepancy has apparently been cleared up as is indicated in the figure by the excellent agreement of the measurements since 1969. These measurements have been made using a wide variety of techniques which are discussed at the end of Section 1.2. There was never any

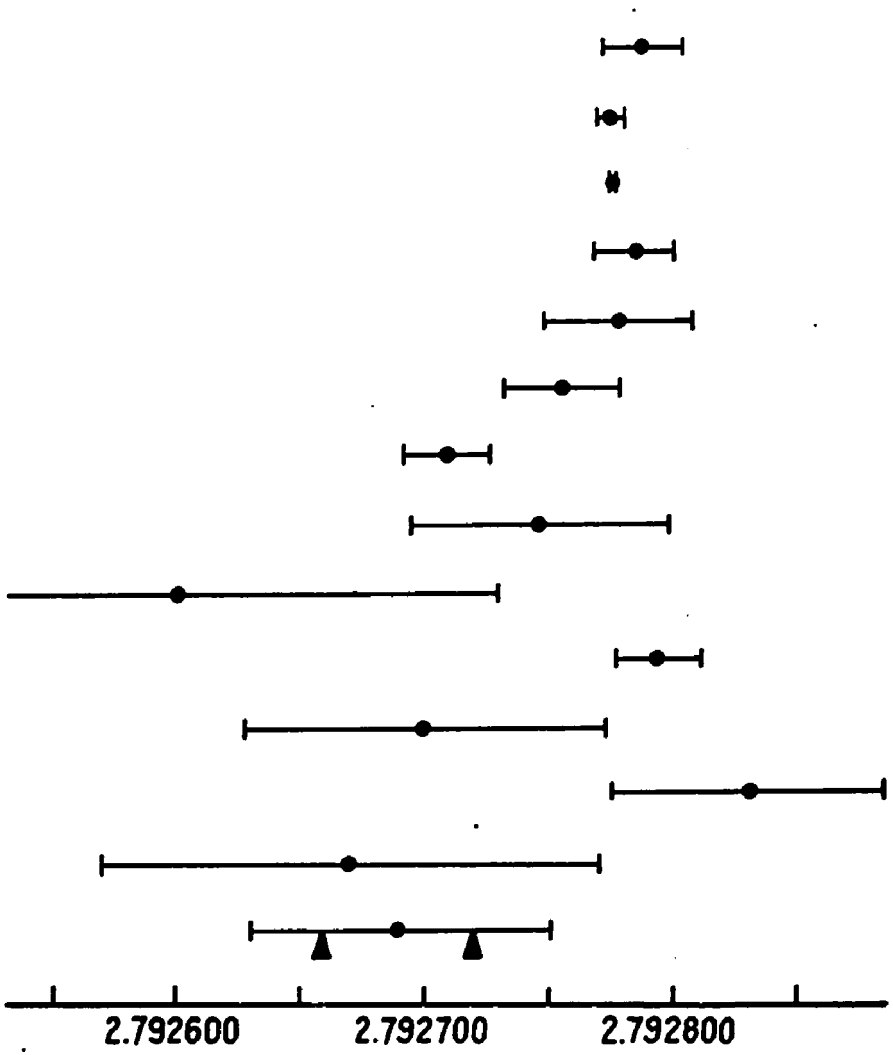

	Assigned Error
Luxon & Rich (1972)	*6.0*
*Petley & Morris (1972)**	*1.8*
Mamyrin et al. (1971)	*0.4*
*Fystrom (1970)**	*6.0*
Zürich: Gubler et al. (1970)	*11.0*
*Petley & Morris (1970)**	*8.2*
Taylor et al., best value (1969)	*6.2*
*Petley & Morris (1967)**	*19*
Marion & Winkler (1967)	*45*
Mamyrin & Frantsuzov (1965)	*6.2*
Sanders et al. (1963)	*26*
*Boyne & Franken (1961)**	*20*
Trigger et al. (1956)	*36*
*Sommer, Thomas, Hipple (1951)**	*22*

FIG. 1 SUMMARY OF THE DATA FOR μ_p/μ_n. * INDICATES MEASUREMENTS MADE USING VARIOUS FORMS OF THE OMEGATRON.

misunderstanding of physical theory discovered and the value which is now indicated is very near the average of the earlier high and low groups. In fact, the weighted average of all of the experimental values available to Taylor et al. ($\overline{\mu'_p/\mu_n}$ = 2.792 783) is consistent with the average of the recent values. This is true even if the value of Sommer et al., is assigned an accuracy of 11 ppm ($\overline{\mu'_p/\mu_n}$ = 2.792 768). Thus one possibility is that the discrepancy was really only a statistical fluctuation.

At the same time, confidence in the determinations of the value of the Faraday has decreased. A recent reevaluation of the error assignment for the measurement of Craig et al. indicates that the error should probably be taken as 11 ppm (Bower, 1970). Furthermore, new data have become available (Bower, 1970; and Marinenko and Taylor, 1968) that are in disagreement with one another by 40 ppm. Thus, while the discrepancies in the value of μ_p/μ_n have been resolved, similar discrepancies have arisen in the value of the Faraday. The effect of this has been to turn attention to the Faraday.

Mass Doublets

The value and interrelation of atomic mass measurements is somewhat different. While the measurements of atomic masses do provide measurements of physical constants, the only one that is normally considered in a tabulation of the so-called fundamental physical constants is the mass of the proton either in atomic mass units or in conventional mass units (e.g., kg). The others are themselves

interrelated, but it is only through this interrelation that they are related to the proton mass and thus the fundamental constants. For this reason, the atomic masses are usually considered as a set in themselves.

Atomic masses can, through the precise techniques of mass doublet spectroscopy, be related to one another and the ^{12}C standard with far more precision than that of many of the fundamental constants (Wapstra and Gove, 1971). This technique measures the difference between the masses of two ions with the same total atomic mass such as

$$^{1}H_2^+ - ^{2}D^+ \qquad \text{or} \qquad ^{12}C_4\ ^{1}H_8\ ^{16}O_2^+ - ^{12}C\ ^{1}H_2\ ^{37}Cl_2^+$$

with respect to one of the masses. Thus one would measure $\Delta M(H_2^+ - D^+)/M(H_2^+)$. Since $\Delta M/M$ is small (in this case ~ 750 ppm) the ratio of these two masses can be measured to far greater accuracy than can either mass. These ratios can then be used to relate the masses back to the ^{12}C standard.

These measurements are usually made in one of two ways: (1) in a conventional deflection spectrometer (Duckworth, 1958) the mass ratio of two ions with masses M_1 and $M_2 = M_1 + \Delta M$ is expressed as the ratio of the deflection voltages V_1 and $V_2 = V_1 + \Delta V$. This relation is

$$\frac{\Delta M}{M_1} = \frac{\Delta V}{V_1} .$$

(2) In the more recent RF mass spectrometers (Smith, 1971) the mass ratio of the two ions is determined by measuring the ratio of their cyclotron frequencies in the same magnetic field. If their cyclotron frequencies are given by ω_{c1} and $\omega_{c2} = \omega_{c1} + \Delta\omega_c$ we have

$$\frac{\Delta M}{M_1} = -\frac{\Delta\omega_c}{\omega_{c2}} \quad . \tag{1.5}$$

These techniques have the advantage that they do not require an absolute measurement of the voltage or the cyclotron frequency, respectively. Thus, if there is a systematic shift in the measured quantity, such as the electric field shift in the cyclotron frequency (Section 2.7), it does not affect the final result. For example, if the cyclotron frequencies in Eq. (1.5) above are shifted by an amount δ, i.e., $\omega_{c1} \to \omega_{c1}(1 + \delta)$, then we would have

$$\frac{\Delta M}{M_1} = -\frac{\Delta\omega_c(1 + \delta)}{\omega_{c2}(1 + \delta)} = -\frac{\Delta\omega_c}{\omega_{c2}} \quad .$$

The mass difference can be calculated in another way using nuclear reaction energies. By accumulating the results of certain nuclear reactions the mass difference of a doublet can be measured in energy units (keV), e.g., (Wapstra, 1970):

$$^{1}H(n,\gamma)^{2}D = (^{1}H + n) - (\gamma + ^{2}D) = 2224.65 \pm 0.04 \text{ keV}$$

$$- \ ^{3}T(\beta^{-})^{3}He = -(^{3}T + \beta^{-}) + ^{3}He = - 18.64 \pm 0.04$$

$$\underline{^{3}T(p,n)^{3}He = (^{3}T + p) - (n + ^{3}He) = -763.84 \pm 0.08}$$

$$^{1}H_{2}^{+}-^{2}D = ^{1}H + p + \beta^{-} + \gamma - ^{2}D = 1442.17 \pm 0.10 \text{ keV}$$

By comparing this to the mass difference in mass units, the best value of which is $H_2^+-D^+ = 1548.287 \pm 0.004$ μu (Smith 1971), we have a direct conversion from energy units to mass units: 1u = 931 461 ± 80 keV. This conversion is a determination of the Einstein mass-energy relation. This relation may be obtained from any number of doublets, but at present the most accurate determination of the energies is for $H_2^+-D^+$. More important, the value of this constant should be the same for all mass doublet pairs. Thus, by comparing the measurements of mass doublets to the restuls of the corresponding nuclear reaction energy measurements, we can test our understanding of atomic masses and the interrelationship of these two areas of physics.

The Einstein mass-energy relation can also be determined from the fundamental constants: $1u = c^2/F$ eV = 931 481 ± 5 keV (Wapstra 1970) to even more precision. Again, we are able to compare the results of nuclear physics and mass spectroscopy to the results of other physical and chemical techniques.

1.2 Measurement Technique

The techniques used to make the measurements tabulated in Fig. 1 are similar in many of their details. The frequencies ω_c and ω_s

are nominally given by $\omega_c = 1.56$ MHz/kG and $\omega_s = 4.24$ MHz/kG. Thus, in typical laboratory fields of 0.1 to 10 kG, these frequencies are in the radio frequency (RF) range. In this section we shall give a brief discussion of the RF resonance technique for measuring ω_c, and the NMR measurements of ω_s.

Resonance Measurements of ω_c

The cyclotron frequency ω_c is determined by a direct measurement of free ions in a magnetic field using an RF resonance process. This process may be illustrated by considering an ion undergoing normal cyclotron motion in a plane perpendicular to a uniform magnetic field $\vec{B} = -B_o\hat{z}$. This motion is described by $r = r_o e^{i(\omega_c t+\theta)}$, where θ is the initial phase angle (Fig. 2(a)). Superposed on the magnetic field is a uniform electric field transverse to the magnetic field given by $\vec{E} = E_o \cos(\nu t + \phi)\,\hat{y}$, where ϕ is the RF phase at $t = 0$. This electric field may be written in complex form as

$$\vec{E} = \frac{iE_o}{2} e^{i(\nu t+\phi)} + \frac{iE_o}{2} e^{-i(\nu t+\phi)} ,$$

where $e^{i(\nu t+\phi)}$ rotates counterclockwise, and $e^{-i(\nu t+\phi)}$ rotates clockwise. If we consider only the component rotating in the direction of the cyclotron rotation, and $\nu = \omega_c$, then the electric field rotates with the velocity vector at an angle $\theta - \phi$ (Fig. 2(b)). For the case $\theta - \phi = 0$ the electric field is always in the direction of the velocity and the ion is continuously accelerated so that it slowly spirals outward (Fig. 2(c)). For the case $\theta - \phi = \pi$ the electric field is

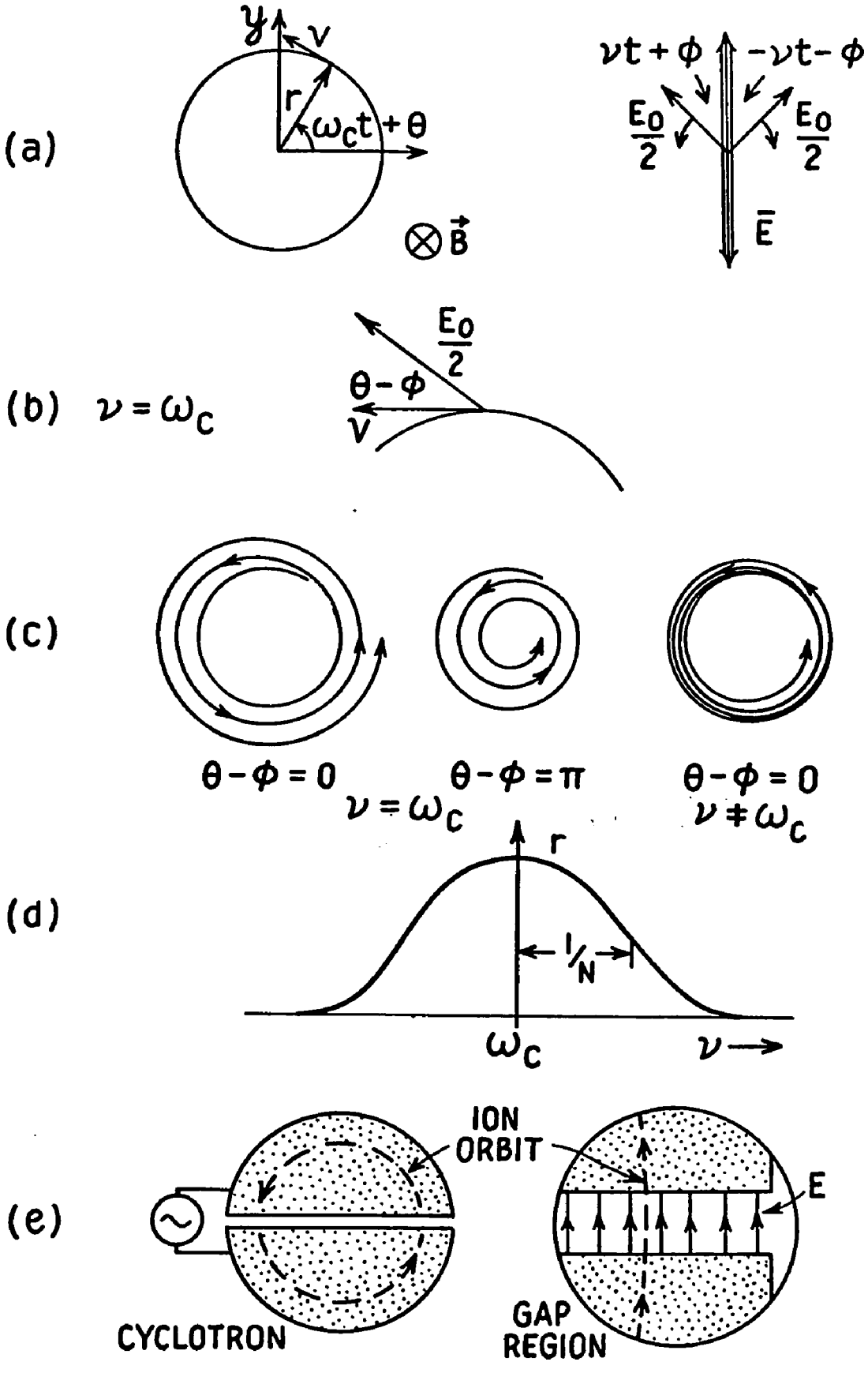

FIG. 2 SCHEMATIC REPRESENTATION OF THE RESONANCE PROCESS.

always in the direction opposite to the velocity vector and it slowly spirals inward. For $\theta - \phi = \pi/2$ the ion does not change radius in the first approximation. If $\omega_c \neq \nu$ the motion is more complex: the RF is alternately in and out of phase with the cyclotron motion and the ion spirals first one way and then the other. Thus we see that for $\nu \cong \omega_c$, there is a mechanism for the ion to change radius, whereas for ν sufficiently far from ω_c, there is no appreciable change in radius. This results in a resonant change in radius r(T) such as that shown in Fig. 2(d) for ions spending a time T in the RF field. In order to estimate the characteristic width $\delta\nu = \nu - \omega_c$ of this resonance process, consider an ion with $\omega_c \neq \nu$ which is initially in phase with the RF ($\theta - \phi = 0$). Let us assume that the ion slowly falls out of phase with the RF voltage so that after completing N cycles in the time T the ion is exactly one-half cycle out of phase ($\theta - \phi = \pi$). The ion will have first been accelerated then decelerated and experience no net change in radius. Thus the characteristic width of the resonance process is approximately $\delta\nu/\nu \cong 1/2N$.

In certain nonuniform RF fields, resonance may be obtained using RF frequencies which are odd harmonics of the cyclotron frequency. For example, consider the cyclotron (Fig. 2(e)) in which the ions only experience the RF field when they are near the gap in the dees. An ion arriving at the gap during the peak of the RF cycle is accelerated once each half revolution. But, the ion cannot distinguish how many half cycles of the RF have taken place except that it is odd. Thus any frequency satisfying the relation $\nu = (2n + 1)\omega_c$, where $n = 0, 1, 2, \ldots$,

will cause a resonant change in radius. To remain in continuous acceleration, the ion must still remain in phase with the RF voltage, and the characteristic width of the resonance process then becomes $\delta\nu/\nu = 1/2N_{RF} = 1/2(2n + 1)N$. Thus by choosing a sufficiently large n, a significant improvement in the linewidth can be obtained.

In each individual apparatus the actual RF field may differ from the examples given here, but the resonance process is essentially the same. The omegatrons use an essentially uniform RF field which does not allow the use of odd harmonics. At the other extreme are the apparatus of Mamyrin et al., with $n \cong 100$ and the mass spectrometer of Smith with $n \cong 500$.

There are two systematic shifts in the zero energy cyclotron frequency ω_o: the relativistic shift and the electric field shift. For an ion moving in a magnetic field with appreciable velocity, the cyclotron frequency is given by

$$\omega_c = \frac{eB}{\gamma Mc} = \frac{\omega_o}{\gamma} , \qquad (1.6)$$

where $\gamma = (1 - v^2/c^2)^{-1/2}$ is the usual relativistic correction. Since for $v^2/c^2 \gtrsim 10^{-6}$, γ is significant at the ppm level, it must be considered whenever the ion energies are of the order of 1 keV or more. In fact, it is a consideration in all of the resonance techniques except that of Boyne and Franken. In some of the experiments, γ is large enough and varies sufficiently during the measurement that its time-average over the motion of the ion must be determined.

In the presence of a radial electric field E_r, the observed cyclotron frequency ω_c' is shifted from the true cyclotron frequency ω_c according to the relation

$$\omega_c' = \omega_c \left[1 - \frac{c}{v_\perp} \frac{E_r}{B} \right] . \tag{1.7}$$

Recalling that the orbital radius r_o of an ion is given by $r_o = Mv_\perp c/eB$, Eq.

$$\omega_c' = \omega_c \left[1 - \frac{c^2 M E_r}{e r_o B^2} \right] . \tag{1.8}$$

All of the RF resonance experiments are affected by this electric field shift. In the omegatrons the axial electric field which is deliberately introduced to trap the ions results in an accompanying radial electric field. In many of the apparatuses there are electric fields present due to either the ion source or the detection systems. Electric fields of sufficient magnitude to cause an appreciable shift can also be caused by the space-charge distribution of the ions themselves if their numbers are allowed to become too large as has often been the case when the ion current has been directly detected using an electrometer. The last but often most troublesome cause is the stray electric fields due to surface potentials variations on neighboring electrodes.

Generally, these electric field shifts are of the order of one standard deviation of the final experimental error or more. Thus, the electric field shift must be experimentally removed by measuring

ω_c as a function of either the ion mass or the magnetic field (Sec. 2.6). However, since several of the causes of these electric fields are not fixed, this experimental removal may be difficult to accomplish accurately.

NMR Determinations of ω_s

The spin-flip frequency ω_s is measured using conventional NMR techniques (Andrew, 1956). Due to the small size of a workable NMR probe (~ 1 cm^3) compared to the typical dimensions of the cyclotron apparatus, it is generally possible to calculate the time-average value of ω_s as experienced by the ions. This time average is based on either theoretical predictions or experimental measurements of the details of the ion's motion. Often, due to complexities in the construction of the apparatus, it is necessary to remove the cyclotron apparatus from the magnetic field before measuring ω_s. In this case any magnetic properties of the apparatus must, of course, be properly accounted for.

The measurement of ω_s using protons in a water sample results in a small correction (~ 26 ppm) which can be made to sufficient accuracy ($\pm$0 .3 ppm) that it does not appreciably affect the final accuracy of the determination of μ_p/μ_n. However since these same problems arise in other measurements to which μ_p/μ_n is related, such as γ_p, it has become conventional to quote the results for all such measurements relative to protons in a spherical water sample. This is normally denoted by a prime ('), e.g., μ_p'/μ_n.

Experimental Apparatus

Having discussed the basic techniques of these experiments, we will now briefly discuss their application to some of the more recent, and more accurate, measurements.

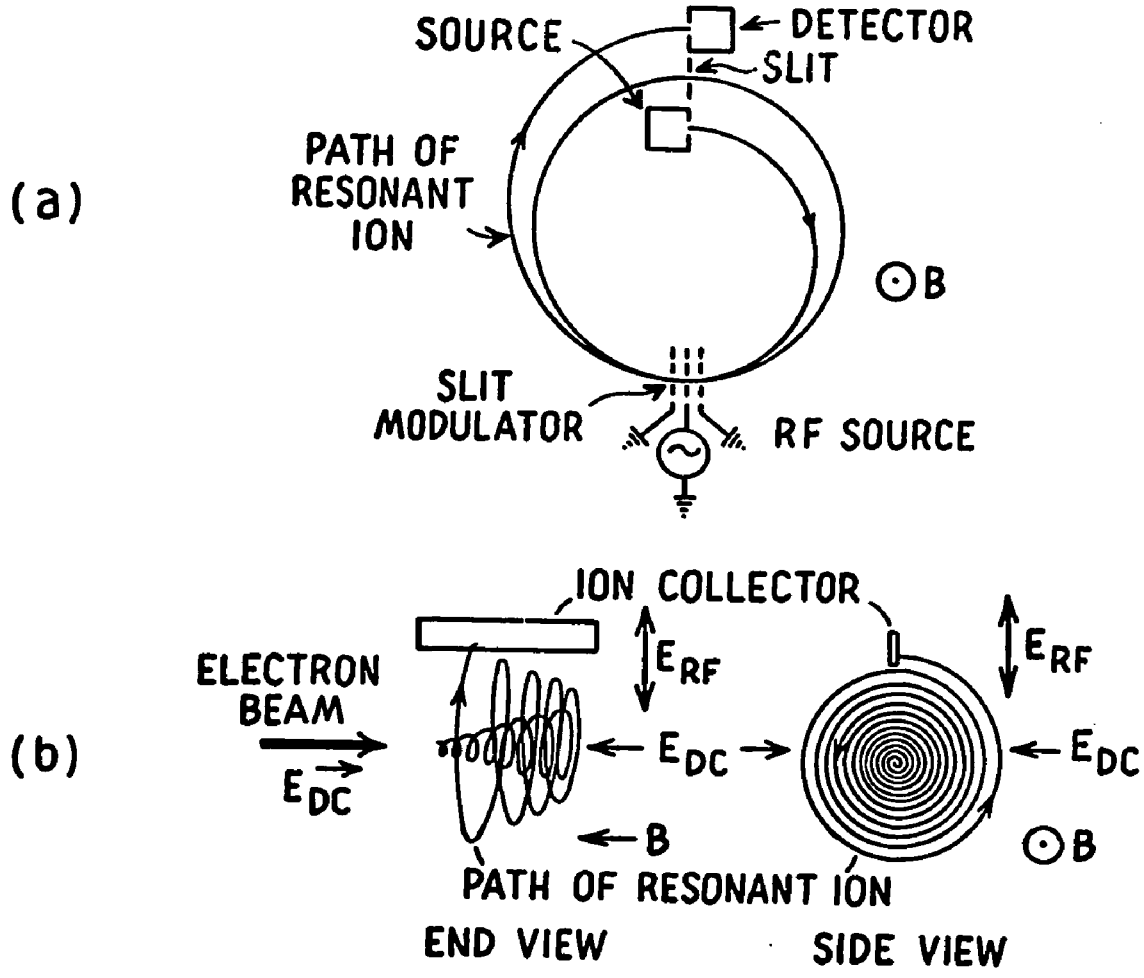

FIG. 3 THREE APPARATUSES USED TO MEASURE μ_p/μ_n.

The mass spectrometer of Mamyrin et al., (1970) (Fig. 3(a)) measures ω_c in only one ion revolution by essentially making a very accurate determination of the ion phase. The ions are produced in a magnetic field of 1.2 kG and their initial orbit is defined by a slit system. The RF field is applied to the ions by a slit modulator which causes the velocity of those ions with the proper phase to increase and they pass through a second slit S_2. Finally, if they remain in phase, the ions receive a second velocity increment in the modulator, and then pass through the slit S_3 and into the detector. Thus, ω_c is measured in the single revolution between the two passes through the modulator. The slit modulator allows very high harmonics of the cyclotron frequency to be applied (n = 100). This results in $N_{RF}^{-1} = 5 \times 10^{-3}$ which is far greater than the actual linewidth of 20 ppm. Thus, it is obvious that the linewidth is very dependent on the phase definition by the narrow slits.

This method of applying the RF field results in a correction of about 10 ppm which is dependent on the precise measurement of the separation of the modulator electrodes. This correction has been both calculated and experimentally verified. Since the resolution is determined by the slit spacing, any improvements in the linewidth are largely dependent on mechanical considerations.

The basic principle of the Omegatrons used by Petley and Morris (1967), Fystrom (1970), and Sommer et al., (1950) is illustrated in Fig. 3(a). Thermal energy ions are produced in the center of the

apparatus by using electron bombardment of a residual gas. The ions are contained in a magnetic field of about 10 kG by a weak electric potential well. They are continuously resonated by a uniform RF field applied across their entire orbit, and their energy is increased to about 1 keV and their radius to about 1 cm whence they strike a detector probe. The linewidth of these instruments is about 200 ppm since the total number of revolutions is limited to less than 10^4 by the drift motion of the ions, and odd harmonics cannot be used.

There are several difficulties in this technique. Both the relativistic factor γ and the electric field correction are difficult to determine. This is due to the large change in velocity which the ion undergoes and the diffuse nature of the ion production process. The electric field shift is proportional to v^{-1} (Eq. (1.6)) and thus it is largest at small radii where the ions are near the electric fields associated with the electron beam and nonresonant ions. Since the electric field shift is determined by varying the ion mass (Sec. 2.7) one must be extremely careful to maintain identical conditions for ions of each mass. Similarly, $\gamma - 1$ increases from zero to about 10 ppm so that its average over the motion of the ion must be determined. The understanding of both of these problems is difficult due to the lack of knowledge of the exact details of the orbit.

The technique of the Zürich group (Gubler et al., 1970) is quite different in that ω_o is not determined directly but instead they measure $\omega_o = \gamma v/r$ for a high energy (1.3 MeV) beam of protons (Fig. 3(c)).

The velocity is determined with a velocity gauge before the ions enter the magnetic field region. The beam is then sent into the magnet and deflected through 180 degrees at a known radius. Thus, ω_c is determined from the velocity and radius, and ω_s is determined by averaging the values obtained from an NMR map along the semicircular path.

1.3 The Present Apparatus

μ_p/μ_n

The essential details of the present apparatus are shown in Fig. 4. The field of a large solenoid is shaped to produce a shallow magnetic mirror well. Within the solenoid is a vacuum system that contains a set of cylindrical electrodes (C's) which surround the experimental region. These C's are electrically connected as shown in Fig. 4(b), for the injection and ejection of ions, and when so connected they will be referred to as the injection and ejection cylinders, respectively. Otherwise they are connected as shown in Fig. 4(c), to allow a transverse RF electric field to be applied to the ions by applying an RF voltage to the C's.

The ions are produced in an external ion source and enter the experimental region through an orbit defining annulus which sets their radius at 4.05 ± 0.05 cm. The ions are then injected into the magnetic well by pulsing the injection cylinder positive. While in the well, the ions undergo both normal cyclotron motion and a slow oscillatory drift between the mirror points. After spending a fixed period of time in the well, the ions are ejected by pulsing the ejection cylinder positive and they then drift down to the detector where they are counted.

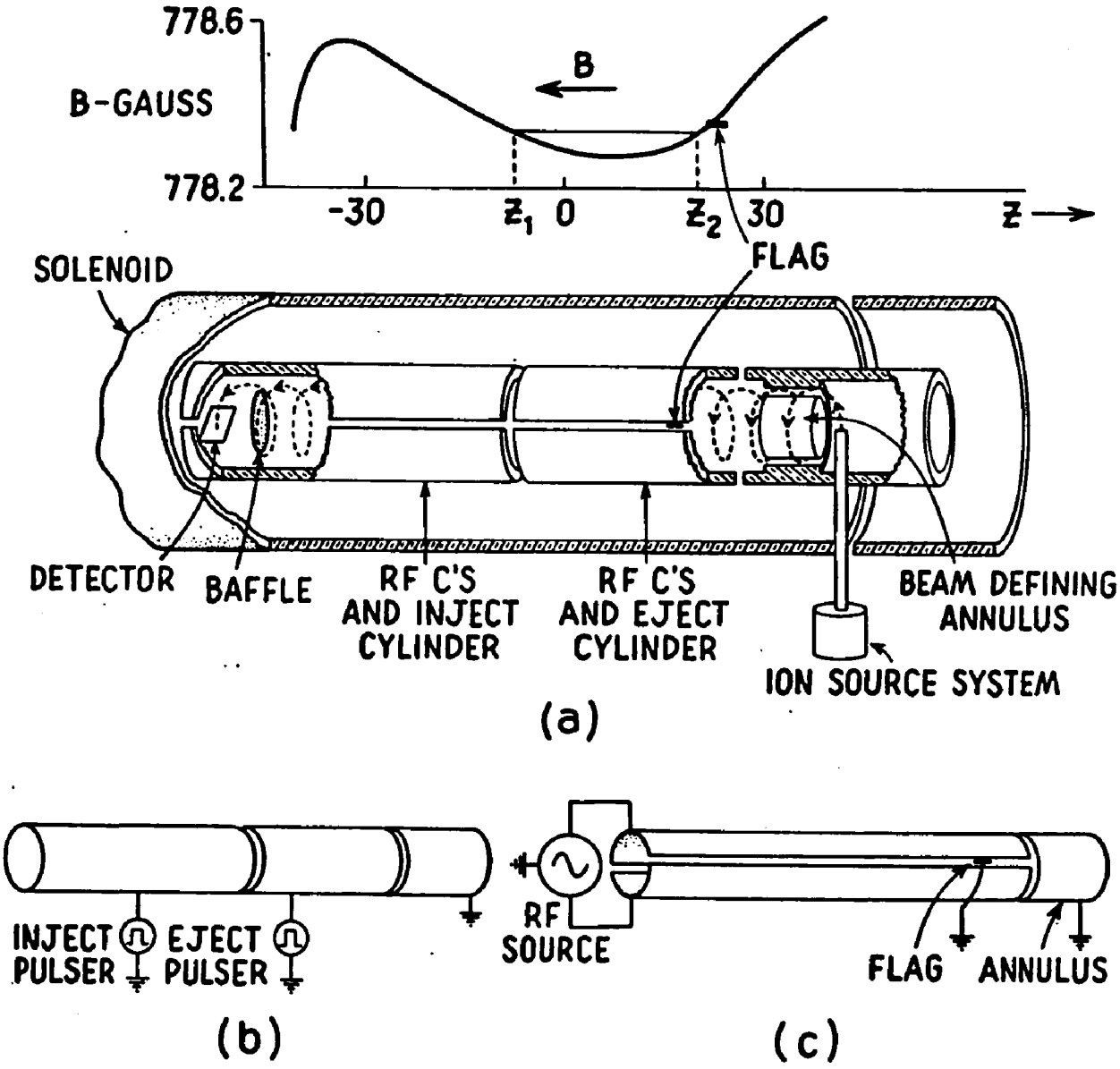

FIG. 4 THE PRESENT APPARATUS. (a) SCHEMATIC DIAGRAM

(b) C's CONNECTED FOR INJECTION AND EJECTION

(c) C's CONNECTED FOR APPLYING THE RF FIELD.

While the ions are in the well, the RF field is applied across their orbit. If the RF frequency is equal to the cyclotron frequency, the ions experience a small continuous change in radius (about 2.5 percent) as discussed in the previous section. The detector is set to detect this change in radius, and resonance is observed by varying the RF frequency on successive machine cycles and recording the counting rate at the detector as a function of frequency. Thus a resonance line similar to that shown in Fig. 2(d) is obtained.

In order to determine ω_s, a small NMR probe is used to make a point by point map of the values of ω_s within the apparatus at the cyclotron radius. These measurements are then used to determine the time-average value of ω_s experienced by the ions as they oscillate axially in the well.

Largely because of the use of magnetic trapping, this technique has several advantages when compared to the other apparatuses discussed above. First, the ions may be held in the experimental region for a large number of cyclotron revolutions. This, along with the use of RF frequencies which are odd harmonics (11th) of the cyclotron frequency has allowed us to make the RF linewidths very narrow. Linewidths of 20 ppm (FWHM) are used for the bulk of the data presented here and lines as narrow as 8 ppm have been used in studies of systematic effects. These linewidths could presumably be improved considerably in a future version of the apparatus.

Second, the well defined orbit and small resonant change in radius allows γ to be accurately determined. In the present apparatus

$\gamma - 1$ is at most 0.5 ppm and can be calculated to 2 percent. Thus, $\gamma - 1$ can become much larger in a future version of this apparatus without contributing significantly to the error.

Third, magnetic trapping of the ions allows us to isolate the experimental region from the electric fields of the source and detection systems. The use of a particle counting detector has allowed us to work with trapping rates which do not produce an appreciable space-charge field. Unfortunately, there is enough residual electric field, apparently due to surface potential variations, to produce an appreciable shift in the cyclotron frequency.

Mass Doublets

The use of the present apparatus to measure the mass difference of closely spaced doublets is a simple extension of the resonance technique described above for measuring ω_c. In order to measure the mass ratio of a doublet such as $H_2^+ - D^+$, both species are produced by the source system and trapped simultaneously in the magnetic well. The resonance lineshape for each specie is then alternately swept and separately recorded. These lineshapes are then shifted to exactly center one on the other, and the total shift is taken as $\Delta\omega_c$. The linewidths in the present apparatus are about 20 ppm and the lines are matched to about 1/2 percent of the linewidth at this reporting, so that the overall accuracy is 1 in 10^7. It is thought that this can be increased by a factor of ten in future work.

This apparatus has the advantage that it measures the mass difference of the low mass doublets directly rather than deducing a

value from measurements on high mass molecular ions as is sometimes done. This is particularly useful in the case of the D_2^+–He^+ doublet as it is difficult to form a high mass ion incorporating He.

CHAPTER II. MEASUREMENT THEORY

This chapter is devoted to understanding the observed experimental quantities and their relation to μ_p/μ_n and ion mass differences. In order to accomplish this, we must first understand the motion of the ions trapped in the well. We must then understand both the effect of the resonance process on the ion motion and the effect of the ion motion on the observed resonance line. Finally, we must apply the observations of this motion to the measurement of μ_p/μ_n and mass differences.

2.1 Orbital Motion of the Trapped Ions

The motion of the ions in the well may be separated into three components: the planar cyclotron motion of the ions about their orbit center in a magnetic field $\vec{B}(\tau_c \simeq 1\ \mu s)$, the axial motion of the orbit center parallel to $\vec{B}$ as the ions oscillate back and forth in the magnetic well ($\tau \simeq 350\ \mu s$), and the slow drift of the orbit center transverse to the direction of $\vec{B}$. The latter point is discussed in Appendix III, and it suffices here to note that certain experimental parameters are adjusted so that this drift is essentially zero.

In the plane transverse to the magnetic field $\vec{B}$, the ion undergoes simple cyclotron motion with frequency ω_c and radius r given by

$$r = \frac{cMv}{eB} \quad . \tag{2.01}$$

Since $T = 1/2\ Mv^2$, this may be written

$$r = \frac{c\sqrt{2MT}}{eB} \quad . \tag{2.02}$$

Since the radius of the apparatus is fixed experimentally so that all ions will experience the same experimental conditions, we have the restriction

$$T \propto \frac{1}{M} \quad . \tag{2.03}$$

That is, the energy of the ions used in the apparatus is inversely proportional to their mass. Typical ions energies are 500 eV for H^+ (protons), 250 eV for H_2^+, and 125 eV for He^{++}.

Axial Motion

The effect of the axial field configuration shown in Fig. 5 as an axial potential well can be easily shown. Consider an ion moving in an axially symmetric magnetic field $\vec{B} = -B_o\hat{z}$ which has a slight well-shaped inhomogeneity as a function of z as shown in the figure. If the axial velocity of the ion is given by $v_z(z)$ and its transverse velocity by $v_\perp(z)$, then the magnitude of the total velocity of the ion $v(z)$ is given by

$$v^2(z) = v_\perp^2(z) + v_z^2(z) \quad . \tag{2.04}$$

Because the speed of a charged particle in a magnetic field is constant, we have

$$v^2(z) = v^2(z_1)$$

for any two points z and z_1. Since the variation in B is slow, we may take as an adiabatic invariant the quantity

$$\mu = \frac{\frac{1}{2} M v_\perp^2(z)}{B_z(z)} \qquad \text{(Jackson, 1962)} \quad . \tag{2.05}$$

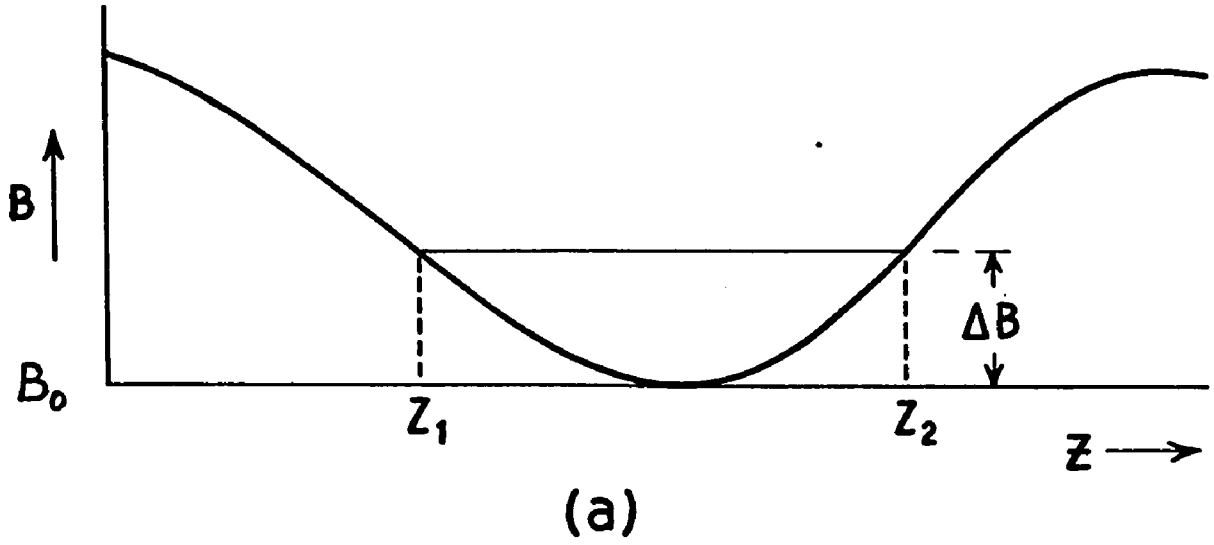

(a)

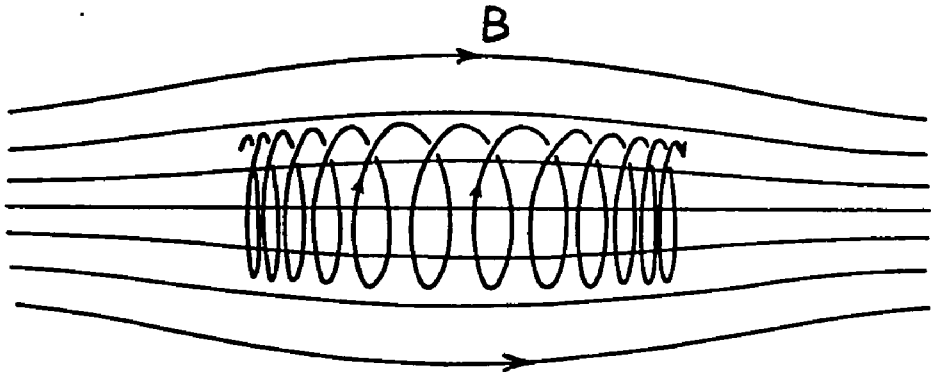

(b)

FIG. 5 A MAGNETIC WELL. (a) A GRAPH OF THE MAGNETIC FIELD AS A FUNCTION OF AXIAL POSITION. (b) THE MOTION OF AN ION IN A MAGNETIC WELL (THE CURVATURE OF THE FIELD LINES IS GREATLY EXAGGERATED).

(See Gilleland (1969) or Northrop (1963) for a more detailed discussion of the approximations made in taking μ as an adiabatic invariant.) If we take μ as a constant, we have

$$\frac{\frac{1}{2} Mv_{\perp}^2(z)}{B_z(z)} = \frac{\frac{1}{2} Mv_{\perp}^2(z_1)}{B_z(z_1)} \quad . \tag{2.06}$$

Thus if the ion is moving in the direction of increasing field strength with small pitch ($v_{\perp}(z) >> v_z(z)$), so that by Eq. (2.06) $v_{\perp}(z)$ is increasing, then the point at which $v^2(z_1) = v_{\perp}^2(z_1)$ must be an endpoint of the motion. If we take z_1 as the endpoint and substitute Eq. (2.04) into Eq. (2.06), we have

$$\frac{1}{2} Mv_z^2(z) = \frac{\frac{1}{2} Mv_{\perp}^2(z_1)}{B_z(z_1)} \left(B_z(z_1) - B_z(z)\right) \quad . \tag{2.07}$$

If we define $T_z(z) = 1/2\ Mv_z^2(z)$ and $T_{\perp}(z) = 1/2\ Mv_{\perp}^2(z)$, this becomes

$$T_z(z) = \frac{T_{\perp}(z_1)}{B_z(z_1)} \left(B_z(z_1) - B_z(z)\right) \quad . \tag{2.08}$$

The other endpoint of the motion z_2 is given by $B(z_2) = B(z_1)$. Thus while the ion undergoes cyclotron motion, its orbit center oscillates back and forth in an axial potential well (Fig. 5(b)). Since in the experimental region, $B_z(z)$ differs from $B(z)$ by less than a ppm, $B_z(z)$ can be replaced by $B(z)$.

This axial motion is identical to the motion in a one-dimensional potential well U(z) given by

$$U(z) = -\frac{T_\perp(z_1)}{B(z_1)}\,(B(z_1) - B(z)) \quad . \tag{2.09}$$

If we let B_{min} denote the bottom of the well, then the magnetic level of an ion in the well $\Delta B(z_1)$ is given by $\Delta B(z_1) = B(z_1) - B_{min}$ and the corresponding energy level ΔU by

$$\Delta U = -\frac{T_\perp(z_1)}{B(z_1)}\,\Delta B \quad . \tag{2.10}$$

In the present experiment $T_\perp \cong 500$ eV for protons and $\Delta B/B$ is typically expressed in ppm, so that $\Delta U/(\Delta B/B) \cong 0.5$ meV/ppm (meV $\equiv 10^{-3}$ eV). If we consider a proton at a level $\Delta B/B = 10$ ppm, it has a peak axial energy of only 5 meV. Thus, understanding the magnetic field which an ion experiences to 1.0 ppm is equivalent to understanding the potential well in which it moves to 0.5 meV.

Such small axial energies in the potential well, especially when compared to the previous lepton g-factor experiments, have pointed up the need to more properly write Eq. (2.09) as

$$U(z) = -\frac{T_\perp(z_1)}{B(z_1)}\,(B(z_1) - B(z)) + V(z) \quad , \tag{2.11}$$

where V(z) is any axially varying potential distribution generally due to surface charges, contact potentials, etc. Unfortunately, since the value of $T_\perp$ is inversely proportional to mass (Eq. (2.03)), the depth

of the magnetic potential well is inversely proportional to the ion mass while V(z) remains unchanged. Equation (2.08) for the axial energy can be written in terms of the spin frequency $\omega_s(z)$ which is the eventual variable of interest as

$$T_z(z) = \frac{T_\perp(z_1)}{\omega_s(z_1)} (\omega_s(z_1) - \omega_s(z)) \quad . \tag{2.12}$$

Similarly, the pitch of an ion's motion is given from Eq. (2.07) by

$$\frac{v_z}{v_\perp} = \left\{ \frac{\omega_s(z_1) - \omega_s(z)}{\omega_s(z_1)} \right\}^{1/2} \quad . \tag{2.13}$$

A particle oscillating at a level 10 ppm from the bottom of the well has a maximum pitch $v_z/v_\perp = 3 \times 10^{-3}$.

Trapping Procedure

The trapping of charged particles in shallow magnetic mirror wells has been discussed thoroughly in the literature of the Michigan lepton g-factor experiments (Gilleland and Rich, 1972, Wesley and Rich, 1971). However, since this experiment may be of interest to an entirely different group of people who are not familiar with these previous experiments, the procedure will be carefully described here. Consider the situation shown in Fig. 6. If a beam of ions spirals down over the well region from the right with sufficient axial energy to clear the right peak, they will continue on over the left peak, but none will be trapped without an external perturbation. Thus, a pair

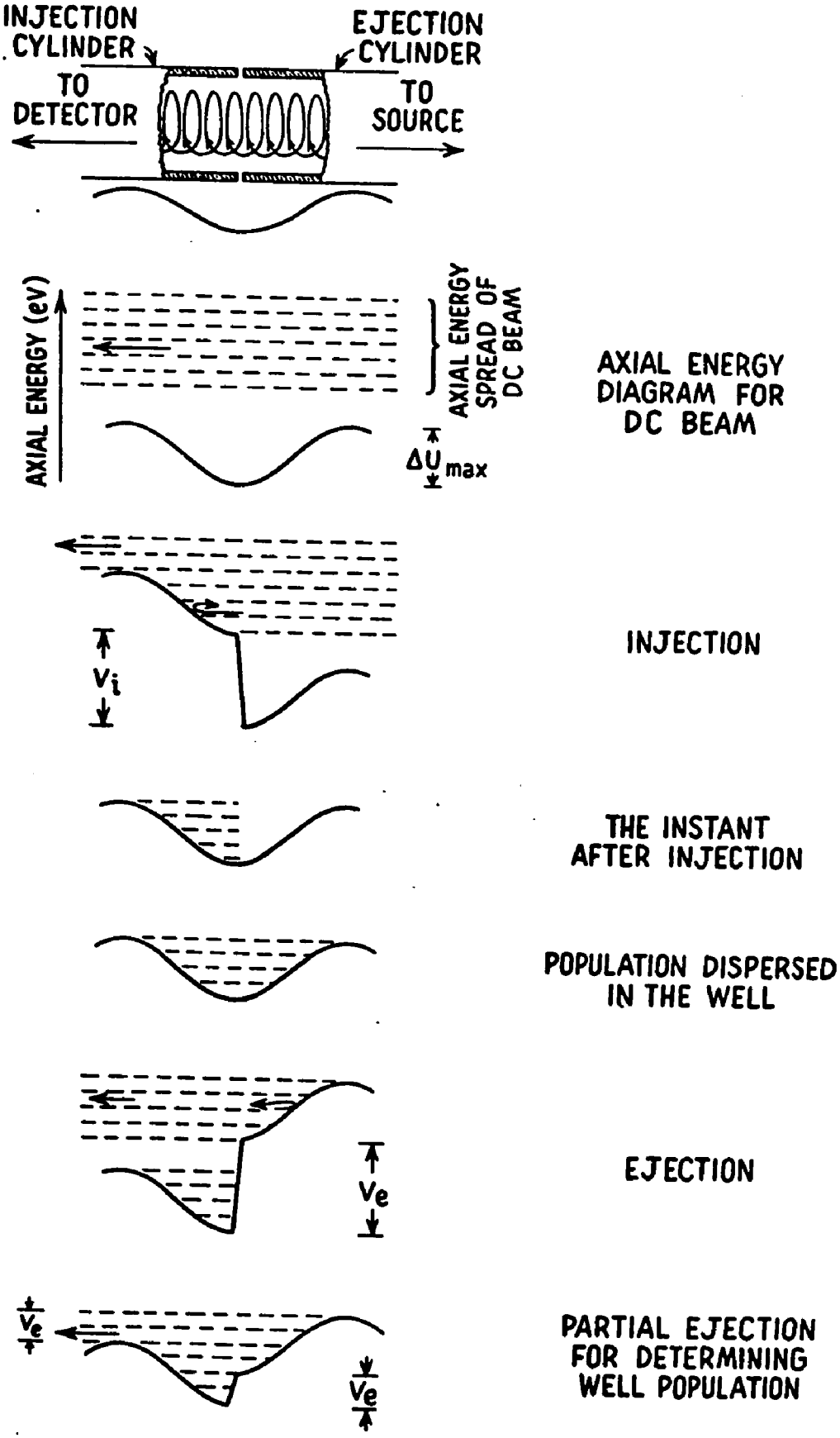

FIG. 6 SCHEMATIC REPRESENTATION OF INJECTION AND EJECTION.

of cylinders are placed around the trapping region concentric with the field center and with a small gap between them at the approximate center of the well. (These cylinders are also split lengthwise for the purpose of applying an RF electric field across the cyclotron orbit, but this does affect the trapping). If the injection (left-hand) cylinder is raised to a potential V_i as shown in Fig. 6, those ions striking the resultant potential barrier will be reflected and spiral back toward the source. If the injection cylinder is then returned to zero potential, those ions within the injection cylinder will remain trapped and will disperse over the entire well. If at some later time it is desired to eject the beam, the ejection (right-hand) cylinder is raised to a positive voltage V_e, and those ions in the ejection cylinder will leave the well and proceed to the detector. In practice the dc beam is only allowed into the well region during the injection period, and the detector is gated to the counters only during the ejection period. Note that if V_e is returned to zero for one-half well period, those ions in the injection cylinder will have moved to the ejection cylinder and can then also be ejected.

2.2 Averaging Over the Motion in the Well

Time-Averages

The period of the axial motion of the ions in the well is given by

$$\tau(z) = \oint dt \quad .$$

If we substitute $v_z = dz/dt$, this becomes

$$\tau(z_1) = \int_{z_1}^{z_2} \frac{dz}{v_z} \quad , \tag{2.14}$$

where z_1 and z_2 are the endpoints of the axial motion. If we substitute for v_z from Eq. (2.13) this becomes

$$\tau(z_1) = \frac{2}{v_\perp} \int_{z_1}^{z_2} \sqrt{\frac{\omega_s(z_1)}{\omega_s(z) - \omega_s(z_1)}}\, dz \quad . \tag{2.15}$$

For a parabolic well the period can be shown to be constant. Since we are normally concerned with particles oscillating in the bottom of the well which is to a good approximation parabolic, the period is approximately constant.

Since r_o is held constant, $v_\perp = r_o\omega_c$ is inversely proportional to the mass of the ion. The axial period of an ion is then proportional to its mass and is typically given by $\tau \cong 350\ M/M_p\ \mu s$.

To obtain the time-average of a quantity in the trapping region, in particular ω_s, it must be averaged over the axial motion of the ion. If we let brackets [ ] denote the time average of a quantity, we have

$$[\omega_s] = \frac{1}{\tau}\oint \omega_s\, dt \quad .$$

Using $v_z(z) = dz/dt$ and taking z_1 and z_2 as the endpoints of the motion, this becomes

$$[\omega_s(z_1)] = \frac{2}{\tau(z_1)} \int_{z_1}^{z_2} \omega_s(z) \frac{dz}{v_z(z)} \quad . \tag{2.16}$$

But $v_z(z)$ is given by Eq. (2.13) so that this may be written as

$$[\omega_s(z_1)] = \frac{2(\omega_s(z_1))^{1/2}}{v_\perp \tau(z_1)} \int_{z_1}^{z_2} \frac{\omega_s(z)}{\{\omega_s(z_1) - \omega_s(z)\}^{1/2}}\, dz \quad . \tag{2.17}$$

Substituting for $\tau(z_1)$ from Eq. (2.15) this becomes

$$[\omega_s(z_1)] = \frac{\int_{z_1}^{z_2} \frac{\omega_s(z)\, dz}{\{\omega_s(z_1) - \omega_s(z)\}^{1/2}}}{\int_{z_1}^{z_2} \frac{dz}{\{\omega_s(z_1) - \omega_s(z)\}^{1/2}}} \quad . \tag{2.18}$$

In this manner, the value of $[\omega_s(z)]$ associated with a particle oscillating at a given level in the well is obtained.

In general ω_s is also a function of the azimuthal position θ, and $\omega_s(z)$ is obtained by a simple average over an appropriate number of evenly spaced θ's:

$$\omega_s(z) = \frac{1}{p} \sum_{i=1}^{p} \omega_s(z,\theta_i) \quad . \tag{2.19}$$

A discussion of the value of p is found in Section 5.2.

Determination of the Median Value of ω_s

The ejection procedure may be extended to determine the population distribution of the ions in the well. If on ejection, the ejection cylinder is raised to a voltage V_e which is less than the depth of the well (Fig. 6, bottom) only those ions with axial energies greater than $U - V_e$ will get out of the well and reach the detector. On successive machine cycles V_e is increased and the number of counts at the detector $N(V_e)$ is plotted as a function of V_e. The result is the integral population of the well (Fig. 7), which may then be differentiated to obtain the population density of the well:

$$\rho(V_e) = \frac{dN(V_e)}{dV_e} \quad . \tag{2.20}$$

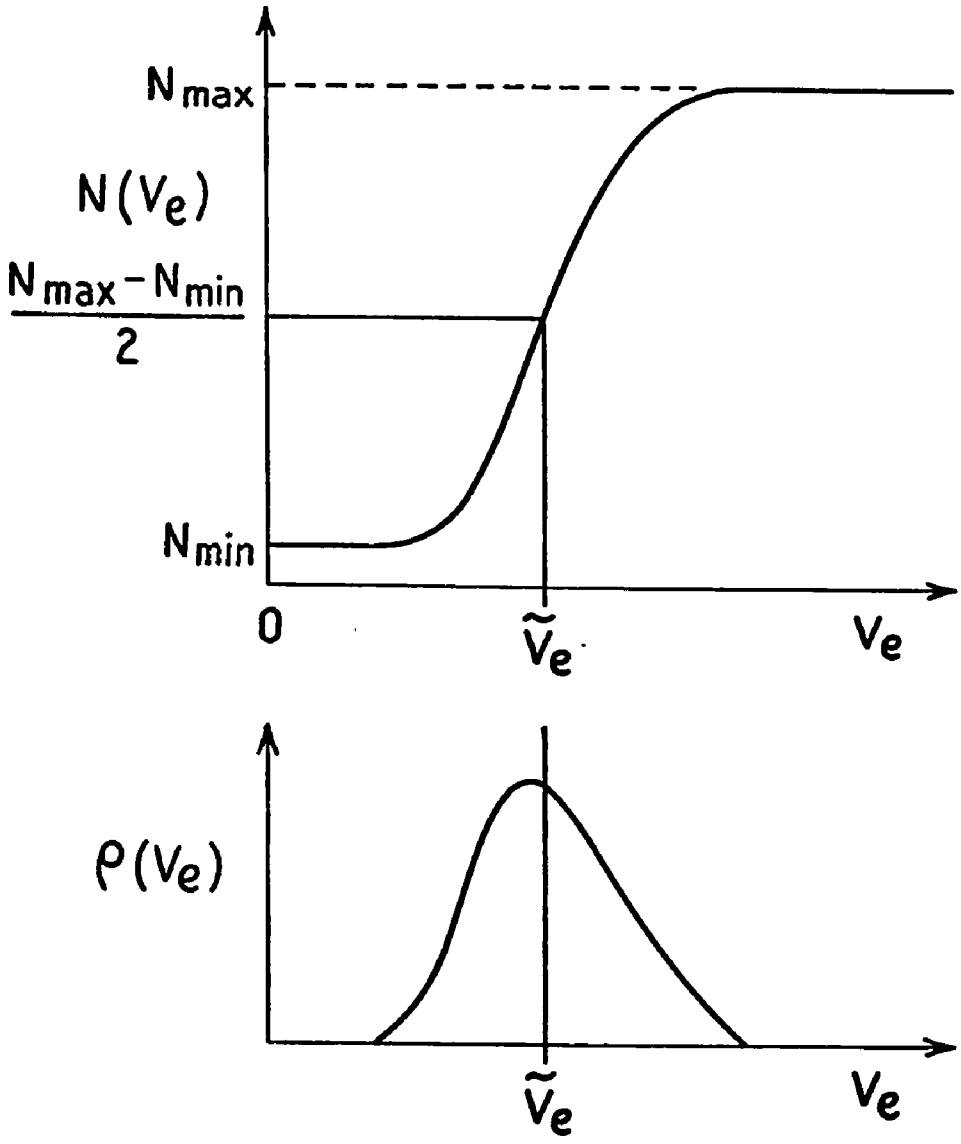

FIG. 7 THE DENSITY FUNCTION.

The median $\tilde{V}_e$ of $\rho(V_e)$ is given by

$$\int_{V_e^{min}}^{\tilde{V}_e} \rho(V_e)\, dV_e = \frac{1}{2} \int_{V_e^{min}}^{V_e^{max}} \rho(V_e)\, dV_e \quad , \tag{2.21}$$

or equivalently by

$$N(\tilde{V}_e) = \frac{N_{max} + N_{min}}{2} \quad . \tag{2.22}$$

Since the time-average spin frequency $[\omega_s(z_1)]$ of an ion at any level in the well is a monotonic function of V_e, the median of the spin frequency is given by

$$[\tilde{\omega}_s(z_1)] = [\omega_s(\tilde{V}_e)] \quad . \tag{2.23}$$

2.3 RF Resonance and Lineshape Theory

Resonant Motion of an Ion

In order to understand the observed resonance lineshapes we must first understand the motion of a single ion near resonance in a uniform magnetic field. Consider the problem of an ion of mass M moving in a magnetic field $\vec{B} = -B_o \hat{z}$ with its orbit center concentric with the center of a longitudinally split conducting cylinder of radius R_c (Fig. 8). An RF voltage $+U_o \cos(\nu t + \phi)$ is applied to the upper C, and $-U_o \cos(\nu t + \phi)$ to the lower C. It is desired to describe the motion of an ion initially at radius r_o, velocity v_o, and angular position θ_o, especially near the resonant condition $\nu \cong \omega_c$. The equations of motion for the ion are

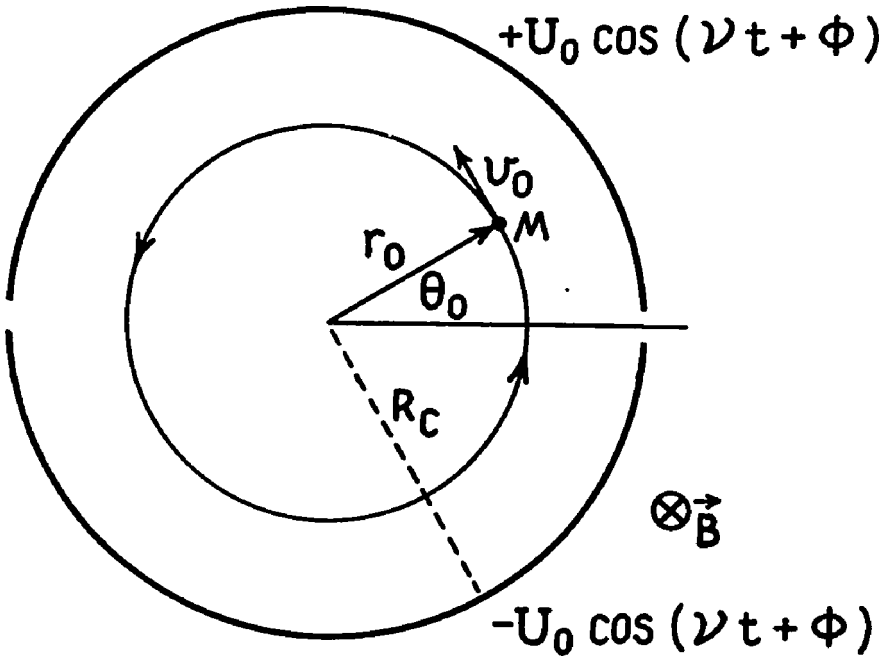

FIG. 8 CYCLOTRON MOTION WITHIN THE C's.

$$\frac{\partial v_x}{\partial t} = \frac{e}{M}\left(E_x - \frac{v_y B_o}{c}\right), \quad \frac{\partial v_y}{\partial t} = \frac{e}{M}\left(E_y - \frac{v_x B_o}{c}\right), \quad \text{and} \quad \frac{\partial v_z}{\partial t} = \frac{e}{M} E_z \ . \tag{2.24(a),(b),(c)}$$

Since the axial motion is separable, we can solve the problem in two dimensions by setting $E = E_x + iE_y$ and $V = v_x + iv_y = v\, e^{i\theta}$. Then, taking Eq. (2.24(a)) + i · Eq. (2.24(b)), we get

$$\frac{dV}{dt} = \frac{e}{M} E + i\omega_c V \ ,$$

where $\omega_c = eB_o/\gamma Mc$. Rearranging terms and multiplying both sides by $e^{-i\omega_c t}$, this becomes

$$e^{-i\omega_c t}\left(\frac{dV}{dt} - i\omega_c t\right) = \frac{e}{M} E\, e^{-i\omega_c t} \ . \tag{2.25}$$

Equation (2.25) may be integrated using the initial conditions $R_o = R(t = 0) = r_o\, e^{i\theta_o}$, and $V_o = V(t = 0) = iv_o\, e^{i\theta_o}$, giving us

$$V\, e^{-i\omega_c t} - V_o = \int_0^t dt\, \frac{e}{M} E\, e^{-i\omega_c t} \ . \tag{2.26}$$

The electric field E has been assumed not to be a function of r in order to obtain an expression for the velocity V which will lend itself to solution. The electric field E is simply the dc electric field of the two C's at $+U_o$ and $-U_o$ which is given by Eq. (I.1) multiplied by $\cos(\nu t + \phi)$, that is

$$E = \frac{4eU_o}{\pi R_c} \frac{1}{1 - \left(\frac{r}{R_c}\right)^2 e^{-2i(\omega_c t+\Theta_o)}} \cos(\nu t + \phi) \qquad (2.27)$$

where $\Theta = (\omega_c t + \Theta_o)$. The electric field of the C's violates our condition of the independence of E from r. However, E may be assumed reasonably constant over a small range of r and the integral performed holding r constant, $r = r_o$. The implications of this limitation are discussed in Section 2.5. Thus the velocity may be written as

$$V = V_o e^{i\omega_c t} + i \frac{4eU_o}{\pi M R_c} \int_0^t dt \frac{e^{-i\omega_c t} \cos(\nu t + \phi)}{1 - \left(\frac{r_o}{R_c}\right)^2 e^{-2i(\omega_c t+\Theta_o)}} . \qquad (2.28)$$

The integral, denoted by I, is evaluated by expanding the denominator as an infinite series and writing the cosine function as an exponential, which gives us

$$I = \frac{1}{2} \int_0^t dt\, e^{-i\omega_c t} \left(e^{i(\nu t+\phi)} + e^{-i(\nu t+\phi)}\right) \sum_{n=o}^{\infty} \left(\frac{r_o^2}{R_c}\right)^{2n} e^{-i2n(\omega_c t+\Theta_o)} .$$

Moving the sum outside the integral and integrating gives us

$$I = -\frac{i}{2} \sum_{n=o}^{\infty} e^{-i2n\Theta_o} \left(\frac{r_o}{R_c}\right)^{2n} \left\{ \frac{e^{i\{\nu-(2n+1)\omega_c\}t} - 1}{\nu - (2n+1)\omega_c} e^{i\phi} \right.$$

$$\left. - \frac{e^{-i\{\nu+(2n+1)\omega_c\}t} - 1}{\nu + (2n+1)\omega_c} e^{-i\phi} \right\} .$$

Thus we have an expression for the velocity as an infinite series given by

$$V = V_o e^{i\omega_c t} + \frac{2eU}{\pi MR_c} e^{i\omega_c t} \sum_{n=o}^{\infty} \left(\frac{r_o}{R_c}\right)^{2n}$$
$$\cdot \left\{ \frac{e^{-\{\nu-(2n+1)\omega_c\}t} - 1}{(\nu - (2n+1)\omega_c)t} e^{i(\phi-2n\theta_o)} - \frac{e^{-i\{\nu+(2n+1)\omega_c\}t} - 1}{(\nu + (2n+1)\omega_c)t} e^{-i(\phi+2n\theta_o)} \right\} . \quad (2.29)$$

It is apparent at this point that for an applied frequency $\nu \cong (2n+1)\omega_c$, $n = 0,1,\ldots,$ the first term in the brackets will exhibit resonant behavior for one term in the series. The maximum amplitude of this term at resonance may be found by taking the limit:

$$\lim_{\nu \to (2n+1)\omega_c} \frac{e^{i\{\nu-(2n+1)\omega_c\}t} - 1}{(\nu - (2n+1)\omega_c)t} = i .$$

Thus the magnitude of the resonant term in the brackets is of order unity. The magnitude of each of the other bracketed terms in the series is at most $1/\omega_c t = 1/2\pi N$, where N is the total number of cycles. In general, we are only interested in cases where N is large (in this work $N \cong 10^4$) and all terms but the resonant term can be dropped. Thus if we let $\nu = (2n+1)\omega_c + \delta\nu$ and ignore all nonresonant terms, we have a simplified expression for the velocity near resonance:

$$V = V_o e^{i\omega_c t} + \frac{2eU_o}{\pi MR_c} \left(\frac{r_o}{R_c}\right)^{2n} e^{i(\phi-2n\theta_o)} \frac{e^{i\delta\nu t} - 1}{\delta\nu} e^{i\omega_c t} . \quad (2.30)$$

Recalling that $V_o = iv_o e^{i\theta_o}$, setting $v_1 = \frac{2eU_o}{\pi MR_c\omega_c}\left(\frac{r_o}{R_c}\right)^{2n}$, and noting that $e^{i\delta\nu t} - 1 = 2 \sin(\delta\nu t/2)\, e^{i\delta\nu t/2}$, the velocity may be written as

$$V = \left\{ iv_o e^{i\theta_o} + v_1 \omega_c t e^{i(\phi - 2n\theta_o)} \frac{\sin(\delta\nu t/2) e^{i\delta\nu t/2}}{\delta\nu t/2} \right\} e^{i\omega_c t} . \quad (2.31)$$

Thus the velocity vector consists of two terms: the first, $iv_o e^{i(\omega_c t + \theta_o)}$, describes the motion with no RF field applied, while the second is the change in the velocity due to the RF field. The latter has a characteristic magnitude given by $v_1 \omega_c t = 2\pi N v_1$.

The radius vector may be obtained by direct integration:

$$R(\delta\nu t) = \left\{ r_o e^{i\theta_o} - i\rho_1 \omega_c t \frac{\sin \delta\nu t/2 \; e^{i\delta\nu t/2}}{\delta\nu t/2} e^{i(\phi - 2n\theta_o)} \right\} e^{i\omega_c t} , \quad (2.32)$$

where $r_o = v_o/\omega_c$, $\rho_1 = v_1/\omega_c$, and terms of order $\delta\nu/\omega_c$ have been dropped. Note that $R(\delta\nu t)$ rotates at ω_c and consists of the radius vector with no applied RF field which is denoted R_o, plus a component due to the RF field $R_1(\delta\nu t)$ (Fig. 9). Thus $R(\delta\nu t)$ may be written

$$R(\delta\nu t) = \left\{ R_o + R_1(\delta\nu t) \right\} e^{i\omega_c t} , \quad (2.33)$$

where

$$R_o = r_o e^{i\theta_o} , \quad (2.34)$$

and

$$R_1(\delta\nu t) = -i\omega_c t \rho_1 \frac{\sin \delta\nu t/2 \; e^{i\delta\nu t/2}}{\delta\nu t/2} e^{i\phi - 2n\theta_o} . \quad (2.35)$$

If we define $r_1(\delta\nu t)$ as the magnitude of $R_1(\delta\nu t)$, we have

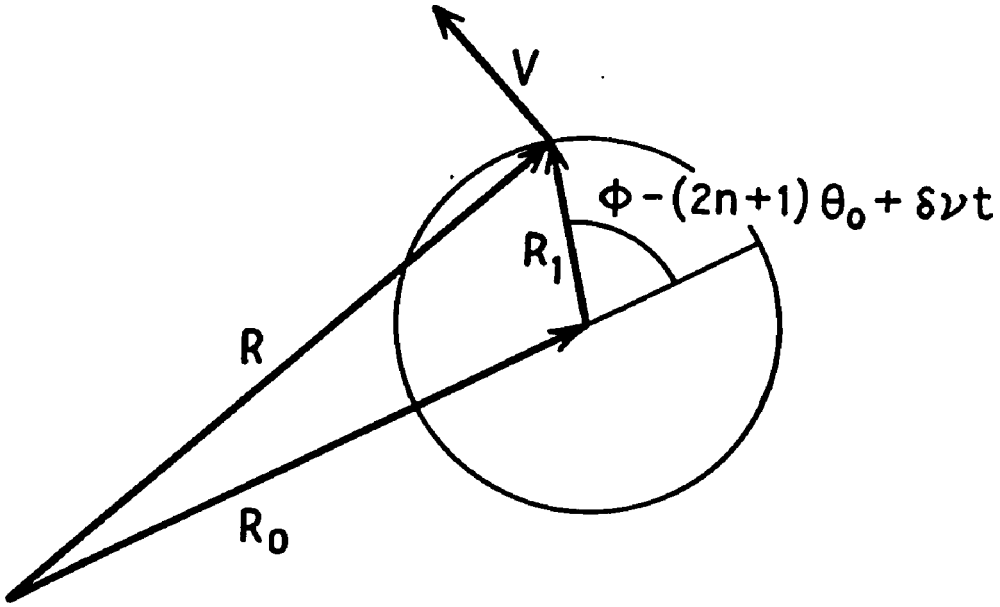

FIG. 9 THE RESONANT RADIUS VECTOR.

$$R_1(\delta\nu t) = r_1(\delta\nu t)\, e^{i(\delta\nu t/2 + \phi - 2n\theta_o)} \tag{2.36}$$

where

$$r_1(\delta\nu t) = \frac{\sin \delta\nu t/2}{\delta\nu t/2}\, \rho_1\omega_c t \ . \tag{2.37}$$

The zeros of $r_1(\delta\nu t)$ occur when $\delta\nu t/2 = m\pi$, where $m = 1,2,\ldots$ (Fig. 10(b)). Since for ions experiencing the RF field for a total time T we have $\omega_c T = 2\pi N$, where N is the total number of cyclotron revolutions, and since $\nu \cong (2n + 1)\omega_c$, the first zero of $r_1(\delta\nu T)$ is given by

$$\frac{\delta\nu}{\nu} = \frac{1}{(2n + 1)N} \ : \tag{2.38}$$

This is the characteristic width of the resonant change in $r_1(\delta\nu T)$, and it will establish the characteristic width of the detection processes described later in this section. In this experiment, $N \tilde{=} 10^4$ and $n = 5$ were generally used resulting in $\delta\nu/\nu \tilde{=} 9$ ppm. Since the angle between $R_1(\delta\nu T)$ and $R_1(0)$ is $\delta\nu T/2$, $R_1(\delta\nu T)$ appears to move along the heavy solid line shown in Fig. 10(a) as the applied RF frequency moves $\delta\nu$ off resonance.

Finally, let us consider the manner in which $R_1(\delta\nu T)$ goes from $R_1(0) = 0$ when the RF field is first applied to its final value $R_1(\delta\nu T)$. The time dependent part of $R_1(\delta\nu T)$ is given from Eq. (2.35) by

$$\rho_1\omega_c T\, \frac{\sin \delta\nu T/2\ e^{i\delta\nu T/2}}{\delta\nu T/2} = \frac{\rho_1\omega_c}{\delta\nu}\,(e^{i\delta\nu T} - 1) \ .$$

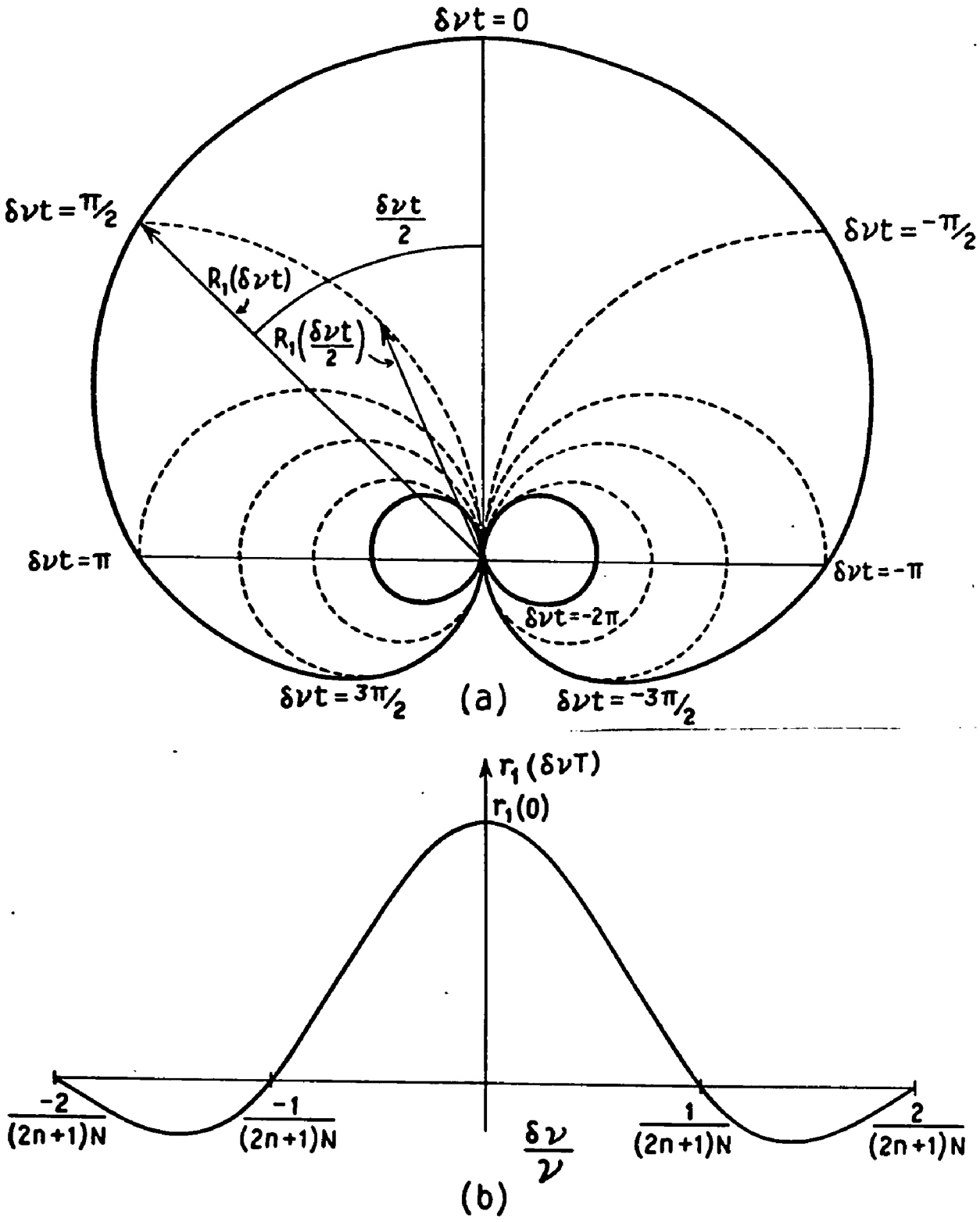

FIG. 10 THE RESONANT CHANGE IN RADIUS.

(a) THE DOTTED LINES SHOW THE APPARENT MOTION OF THE RESONANT VECTOR.

(b) THE MAGNITUDE OF THE RESONANT COMPONENT AS A FUNCTION OF $\delta\nu$.

This describes a circle of radius $\omega_c\rho_1/\delta\nu = 2\pi N\rho_1/\delta\nu T$ centered on the x-axis at $-\omega_c\rho_1/\delta\nu = -2\pi N\rho_1/\delta\nu T$, and passing through the origin at $t = 0$. Thus, as t increases from 0 to T, R_1 appears to move along a circular trajectory as indicated by the dotted lines shown in Fig. (10(a)). Of particular interest is the case $\delta\nu T/2 = \pi$, where R_1 first increases and then decreases, finally returning to $R_1(\delta\nu T) = 0$. This illustrates how an ion slightly off of resonance first experiences a resonant increase in r_1, but then as its phase with respect to the RF field shifts, r_1 begins to decrease and finally $r_1 = 0$ and there is no net change in radius.

There are no experimental restrictions on Θ_o and ϕ, and they are essentially random. Thus, it is convenient to leave the idea of one ion, and consider an ensemble of ions spread over all possible values of Θ_o with any value being equally likely. This makes the value of ϕ insignificant since we are only interested in what happens after a large number of revolutions, and we can always imagine our sample being rotated through a fraction of a revolution to establish the appropriate ϕ.

For fixed initial conditions with only Θ_o and ϕ being allowed to vary, $r_1(\delta\nu T)$ is constant and the locus of all of the vectors $R_1(\delta\nu T)$ is a circle of radius $r_1(\delta\nu T)$ about the tip of R_o (see Fig. 11(a)).

Depending on their phase, some ions will move to larger radii, some will move to smaller radii, and others will not change at all. The result will be a spreading of the initial radius r_o into a band of radii from $r_o - r_1$ to $r_o + r_1$. An insight into what is happening may be had by considering a large ensemble of ions uniformly distributed in

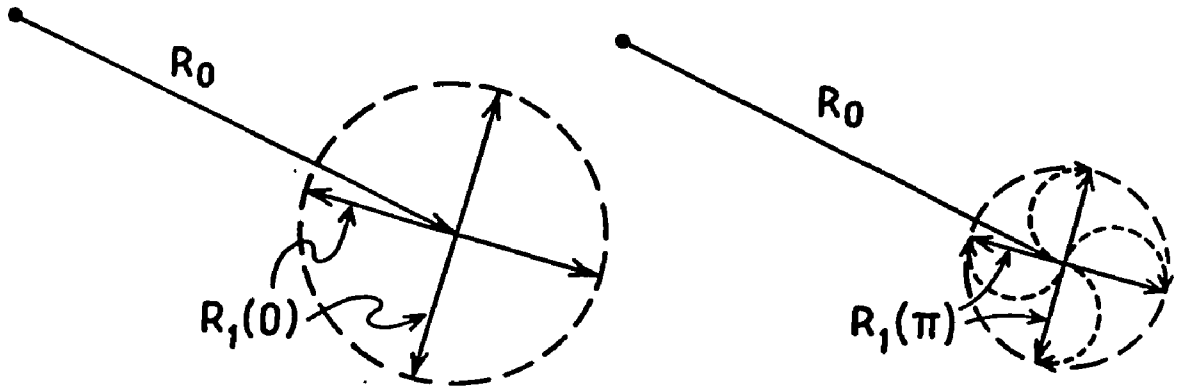

(a)

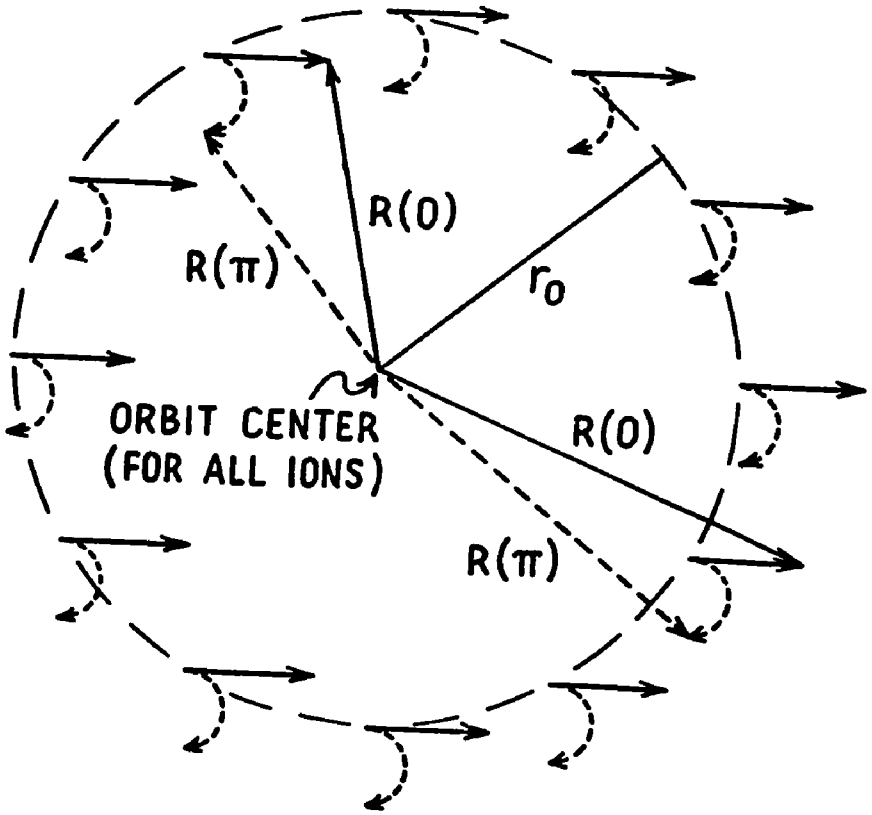

(b)

FIG. 11 ION MOTION NEAR RESONANCE. (a) FOR VARIOUS VALUES OF THE RF PHASE. (b) FOR VARIOUS VALUES OF THE ION'S PHASE.

θ_o with $\nu \cong \omega_c$ (n = 0). Figure 11(b) shows the apparent motion of the ions if a strobed snapshot is taken of the ions with a camera operating once every cyclotron revolution. The small straight arrows show the motion for $\delta\nu t = 0$, and the small curved arrows show the motion for $\delta\nu t/2 = \pi/2$.

RF Lineshape

There are two ways in which the resonant change in radius may be directly used to detect resonance: First, by observing ions which move to either a larger or a smaller radius as a function of applied RF frequency ν. These processes will be referred to as outward and inward resonances, respectively. Second, by observing the number of ions at the initial beam radius as a function of ν. This will be referred to as a removal resonance.

Let us assume that we have a detector set to detect only those ions which reach a radius greater than $r_o + \Delta R$ as is shown in Fig. 12(a). A bunch of ions which is randomly distributed in phase is injected into the well and an RF field at a fixed frequency ν is applied for a total time T. The ions are then ejected from the well and those reaching the detector are counted. Then, another bunch is injected and the process is repeated using another value of the applied frequency ν. Recall that the detector is located outside the trapping region so that the ions complete their resonant motion before being ejected and detected.

If the ions experience the RF field for a total time T, the magnitude of $r_1(\delta\nu T)$ is given from Eq. (2.37) as

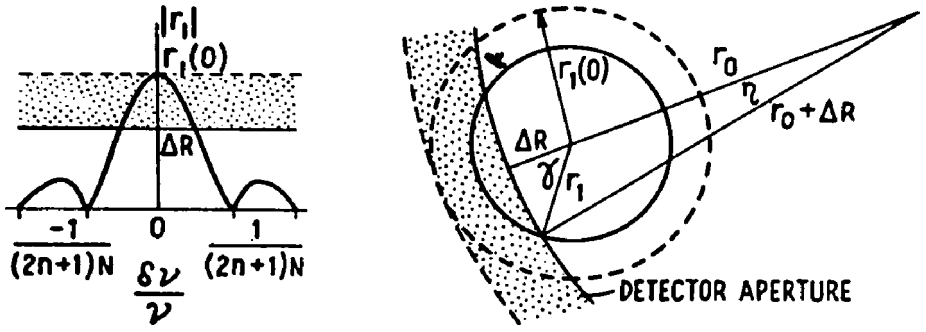

A. OUTWARD RESONANCE

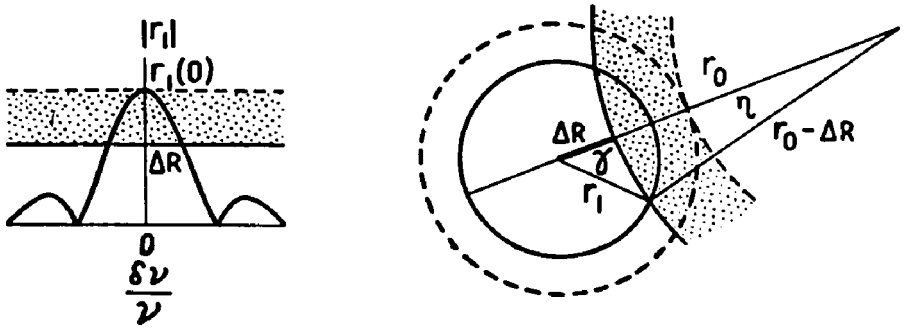

B. INWARD RESONANCE

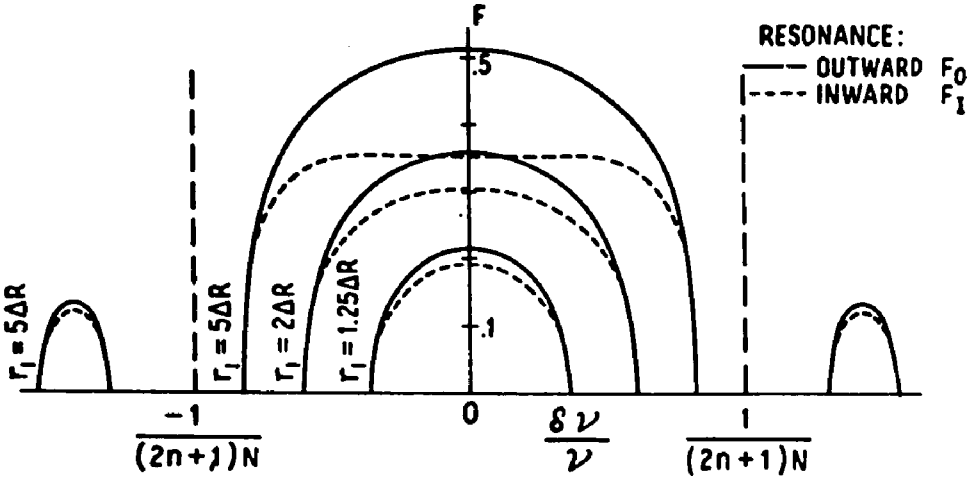

C. LINE SHAPE

FIG. 12 INWARD AND OUTWARD RESONANCE.

(COMPARE FIG. 10(b))

$$r_1(\delta\nu) = \frac{\sin(\delta\nu T/2)}{\delta\nu T/2}\ \rho_1\omega_c T \quad . \tag{2.39}$$

It can be seen from Fig. 12(a) that the fraction of the ions reaching the detector is characterized by the angle $\gamma(\delta\nu)$ between r_o and the intersection of $r_1(\delta\nu)$ and the radius of the detector aperture. From the geometry of the figure, we can write

$$r_1(\delta\nu)\sin\gamma = (r_o + \Delta R)\sin\eta \quad \text{and} \quad r_1(\delta\nu)\cos\gamma = (r_o + \Delta R)\cos\eta - r_o \quad .$$

Eliminating η and solving for $\cos\gamma$ we have

$$\cos\gamma = \frac{\Delta R^2 - r_1^2(\delta\nu) + 2r_o\Delta R}{2r_o r_1(\delta\nu)} \quad .$$

Thus if we define $F_o(\delta\nu) = \gamma(\delta\nu)/\pi$ as the fraction of the ions reaching the detector then

$$F_o(\delta\nu) = \frac{1}{\pi}\cos^{-1}\frac{\Delta R^2 - r_1^2(\delta\nu) + 2r_o\Delta R}{2r_o r_1(\delta\nu)} \quad . \tag{2.40}$$

F_o is plotted for several values of ΔR in Fig. 12(c) using the typical condition $r_1(0) = 0.1\ r_o$.

Those ions reaching the detector have values of $r_1(\delta\nu) > \Delta R$ as indicated in Fig. 12(a), (but not all ions with $r_1(\delta\nu) > \Delta R$ reach the detector). Thus it can be seen that if $\Delta R < 0.21\ r_1(0)$, then sidepeaks will show up on either side of the main resonance. These peaks

correspond to ions that have spiraled first away from the initial radius and then back, and finally away again.

A similar procedure may be carried out for an inward resonance where only those ions reaching a radius less than $r_o - \Delta R$ are detected, as is shown in Fig. 12(b). Defining $F_I(\delta\nu)$ as that fraction of ions reaching the detector, the result is

$$F_I(\delta\nu) = \frac{1}{\pi} \cos^{-1} \frac{-\Delta R^2 + 2r_o\Delta R + r_1^2(\delta\nu)}{2r_o r_1(\delta\nu)} \quad . \tag{2.41}$$

Some typical values of F_I are shown as dashed lines in Fig. 12(c).

It should be noted that in both of these processes that there is no upper limit set on the detection radius, whereas at least in the present apparatus there is an upper limit set by the finite size of the detector window. This must be accounted for by not allowing $r_1(0)$ to become too large. In the present work, this set an upper limit on $r_1(0)$ of $r_1(0) \cong 2\Delta R$ with $\Delta R = 4.0$ mm.

Another limit on the detector aperture is the systematic shifts in the time-average magnetic field experienced by the ions as they change radius as discussed in Section 2.4. In order to evaluate these shifts it is necessary to know the final radius of the ion reasonably well. This generally requires a limit on the detector aperture of only a few millimeters.

The removal resonance may be discussed in terms of the results for the inward and outward resonances. If we consider a detector aperture of width ΔR, where $\Delta R = \Delta R_I + \Delta R_O$, placed symmetrically across

the initial radius as is shown in Fig. 13(a), then the fraction of ions reaching the detector in a removal resonance, $F_R(\delta\nu)$, is given by

$$F_R(\delta\nu) = 1 - F_I(\delta\nu) - F_O(\delta\nu) \quad .$$

Substituting from Eqs. (2.40) and (2.41) this becomes

$$F_R(\delta\nu) = 1 - \frac{1}{\pi}\cos^{-1}\frac{-\Delta R_I^2 + 2r_o\Delta R_I + r_1(\delta\nu)^2}{2r_o r_1(\delta\nu)} - \frac{1}{\pi}\cos^{-1}\frac{-\Delta R_O^2 - r_1(\delta\nu)^2 + 2r_o\Delta R_O}{2r_o r_1(\delta\nu)} \quad . \tag{2.42}$$

The function F_R is graphed in Fig. 13(b) for the typical experimental values of $r_o = 4.0$ cm, and $\Delta R = 2.0$ mm, and is the same for any values in the same ratio. So long as r_1 and ΔR are relatively small compared to r_o, F_R is largely determined by the ratio $r_1{:}\Delta R$. Again, it may be seen that if we allow $\Delta R < 0.42\ r_1(0)$, side peaks will begin to show on either side of the resonance.

The equations given for F_R above do not depend on the detector being centered. If the detector is not centered, F_R may be evaluated by using the appropriate values for ΔR_I and ΔR_O. Since both F_I and F_O are symmetric about the center frequency, F_R will also be symmetric. That is, there will be no shift in the center or symmetry of the resonance line due to the detector being off-center as long as the initial ($r_1 = 0$) beam falls within the aperture. This may be further extended to show that nonuniformities in the detector response and spreading in the radii of the

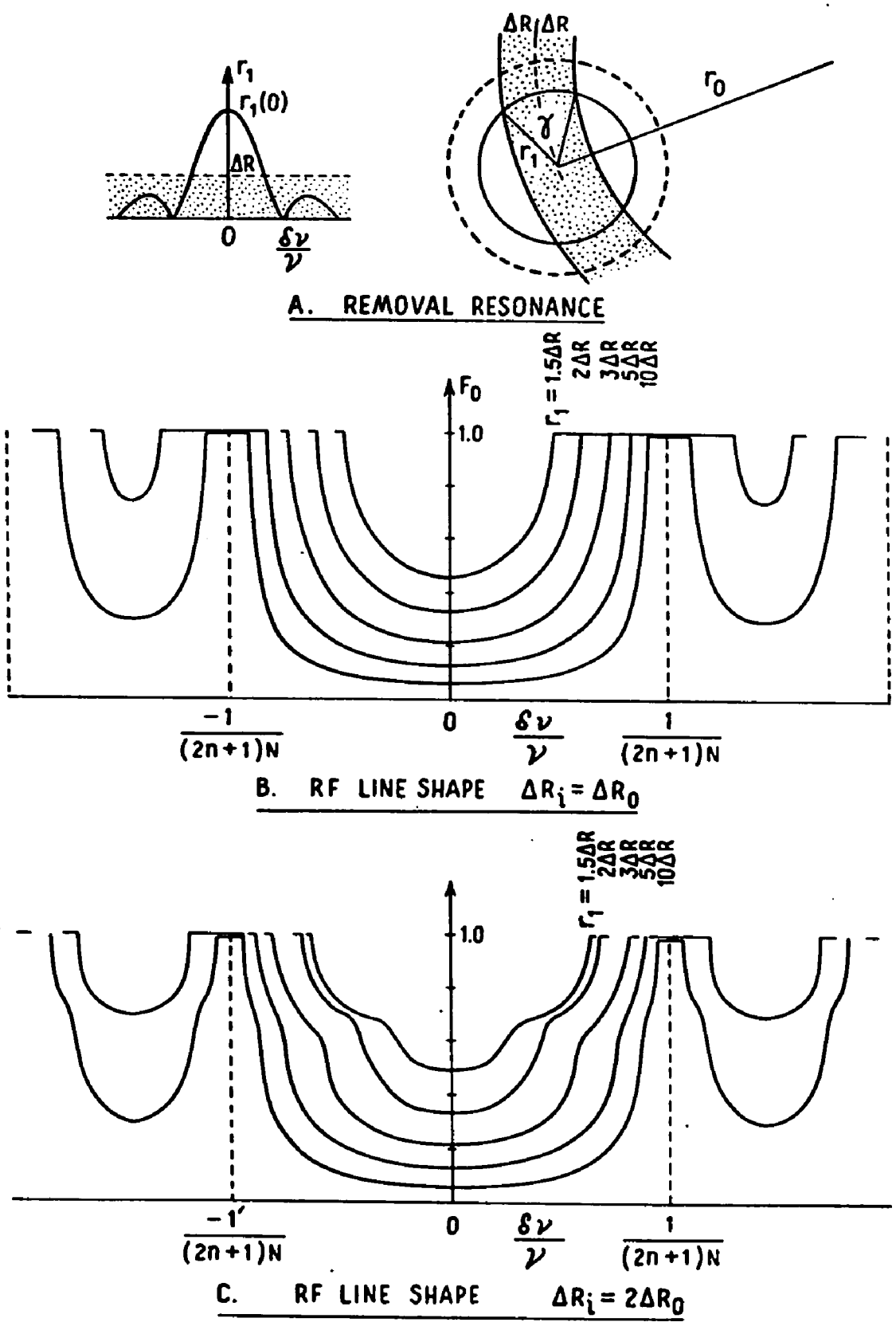

FIG. 13 REMOVAL RESONANCE.

(COMPARE FIG. 10(b))

trapped ions so long as it is less than ΔR will not affect the resonance symmetry or center. Figure 13(c) shows F_R for the same aperture as used in Fig. 13(b) except that the gap is off-center with $\Delta R_I = 1.33$ mm and $\Delta R_O = 0.67$ mm.

Observed Lineshape

The lineshape theory developed thus far has been based on the assumption of a homogeneous magnetic field. What happens if the theory is applied to the ions in our well-shaped field which experience time-average field which differ over a range ΔB? If we let $F(\nu - (2n + 1)\omega_c) = F(\delta\nu)$ represent the RF lineshape functions $F_I(\delta\nu)$, $F_O(\delta\nu)$, or $F_R(\delta\nu)$ discussed in the previous section with characteristic width $1/(2n + 1)N$, then we must make the explicit assumption

$$F(\nu - (2n + 1)[\omega_c]) = [F(\nu - (2n + 1)\omega_c)] \quad . \tag{2.43}$$

That is, we must make the assumption that we can replace the ω_c with its time-average $[\omega_c]$. Let us take $\rho([\omega_c])$ as the density function of the ions in the well with median $[\tilde{\omega}_c]$ and fractional width $\Delta[\omega_c]/[\omega_c]$. Then, the observed lineshape function $f(\nu)$ is given by

$$f(\nu) = \int_0^\infty F(\nu - (2n + 1)[\omega_c])\rho([\omega_c])\, d[\omega_c] \quad . \tag{2.44}$$

The median $\tilde{\nu}$ of this function is given by

$$\int_0^{\tilde{\nu}} f(\nu)\, d\nu = \frac{1}{2} \int_0^\infty f(\nu)\, d\nu \quad , \tag{2.45}$$

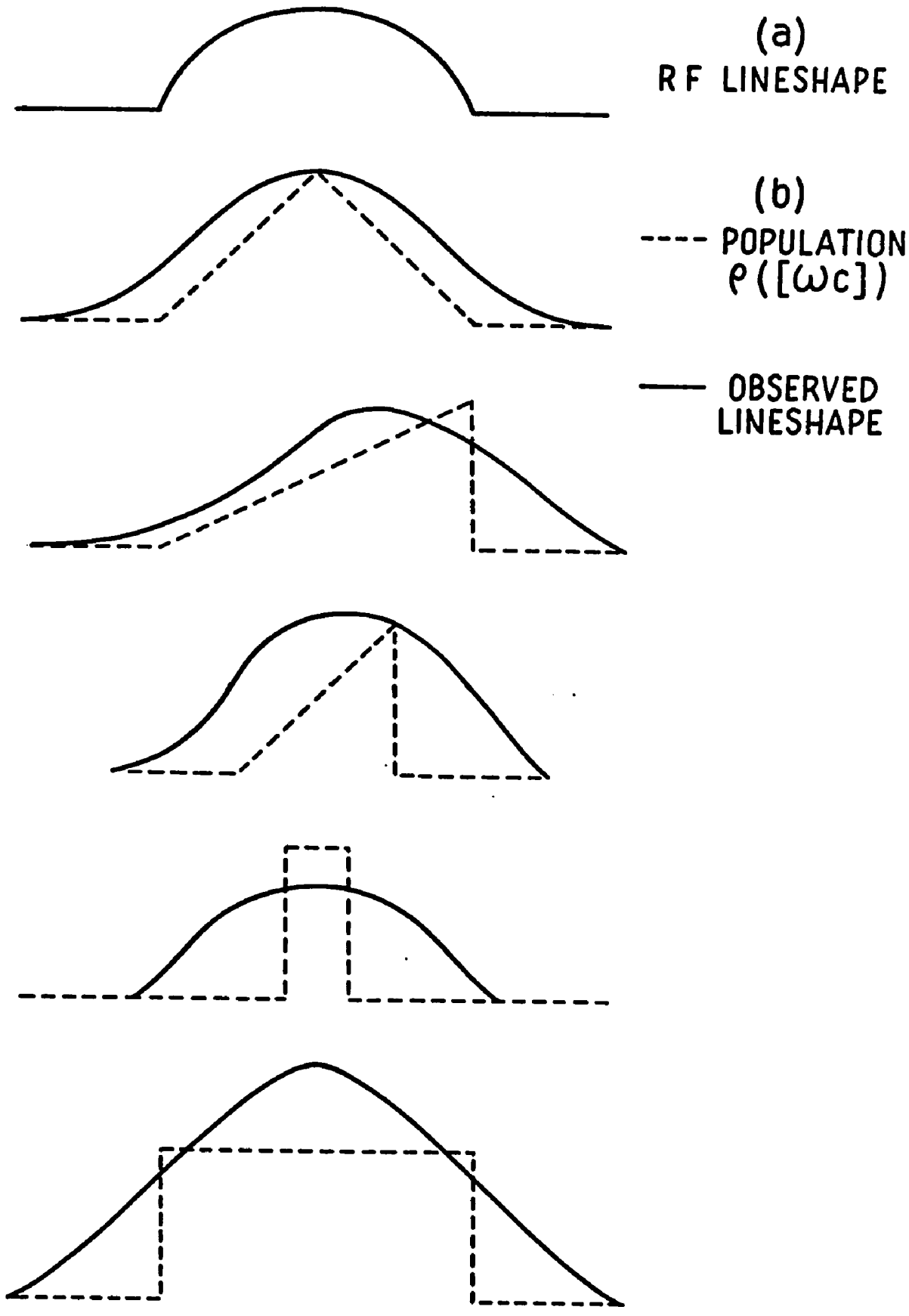

FIG. 14 EXPECTED LINESHAPE $f(\nu)$ FOR THE APPROXIMATE RF LINESHAPE $F(\nu)$ SHOWN IN (a) AND VARIOUS POPULATION DISTRIBUTIONS (SHOWN DOTTED).

and the characteristic width is defined as $\Delta\nu$ (FWHM). If the width of the density function is much greater than the width of the RF lineshape, $\Delta[\omega_c]/[\omega_c] >> 1/(2n + 1)N$, then $f(\nu) \cong \rho(\nu/(2n + 1))$ and the lineshape is dominated by the density function. But, the relative amplitude of the line will be decreased since only a fraction of the ions in the well will be resonated at any given RF frequency. If $\Delta[\omega_c]/[\omega_c] << 1/(2n + 1)N$, then $f(\nu) \cong F(\nu)$ and the observed lineshape is the RF lineshape. Several intermediate cases are illustrated in Fig. 14.

We now make the explicit and important assertion that

$$\frac{\tilde{\nu}}{2n + 1} \cong [\tilde{\omega}_c] \quad . \tag{2.46}$$

If $\rho([\omega_c])$ is symmetric about $[\tilde{\omega}_c]$ the equality holds. In the two limits cited in the previous paragraph, the approximation is clearly excellent, approaching equality. For the intermediate case $\Delta[\omega_c]/[\omega_c] \cong 1/(2n + 1)N$, the approximation holds to better than 0.01 $\Delta\nu$ for any reasonable $\rho([\omega_c])$ including those shown in Fig. 14.

Changes in the Effective RF Field with Harmonic Order

One point of experimental concern is the equivalent amplitude of the RF voltage U_o necessary to hold the resonant change in radius r_1 constant as the harmonic order n is increased. At resonance ($\delta\nu = 0$) and with $\omega_c T = 2\pi N$, r_1 is given from Eq. (2.39) by

$$r_1 = 2\pi N\rho_1 = \frac{2eU_o}{\pi M R_c \omega_c^2} \left(\frac{r_o}{R_c}\right)^{2n} \quad . \tag{2.47}$$

The only quantity which depends on the harmonic order of the resonance is the index n. Thus if we desire to keep r_1 constant as the harmonic order of the resonance is changed, we require

$$U_o \propto \left(\frac{r_o}{R_c}\right)^{-2n} , \tag{2.48}$$

where r_o/R_c must be less than unity and is 0.75 in the present apparatus. This can impose severe requirements on the RF source at higher harmonics as is shown in Fig. 15. In practice, it is desired to make r_o as large as possible in order to use higher harmonics at reasonable RF voltages while it is also desirable to keep r_o from too nearly approaching R_c because of the approximation of the gap between the C's as infinitesimal made in Appendix I and because of stray electric fields which might be present near the surfaces.

In the present experiment, using the 11th harmonic, n = 5, results in a substantial improvement in the linewidth with only a moderate increase in the applied RF voltage. However, an identical improvement in the linewidth by going to the 121st harmonic (n = 60) would require increasing the RF level by 16 orders of magnitude. Thus it is obvious that any substantial decrease in the linewidth by going to higher harmonics would require that r_o/R_c be nearer to unity.

If we hold U_o constant in Eq. (2.47) above, we can form the differential relationship

$$\frac{dr_1}{r_1} = 2n \frac{dr_o}{r_o} . \tag{2.49}$$

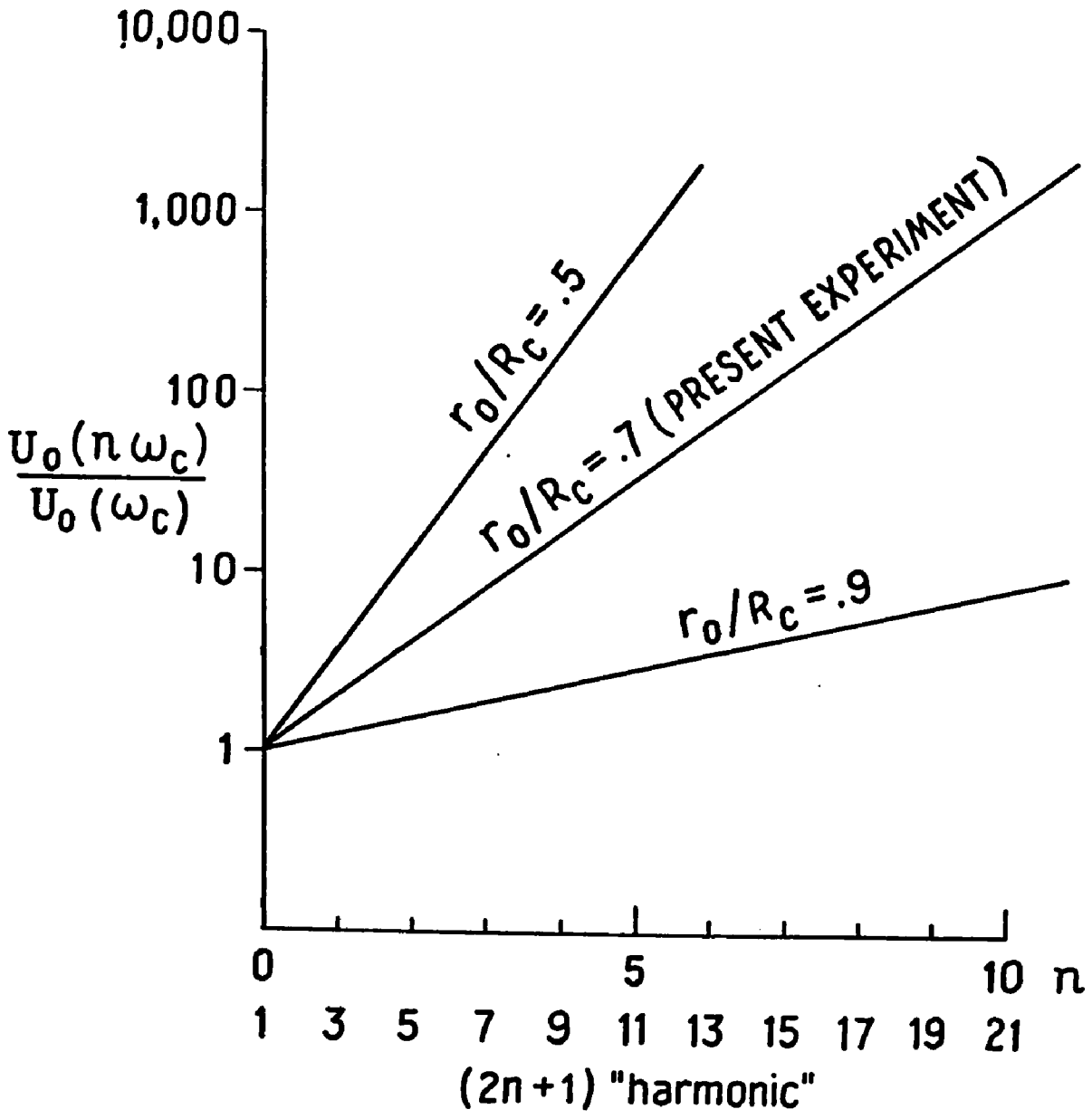

FIG. 15 RF AMPLITUDE REQUIRED TO MAINTAIN A CONSTANT RESONANT CHANGE IN RADIUS VS. HARMONIC ORDER.

The differential dr_1/r_1 is a measure of the variation in the effective RF field. Thus as the harmonic order increases, it is increasingly difficult to maintain limits on r_o such that dr_1/r_1 remains small. However, the original equations of motion were solved on the premise that r_o was constant, and that only relatively small variations in r_o would be allowed. Note that this variation is not present at all when using the fundamental frequency ($n = 0$).

Alignment of the Orbit Center

In the derivation of the RF resonance theory, it has been assumed that the orbit center of the ions is the mechanical axis of the C's. Experimentally, this not necessarily the case. In order to understand the effect of a small misalignment of the orbit center, we will first review the resonant motion of an ion when the applied RF frequency is an odd harmonic of the cyclotron frequency.

Consider the special case of an ion exactly on resonance with $\nu = 3\omega_c$, and $\theta_o = \phi = 0$ as is shown in Fig. 16. The three dotted lines in the figure indicate the position of the ion each time the RF field passes through zero. In the sectors nearest the gaps, the ion experiences an essentially decelerating field while the contributions in the other four sectors can be seen to cancel one another. Thus the ion will slowly spiral inward. Similarly, an ion with $\theta_o = \pi$ experiences an accelerating field in the sectors near the gaps and spirals outward.

Experimentally, the orbit center cannot be expected to fall exactly on the mechanical center of the C's. Consider an ion whose

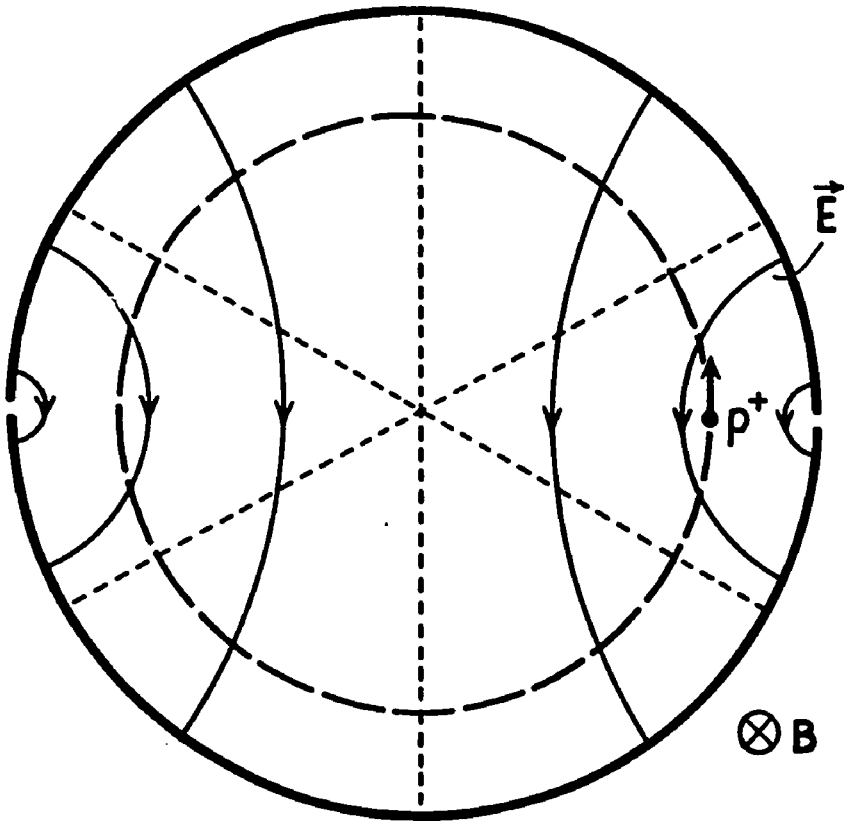

FIG. 16 AN ION MOVING IN PHASE WITH THE RF FIELD AT THE THIRD HARMONIC. THE DOTTED LINES INDICATE POINTS ON THE ORBIT WHERE THE RF FIELD IS AT ZERO.

orbit center is displaced a small amount along the x-axis to the right. The rate of change of the effective field is given to a first approximation by

$$\frac{dr_1}{r_1} = 2n \frac{dr_o}{r_o} \quad . \tag{2.49}$$

Thus the effective electric field will increase in the sector near the right gap and decrease in the sector near the left gap. The ion at $\theta_o = \pi$ discussed above will gain velocity at the right gap which in turn causes a slight shift in the orbit center to the left. At the left gap the ion gains somewhat less velocity causing its orbit center to move back to the right by a lesser amount. Thus there will be a net drift to the left which will damp out as the ion nears the center. Had the ion started with $\theta_o = 0$, just the opposite would happen and the ion drifts off center. These effects are more pronounced at higher harmonics because of the dependence of Eq. (2.49) on n, but we would not expect them at all at the fundamental since n = 0.

Normally, resonance is not expected at even harmonics of the cyclotron frequency. This may be simply seen by observing that if the orbit is cut up into sectors for an even harmonic as was done for the third harmonic above, the sectors nearest the gaps also cancel leaving no net effect. However, if the orbit center is off the mechanical center, the contributions near each gap will not cancel and a resonance can occur. This may happen with relative ease at higher harmonics since for example at the 10th harmonic, with $dr_o = 2$ mm and $r_o = 4.0$ cm, we have $dr_1/r_1 \cong 1/2$.

The overall picture is not quite this simple because one must also consider the motion of the orbit center about the field center (Appendix III), and the field center need not be either the orbit center or the mechanical center. This may be all summed up by stating that even harmonics have been observed at RF levels which were higher than those used for the corresponding nearest odd harmonics.

2.4 The Effect of a Change in Radius on the Time-Average Field

When an ion undergoes a resonant change in radius, three systematic shifts occur. First, the ion experiences a change in the magnetic field, $\partial B_z/\partial r \neq 0$. Second, the effective level of the ion in the well changes due to the resonant change in the ions radius. Third, there is also a small change in $\gamma = (1 - v^2/c^2)^{-1/2}$ which is given by

$$\frac{d\gamma}{\gamma} = \frac{dv}{v} = \frac{dr}{r} .$$

Since $\gamma - 1 < 0.5$ ppm in the present experiment, this change is insignificant. Theoretical predictions of the first two effects are made here, and these predictions are verified in Section 5.1.

The Change in the Magnetic Field with Radius

In order to determine the change in magnetic field with radius, we must evaluate $\partial B/\partial r$. This is accomplished by approximating the magnetic well shape with an analytic function known as the Garren well (Garren et al., 1958) which is discussed in Appendix II. The axial well shape is then approximated to first order in r by

$$B_z = B_o \left\{ 1 + \alpha \left(1 + \frac{1}{2} \frac{2\pi r}{L} \right) \cos \frac{2\pi z}{L} \right\} . \qquad \text{(II.2)}$$

When this function is fitted to the well used in the present experiment (see Appendix II), we get $B_o \simeq 776$ G, $\alpha \simeq 160$ ppm, and $L \simeq 80$ cm. Taking the derivative of Eq. (II.2) with respect to r, we have

$$\frac{1}{B_o} \frac{\partial B}{\partial r} = \frac{1}{B_o} \frac{\partial B_z}{\partial r} \cong - \alpha \frac{2\pi^2 r}{L^2} \cos \frac{2\pi z}{L} , \qquad \text{(II.4)}$$

to excellent approximation. Using the characteristic values given above along with r = 4.04 cm, this becomes

$$\frac{1}{B_o} \frac{\partial B}{\partial r} \cong -2.0 \cos \frac{2\pi z}{L} \text{ ppm/cm} . \qquad (2.50)$$

Thus we have a maximum shift of about 2 ppm/cm but it is a maximum at the bottom of the well where, for other reasons, it is desirable to work. For a typical inward or outward resonance with $\Delta R = 4.0$ mm this produces a maximum shift of about 0.8 ppm, while for a removal resonance with $\Delta R = 1.0$ mm it is only 0.2 ppm and negligible.

The Effect of a Change in Radius on the Axial Motion

To evaluate the effect of changing the transverse energy $T_\perp = 1/2\ Mv_\perp^2 \cong 1/2 Mv^2$ on the axial motion of the ion in the well, we will introduce another adiabatic invariant known as the longitudinal invariant (Chandrasekhar, p. 63)

$$J_z = \oint p_z \, dz . \qquad (2.51)$$

Since the axial motion is completely nonrelativistic, we can set $p_z = Mv_z$, substitute for v_z from Eq. (2.13), and write

$$J_z = Mv_\perp \oint \sqrt{\frac{B(z_1) - B(z)}{B(z_o)}}\, dz \quad . \tag{2.52}$$

Using the Garren well field (Eq. II.1) this becomes

$$J_z = \frac{Mv_\perp}{\sqrt{B(z_o)}} 4\sqrt{\alpha I_o} \int_0^{z_o} \sqrt{\cos\frac{2\pi z}{L} - \cos\frac{2\pi z_o}{L}}\, dz \quad ,$$

where z_o is the endpoint of the motion. This is a rigorous adiabatic invariant for the entire well, and can be used to find a new endpoint for the motion with changing $v_\perp$. This assumes that any changes in $v_\perp$ are slow. In the present experiment $v_\perp$ changes by less than 10 percent in 10^4 revolutions.

To perform the integration, we expand the cosine terms as infinite series and keep only the terms through second order. Thus we have

$$J_z \cong Mv_\perp \sqrt{\frac{\alpha I_o}{B(z_o)}} \int_0^{z_o} \sqrt{\frac{1}{2}\left(\frac{2\pi z_o}{L}\right)^2 - \frac{1}{2}\left(\frac{2\pi z}{L}\right)^2}\, dz \quad , \tag{2.53}$$

or

$$J_z \cong \pi M \sqrt{\frac{\alpha I_o}{8B(z_o)}}\, v_\perp z_o^2 \tag{2.54}$$

to good approximation for the bottom quarter of the well (i.e., $\Delta B = \{B(z_o) - B(0)\} < \alpha/2 = 80$ ppm).

Thus we can write

$$v_\perp z_o^2 \cong \text{constant} \tag{2.55}$$

for this portion of the well since all of the other factors remain constant to an accuracy far better than the approximations already made.

For the Garren well we have

$$\Delta B = B(z_o) - B(0) \cong \alpha B_o \left(1 - \cos \frac{2\pi z_o}{L}\right) . \tag{2.56}$$

By expanding the cosine function and keeping only the first term as before, this becomes

$$\Delta B \cong \frac{1}{2} B_o \left(\frac{2\pi z_o}{L}\right)^2 .$$

Combining this with Eq. (2.55) gives us the result

$$v_\perp \Delta B(z_o) \cong \text{constant} . \tag{2.57}$$

Thus we may write the differential relation

$$\frac{\delta v_\perp}{v_\perp} = - \frac{\delta(\Delta B)}{\Delta B} . \tag{2.58}$$

But, since $\delta v_\perp / v_\perp = \delta r / r_o$ we have finally

$$\frac{\delta r}{r_o} = - \frac{\delta(\Delta B)}{\Delta B} . \tag{2.59}$$

Thus we can see that the level of the ion in the well changes linearly in proportion to the change in radius. The fractional error in this approximation is less than 10 percent for $z_o < L/6$ which corresponds to the lower 1/4 of the Garren well ($\Delta B(z_o) < 80$ ppm). Typically, $\Delta B(z_o) < 50$ ppm, and $\delta r/r_o = 0.10$ for a typical inward or outward resonance, so that the worst case change in the level of an ion in the well is 5 ppm. However, this is reduced by one-half in the normal time-averaging of the magnetic field, and by another one-half since the average field seen by the ion is the mean of the initial and final values. Thus we have a worse case effect for the present experiment of only about 1.25 ppm. For removal resonances where the change in radius is only 2.5 percent the effect is completely negligible.

Both of these effects point up the need to know the change in the ions radius reasonably well, and particularly to keep the detector aperture less than ΔR for inward and outward resonances. These effects produce only a (negligible) broadening of the removal resonance line.

2.5 Comparison of the Various Techniques for Observing Resonance

In order to make a clear comparison of the techniques for observing resonance, let us first review the pertinent details of the resonance process. First, a bunch of ions is injected into the well. An RF field at a fixed frequency is then applied across their orbit for a fixed period of time T. Finally, the ions are ejected and move on to the detector where those within a given radial aperture are detected. A new bunch of ions is then injected and the process is repeated at another

frequency. Resonance is observed as a change in counting rate as a function of frequency. The population of the well can be limited by a mechanical flag which limits the amplitude of the axial motion of the ions in the well. This flag is on the source side of the well and the ions are given enough pitch when they enter from the source system to pass over it, but once the ions are confined to the well their pitch is small enough that they must strike the flag if their axial motion carries them that far.

Normally, in order to make a measurement of μ_p/μ_n, the population of the well is first determined and then the RF resonance lineshape corresponding to the entire population is obtained. It will generally be assumed that the RF linewidth is slightly greater than the width of the population distribution as this is experimentally convenient (see Section 4.5).

It is desirable to keep the resonant change in radius defined to within 1 to 2 mm and as small as possible for several reasons. First, a small change in radius is consistent with the approximation that the radius was constant which was made in Section 2.3 in order to integrate the equations of motion. This problem is compounded when the frequency of the applied RF field is at an odd harmonic of the cyclotron frequency (Eq. (2.49)). Second, from Section 2.4 there are several shifts in the time-average field experienced by the ion which accompanies a change in radius. Third, the applied RF fields are kept to a minimum and result in only small changes in the initial velocity (energy) of the ions.

Removal Resonances vs. Inward or Outward Resonances

Because of the conditions indicated above, it is generally preferable to use the removal resonance process over the inward or outward resonances. The latter by their very nature require a larger change in radius. Since the change in radius must also be well-defined the detector aperture must be small (~ 2 mm). Thus for an inward or outward resonance with a well-defined radial aperture ($r_1 \sim 1.25\ \Delta R$; Fig. 12(c)), a relatively narrow resonance line would be produced, but only a small fraction (~ 20 percent) of the ions in the well contribute to the resonance line. The removal resonance has the further advantage that the average trapping rate is immediately obvious from the shoulders of the resonance, and thus the fraction of the ions in the well contributing to the resonance line can be immediately estimated. For an inward or outward resonance this can only be determined by separately monitoring the trapping rate.

Other Ways of Observing Resonance

There are several other techniques for observing resonance which might be particularly useful in measurements of μ_p/μ_n where both the cyclotron frequency and corresponding spin frequency must be determined.

The change in the amplitude of the axial motion of the ions which accompanies the resonant change in the transverse velocity (Section 2.4), can also be used to observe a resonance condition. Consider a bunch of ions trapped in the well with the flag used to limit their axial motion, but with the detector set to a somewhat wider aperture so that

all of the ions are detected on ejection in spite of small changes in their radius. The resonant motion of the ions in the well must still satisfy the longitudinal invariant discussed in Section 2.4, and those ions which move to a smaller radius will also move to a higher level in the well (Eq. (2.59)). However, those ions at a level in the well just below the flag would then strike the flag and be lost. Thus there would still be a resonant decrease in the counting rate which would correspond to those ions which are at a level in the well just below the flag.

In the typical measurement of μ_p/μ_n, the population distribution of all of the ions in the well and the corresponding cyclotron resonance line are determined. This process can be modified by first applying the RF field and then looking at the population distribution of the resonant ions. Initially, a crude inward or outward resonance line would be determined, and then the RF frequency returned to a value within the resonance line and left constant. The population distribution could then be determined for the resonant ions reaching the detector. This population should have a characteristic width which is approximately equal to the linewidth of the RF resonance since the ions reaching the detector must have a time-average cyclotron frequency which is within one linewidth of the applied frequency. Thus, the frequency of the applied RF field is fixed and the corresponding level in the well is clearly defined. This technique allows a narrow resonance process to be established without using the flag to limit the population. It should allow useful systematic studies for a measurement of μ_p/μ_n, but its application in the present experiment has been limited.

The radial electric field shift of the cyclotron frequency can also be used to determine the resonant cyclotron frequency distribution of the ions (after Smith, 1971). Assume that a conductor is placed down the center of the apparatus concentric with the orbit center. If a potential is placed on this conductor, it will introduce a uniform radial electric field in the well region. Then a constant RF frequency is applied to the C's and the radial electric field can be swept in order to observe the resonant lineshape. This technique has the advantage of keeping the applied frequencies and RF amplitudes constant in time, and would result in a further check of the electric field shift. This might prove especially valuable with mass doublet measurements as it would allow both frequencies to remain constant and identical electric field sweeps to be applied to both.

2.6 Determination of Ion Mass Ratios

If two species of ion with slightly different masses M_1 and $M_2 = M_1 + \Delta M$ are trapped in the well at the same time, their observed cyclotron frequencies are given by ω'_{c1} and $\omega'_{c2} = \omega'_{c1} + \Delta\omega_c$ where

$$\omega'_{c1} = \frac{eB}{\gamma_1 M_1 c}\left(1 + \frac{c[E_r]}{v_{\perp 1} B}\right) = \frac{eB}{\gamma_1 M_1 c}\left(1 + \frac{c^2 M_1 [E_r]}{B^2 e\, r_o}\right) \qquad (2.60a)$$

and

$$\omega'_{c2} = \frac{eB}{\gamma_2 M_2 c}\left(1 + \frac{c[E_r]}{v_{\perp 2} B}\right) = \frac{eB}{\gamma_2 M_2 c}\left(1 + \frac{c^2 M_2 [E_r]}{B^2 e\, r_o}\right), \qquad (2.60b)$$

with $[E_r]$ being the time-average radial electric field experienced by the ions as they oscillate in the well.

If the velocities are identical ($v_{\perp 1} = v_{\perp 2}$), then the electric field shifts are identical and $\gamma_1 = \gamma_2$, but there is a small difference in the ion radii due to the mass difference which is given by $\Delta r = r_o \Delta M/M_2$. Because of the radial magnetic field gradient dB/dr (Section 2.4), this slight difference in radius results in a small shift in the mass difference and we have

$$\frac{\Delta M}{M_2} = -\frac{\Delta\omega_c'}{\omega_{c1}'} - \frac{1}{B}\frac{dB}{dr}\Delta r \quad . \tag{2.61}$$

Since $B^{-1}\, dB/dr \cong -2$ ppm/cm (Section 2.4) and $\Delta r = r_o \Delta\omega_c'/\omega_{c1}$ we have

$$\frac{\Delta M}{M_2} = -\frac{\Delta\omega_c'}{\omega_{c1}'}(1 - 8 \text{ ppm}) \quad .$$

This error is negligible at the present level of accuracy, and since the beam system apparently behaves as a velocity filter (Section 3.4) this treatment is probably sufficient.

If, however, we consider that the radial aperture of the annulus might allow the mean radii of the ion species to differ by as much as $\delta r/r_o = 0.01$ (Section 3.6), there are additional shifts which must be considered, and we have

$$\frac{\Delta M}{M_2} = -\frac{\Delta\omega_c'}{\omega_{c2}'} + \frac{c^2 M_1 [E_r]}{B^2 e r_o}\left\{\frac{2\delta r}{r_o} - \frac{\Delta M}{M}\right\} - \frac{1}{B}\frac{dB}{dr}\delta r \quad , \tag{2.62}$$

where $[E_r]$ has been taken as proportional to r_o^{-1}. Taking $B^{-1}\, dB/dr =$ 2 ppm/cm, the shift due to the magnetic field gradient is at most 80 ppb.

A reasonable estimate of the electric field shift is $c^2 M_1 [E_r]/B^2 e r_o$ = 10 ppm. Thus the differential electric field shift can be as large as 200 ppb. This shift is large enough to point out the need for careful consideration of the relative radial positions of the two ions. The effect of this shift could be removed by experimentally adjusting $[E_r]$ to zero by introducing the appropriate potentials while using the extrapolation procedure described for μ_p/μ_n.

In order to determine the experimental values of $\Delta\omega_c'$ you can, in principle, determine the medians $\tilde{\nu}_1$ and $\tilde{\nu}_2$ of the two resonance lineshapes $f(\nu_1)$ and $f(\nu_2)$, and then you have

$$\Delta\omega_c = \frac{\tilde{\nu}_2 - \tilde{\nu}_1}{2n+1} = \frac{\Delta\tilde{\nu}}{2n+1} \quad .$$

However, in order to extract the maximum amount of information from the data, the difference

$$f(\nu_1 + \Delta\nu) - f(\nu_2)$$

is formed. Then $\Delta\nu$ is varied and the difference is fitted to a straight line at zero:

$$f(\nu_1 + \Delta\tilde{\nu}) - f(\nu_2) = 0 \quad . \tag{2.63}$$

This procedure has the advantage that if the two species do not experience identical conditions, then the difference cannot be made exactly zero for any value of $\Delta\nu$ and the residual function is an indicator of this.

2.7 Determination of μ_p'/μ_n

The Observed Value of μ_p/μ_n

The observed value of μ_p/μ_n for an ion of mass M(amu) with the applied RF frequency near the (2n + 1)st harmonic of the cyclotron frequency is given by

$$\left(\frac{\mu_p}{\mu_n}\right)_{\text{observed}} = \frac{[\tilde{\omega}_s]}{\tilde{\nu}/(2n+1)} \frac{M_p}{M} \quad . \tag{2.64}$$

The expectation value of the spin frequency is obtained by first determining the median $\tilde{V}_e$ of the ejection function $N(V_e)$ for the sample, and then using the field maps of the well region to determine $[\tilde{\omega}_s] = [\omega_s(\tilde{V}_e)]$ (Eq. (2.22)). The median value of the observed cyclotron frequency is determined from the RF resonance $[\tilde{\omega}_c] \cong \tilde{\nu}/(2n+1)$ (Eq. (2.46)). The quantities $[\tilde{\omega}_s]$ and $\tilde{\nu}$ may be taken as applying to identical samples only to the extent that the population and cyclotron resonance are drawn from the same sample population, i.e., $\rho([\omega_s]) = \rho(K[\omega_c])$. This might not be true if, for example, ions are scattered out of the well because of the resonance process, as occurs during an inward resonance when ions move upward in the well and those near the flag strike it (Section 5.1).

Extrapolation

As was pointed out in Section 1.2, in the presence of a time-average radial electric field $[E_r]$ the observed cyclotron frequency ω_c' is shifted from the true cyclotron frequency ω_c by an amount given by

$$\omega_c' = \omega_c \left(1 + \frac{c[E_r]}{v_\perp B}\right) . \qquad (1.6')$$

The magnitude of this shift for 475 eV protons in a field of 775 gauss is 4.3 ppm per mV/cm of electric field. Since such small electric fields are impossible to measure directly, they must be assumed to be present and their effect accounted for by an extrapolation procedure. Since $r_o = Mv_\perp c/eB$, Eq. (1.6') may be written as

$$\omega_c' = \omega_c \left(1 + \frac{c^2 M[E_r]}{B^2 e r_o}\right) , \qquad (1.7')$$

where r_o is held constant in the apparatus. Thus, the dependence of μ_p/μ_n on $[E_r]$ may be determined by varying M and linearly extrapolating $[\tilde{\omega}_s]/\{(M/M_p)\ \tilde{\nu}/(2n+1)\}$ as a function of M to M = 0, or by varying B and linearly extrapolating $[\tilde{\omega}_s]/\{\tilde{\nu}/(2n+1)\}$ as a function of B^{-2} to $B^{-2} = 0$.

CHAPTER III. APPARATUS

The apparatus was originally built to demonstrate a new and untried technique, and it has been developed and modified as the application of the technique progressed. The main apparatus (Fig. 17) consists of the solenoid to provide the magnetic field, the main vacuum tank, and the equipment to trap and resonate the ions. In addition, there is an independent source system to provide the ions.

3.1 The Solenoid

The solenoid was designed to provide a magnetic field of about 1 kG. It was constructed using an existing aluminum form and about 2000 lb of copper wire (Fig. 18). The form consists of a 1/2 inch rolled cylinder with 1 inch flanges welded on the ends. It was machined to finished dimensions of 25.25 in dia. by 59.25 in long. The form was then fitted with a bolt-in water jacket to provide a channel for the coolant.

One gap in the windings is required so that the beam can be injected perpendicular to the field lines. In order to preserve the symmetry of the coil configuration, the coil was wound with two gaps symmetrically placed from the ends. The solenoid was wound with the two end sections 27.25 cm long, a center section 89.5 cm long and 3.0 cm gaps in between. The center section consists of six layers while the outer sections have two additional layers to help correct for the rapid fall-off in field of the relatively short solenoid. The

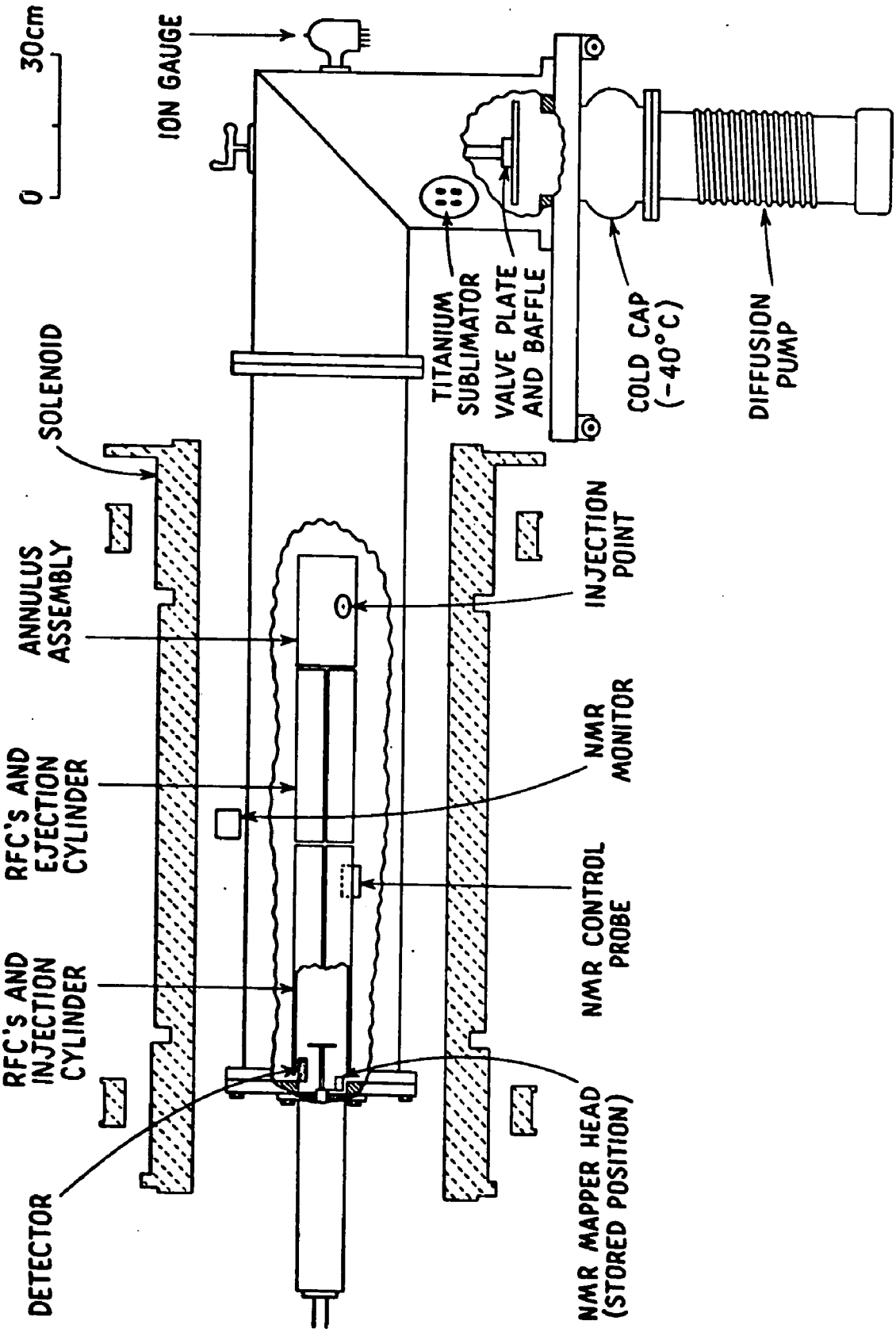

FIG. 17 THE MAIN APPARATUS.

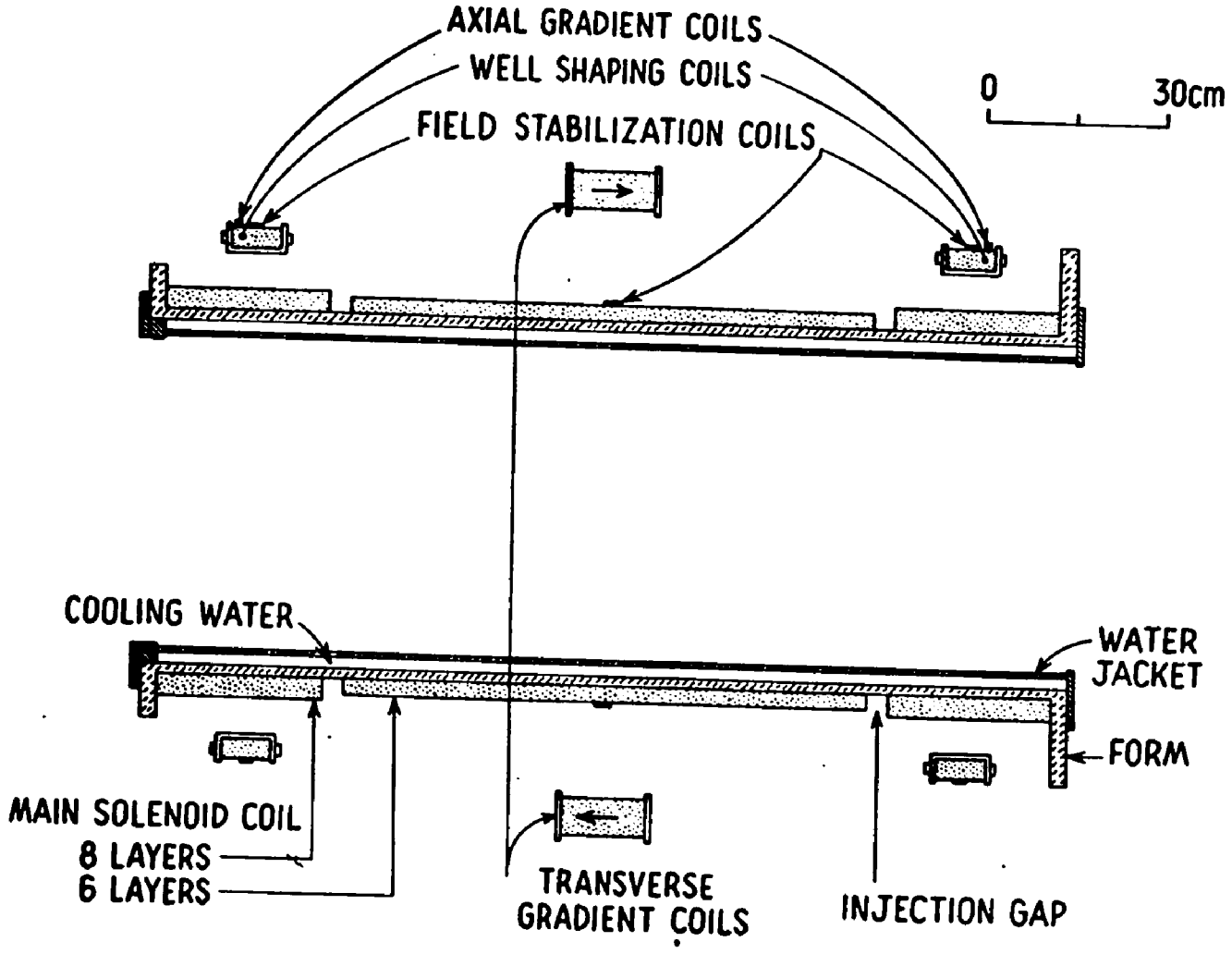

FIG. 18 SOLENOID AND THE AUXILIARY MAGNETIC COILS.

solenoid was wound with 0.100 in. x 0.200 in. copper wire on edge. Insulation is provided by 1 mil of AI-220 varnish on the wire, and a 1 mil layer of Kapton H film between the layers. The entire assembly is bonded together with a thermosetting varnish.

The final well shaping is done by two coils outside of the main solenoid winding each consisting of 280 turns of wire wound in the same manner as the main solenoid. Varying the axial position of these coils changes the depth of the well.

An additional pair of small coils with opposing magnetic moments are mounted 180 degrees apart outside of the solenoid and provide a transverse field gradient of the form const $\cdot \partial B_z/\partial x$, in the experimental region. These coils may be rotated about the axis of the solenoid to establish the direction $\hat{x}$. The magnitude of the gradient is determined by the magnitude of the current through the coils. The effect of these coils as they are used in this experiment is discussed in Appendix III. A more detailed discussion of their effect is given in J. Wesley, (1970, Appendix C).

A small three-turn coil is wound over each well shaping coil. These coils are connected in series with opposite polarity and driven from a separate current source. They serve to produce an axial gradient in the trapping region, and are used to shift the axial position of the bottom of the well.

3.2 Solenoid Power Supply, Cooling, and Field Regulation

The power supply and cooling systems for the solenoid are essentially those developed by J. Wesley (1970) for the most recent

Michigan electron g-factor experiment, g-IV. Although designed for the g-IV apparatus, they performed admirably when connected to the present apparatus. The solenoid normally operated at 400 volts and 28 amps providing a field of 775 G. The current was regulated by a conventional current regulator to about 1 ppm short term. Cooling water for the solenoid was provided by a closed circuit cooling system at the rate of 45 gpm. This water was normally held at a temperature of 10 $\pm$ 0.2°C, and resulted in a maximum temperature on the outside of the solenoid winding of 56°C.

The magnetic field was further regulated by an NMR servo-regulator which operated independently of the power supply current regulator (Fig. 19). The NMR sensing probe is located near the trapping region at z = 33 cm, r = 11 cm. The probe is excited by a marginal oscillator which is in turn phase-locked to the 1.0 MHz crystal standard of the Monsanto model 3100A frequency synthesizer at a multiple of 0.1 MHz. The detected signal from the marginal oscillator is fed to a lock-in amplifier which generates an error signal. The error signal is then fed back through a current amplifier to the field stabilization coils on the outside of the solenoid. In this manner the NMR resonance signal is adjusted to be equal to a standard frequency (3.300 000 MHz) derived from the frequency synthesizer.

The magnetic field just outside the control probe is regulated to 0.2 ppm, but the regulation becomes considerably worse further from the control probe due to thermal-mechanical fluctuations of the

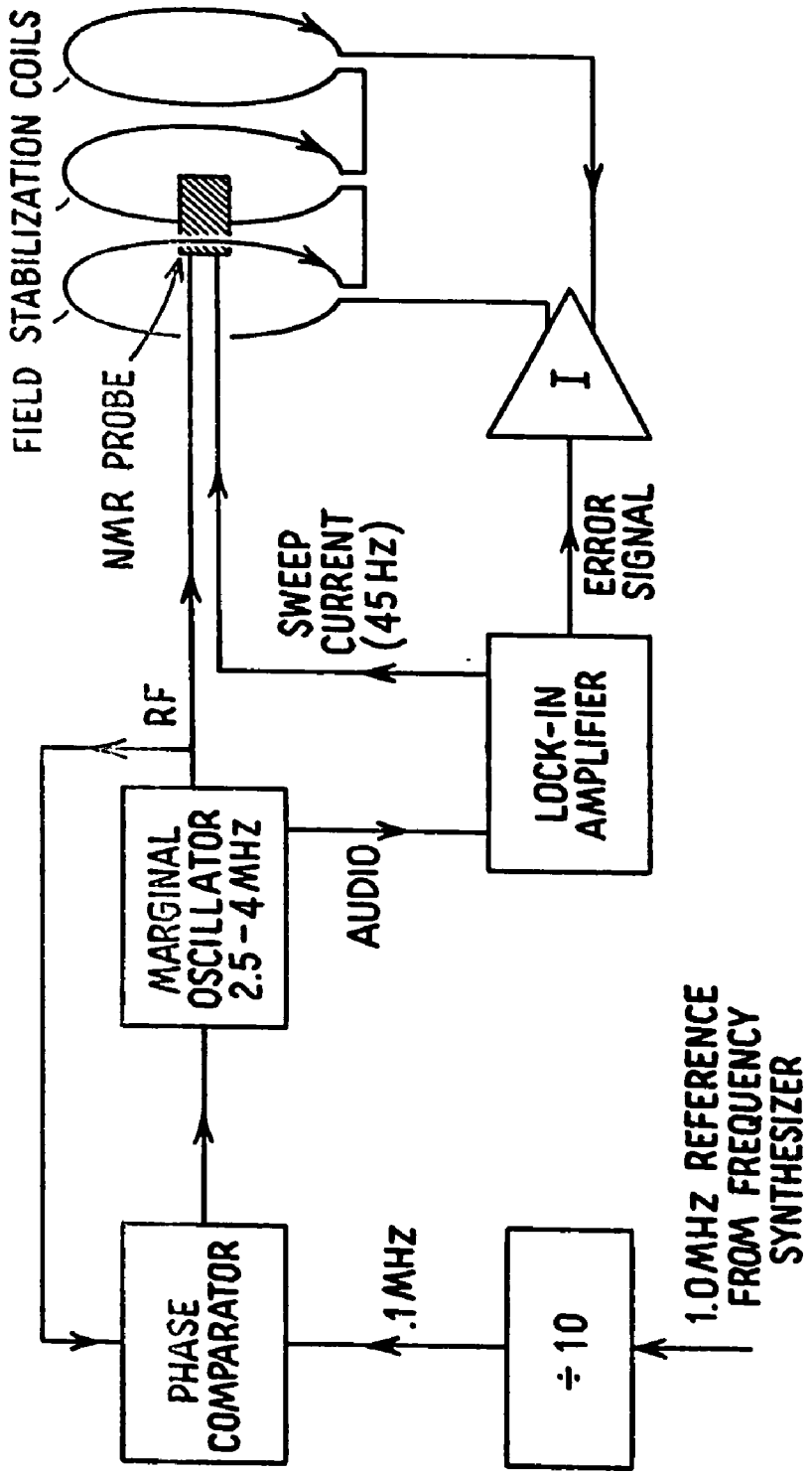

FIG. 19 NMR FIELD REGULATOR.

solenoid. In that portion of the well which was used for precision measurements, the RMS deviation was 1 to 2 ppm, while the mean magnetic field remains essentially constant. There is an additional NMR monitoring probe mounted on the outside of the vacuum system (see Fig. 17), which is used to monitor the day-to-day operation of the solenoid and is a good indicator of fluctuations in the magnetic field.

3.3 Field Mapping System

The magnetic field at the ion cyclotron radius is mapped with an additional movable NMR probe (Fig. 20). This probe is mounted on a support tube which is sealed into the vacuum system faceplate and can map the field within the apparatus without disturbing the vacuum. The probe head is made entirely of plexiglass. The sample is cylindrical and contains 0.65 cc of 0.2 m $CuSo_4$ in water.

The probe assembly is mounted on a vacuum sealed support shaft which runs down the center of the apparatus. This shaft also serves as a coaxial connection for the RF feed and carries the sweep connection. The electrical connections are brought out the end of the tube with o-ring sealed feedthroughs. Normally, the center of the sample is set at the same radius as the mean radius of the annulus with an accuracy of ± 0.05 mm. The axial position of the probe assembly is controlled from outside the vacuum system with a motor drive and can be set to a given axial position with an accuracy of ± 0.5 mm. It should be noted that we only need to know the relative axial position of the probe in order to perform the field averaging. The probe can also be rotated about its center to any azimuthal position. Mechanical stops are provided every 45 degrees so that the aximuthal positions can be set reproducibly.

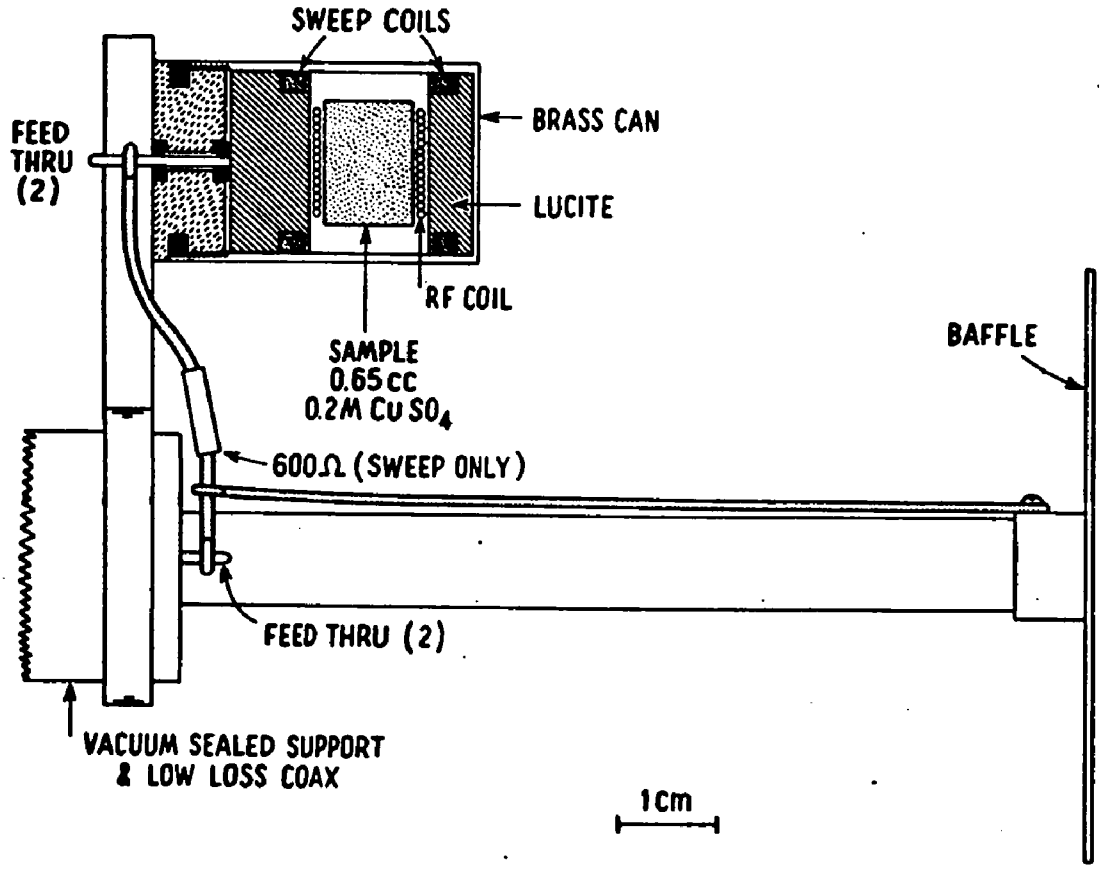

FIG. 20 NMR MAPPER PROBE ASSEMBLY.

When not in use, the probe is retracted to a position behind the detector. The probe shaft carries a circular baffle to provide an electrical shielding for the trapping region. The supporting shaft and mounting parts were all brought up to a separate NMR probe and no shift due to magnetic contamination was observed at the level of 0.3 ppm (1.0 Hz).

The mapping probe was excited with a conventional marginal oscillator which is electrically similar to a Harvey Wells-Magnion 0-503. The oscillator is locked to the magnetic resonance frequency using a lock-in amplifier and feedback tuning of the marginal oscillator with a varicap diode. This system was developed by J. Wesley for g-IV and allows the oscillator to track the probe as it moves. The frequency of the marginal oscillator is read directly on a frequency counter. Using this system the center of the resonance line can be found to $\pm$ 1 Hz or $\pm$ 0.3 ppm, and is independent of sweep amplitude, RF amplitude, overall loop gain, stray pickup, and coupling with the NMR regulator probe.

The mapping probe is experimentally calibrated to the standard probes built by J. Wesley (1970) for g-IV. The probes are built in a cylindrical configuration (with a length to diameter ratio 10:1 and are placed transverse to the magnetic field. This has the advantage of essentially eliminating the effect of nonzero susceptabilities in in the materials used to construct the probe. All three of the mechanically identical g-IV probes were used to eliminate the possibility of variations in the material used for any one probe affecting the

results. The electronics used with the standard probe are similar to those used with the mapper.

3.4 The Ion Source and Beam System

Introduction

The beam system was developed as a separate unit which could be aligned and tested without the main vacuum tank, and then "plugged in" to provide a dc ion beam at the cyclotron radius. The basic beam system is shown in Fig. 21. The beam system consists of an ion source and electrostatic lens to produce a collimated beam of ions, followed by a series of deflection plates to guide the ions on a straight line path into the high field region.

Vacuum System

The vacuum tank for the beam system was built in a T configuration and supported near the center of the T by two heavy rollers which allow the beam system to be rolled back and forth when coupling it with the main vacuum tank. The entire vacuum tank above the support point was constructed of silver-soldered brass.

The vacuum pumping is done with a conventional NRC 4 inch diffusion pump with a cold cap maintained at a -40°C by the closed circuit freon refrigeration system. The pump oil is Dow-Corning DC-705 to minimize the presence of backstreaming oil in the system. Normally, this system attained a vacuum of 3×10^{-8} Torr when the source was not running. This rose to 2.0×10^{-7} Torr with the source in operation. The vacuum system was fitted with a titanium sublimator in the base of the upper T-section which could provide an additional factor of three in pumping speed if needed.

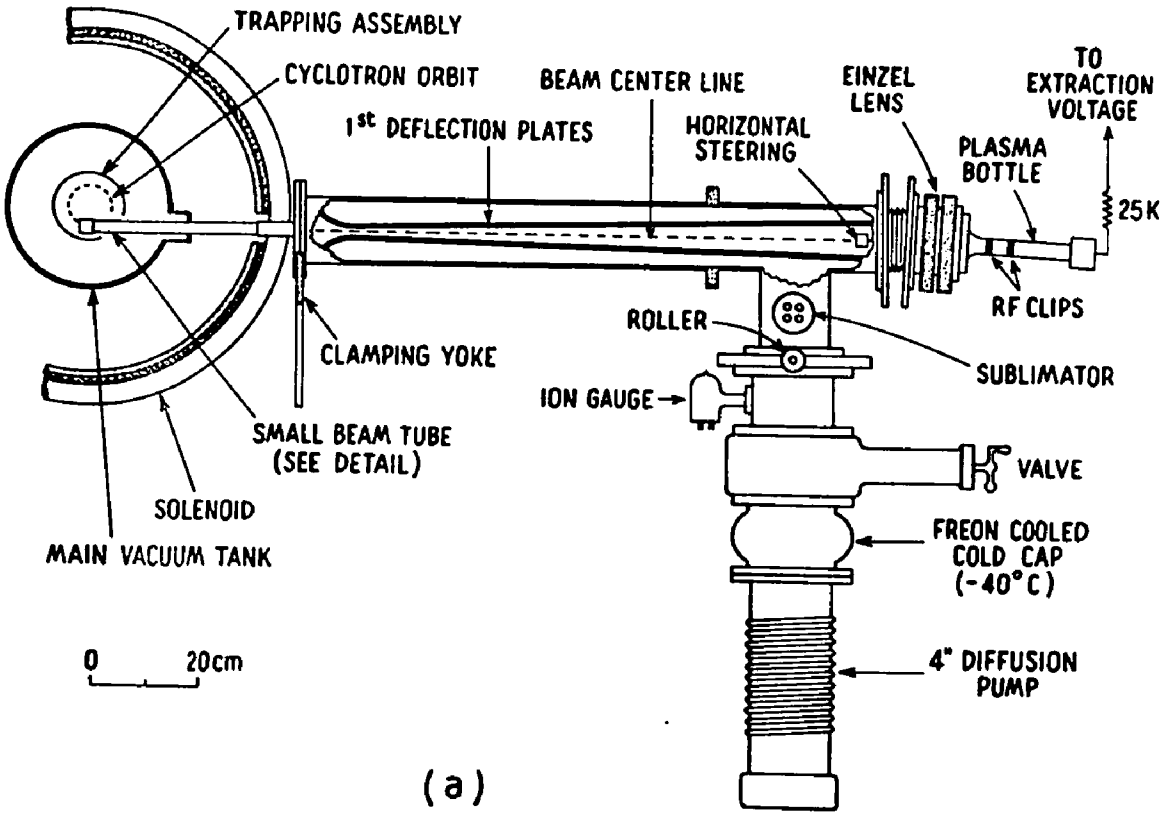

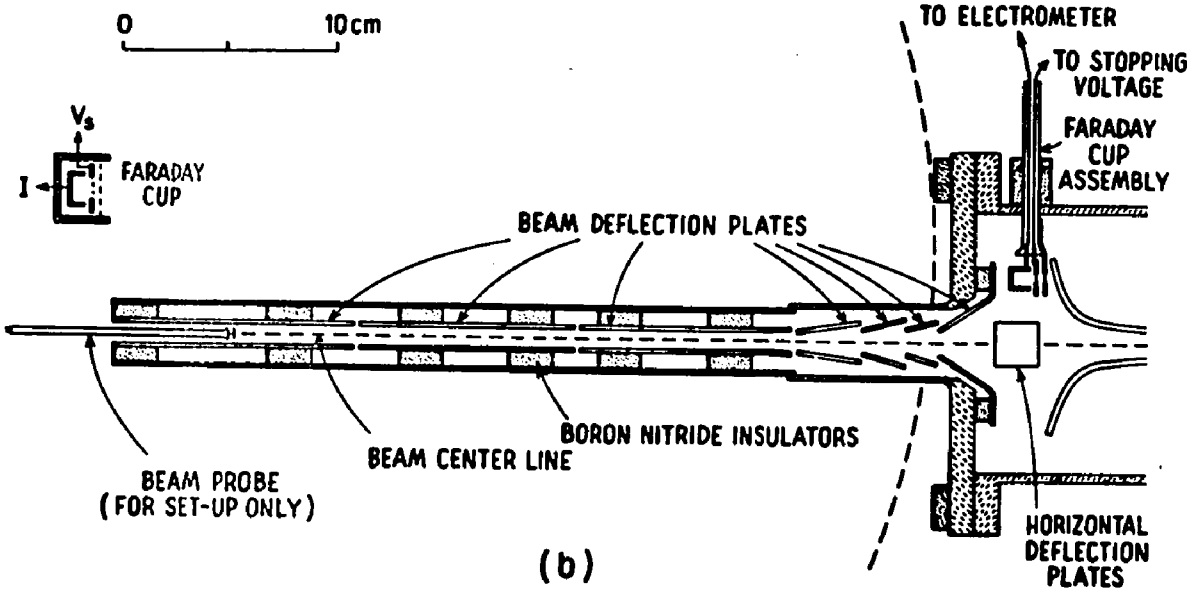

FIG. 21 ION SOURCE SYSTEM. (a) OVERALL SCHEMATIC. (b) BEAM TUBE DETAIL.

In normal operation the beam tube is inserted through a port in the side of the main vacuum tank and sealed with an o-ring seal about its outside diameter. The beam system is further supported with a collar just outside the solenoid which provides mechanical support of the beam tube and allows limited vertical adjustment to position its end at the correct cyclotron radius. The beam tube provides the necessary conductance to allow differential pumping of the two vacuum systems. This conductance allows the two systems to operate at pressures which differ by a factor of 1000 although normally the pressure ratio is 100:1.

The RF Ion Source

The ions used in this experiment are provided by an Ortec 501 ion source. In operation, a gas is leaked into the plasma bottle shown to the right in Fig. 21(a). This gas is then disassociated into a plasma of atomic ions and electrons by a strong 80 MHz RF electric field applied via two conducting rings on the outside of the bottle. A positive voltage V is applied to the terminal on the right causing ions with charge q to be accelerated through a potential V and leave the source through the canal with energy approximately qV. The exit canal defines the direction and divergence of the beam. While the source does not produce molecular (e.g., H_2^+) ions directly, it does produce them by recombination in the canal region. This process is very dependent on the material used for the canal, and nickel was chosen to insure ample numbers of molecular ions.

For a given ion type, the number of ions per second out of the bottle is proportional to the energy of the ions. For different types of ions the output of the source falls off as the square-root of the mass of the ion. In normal operation the overall output from the source was approximately 0.40 μA for hydrogen gas at 500 eV.

The ion source is equipped to operate with hydrogen, deuterium, and helium gases (H_2, D_2, and He). The hydrogen gas flow is controlled by an Ortec palladium leak, and the other gases by a conventional pressure regulator operating at 1 psi followed by a Nupro type B2-S capillary flow valve. While the palladium leak had the advantage of more precise control than the valves, its long thermal time constant made adjustment difficult when mixing gases as discussed below.

The output of the bottle contains several different components including the atomic ion and the molecular ion being used, and in smaller quantities atmospheric gases and bottle contaminants. However, those components which are not of the desired mass are removed from the beam by the crossed field injection system as is explained later in this section.

When two gases (e.g., H_2 and D_2) are leaked into the bottle simultaneously the bottle produces ions of both species. Since these ions are all being drawn from the same plasma, they should come out with the same energy distribution. This has been verified experimentally (Fig. 22). If both of these species have an ion of the same mass number ($^1H_2^+$ and $^2D^+$) these ions pass through the deflection system with identical trajectories. The relative abundance of the two species can be adjusted by adjusting the gas flow. In fact,

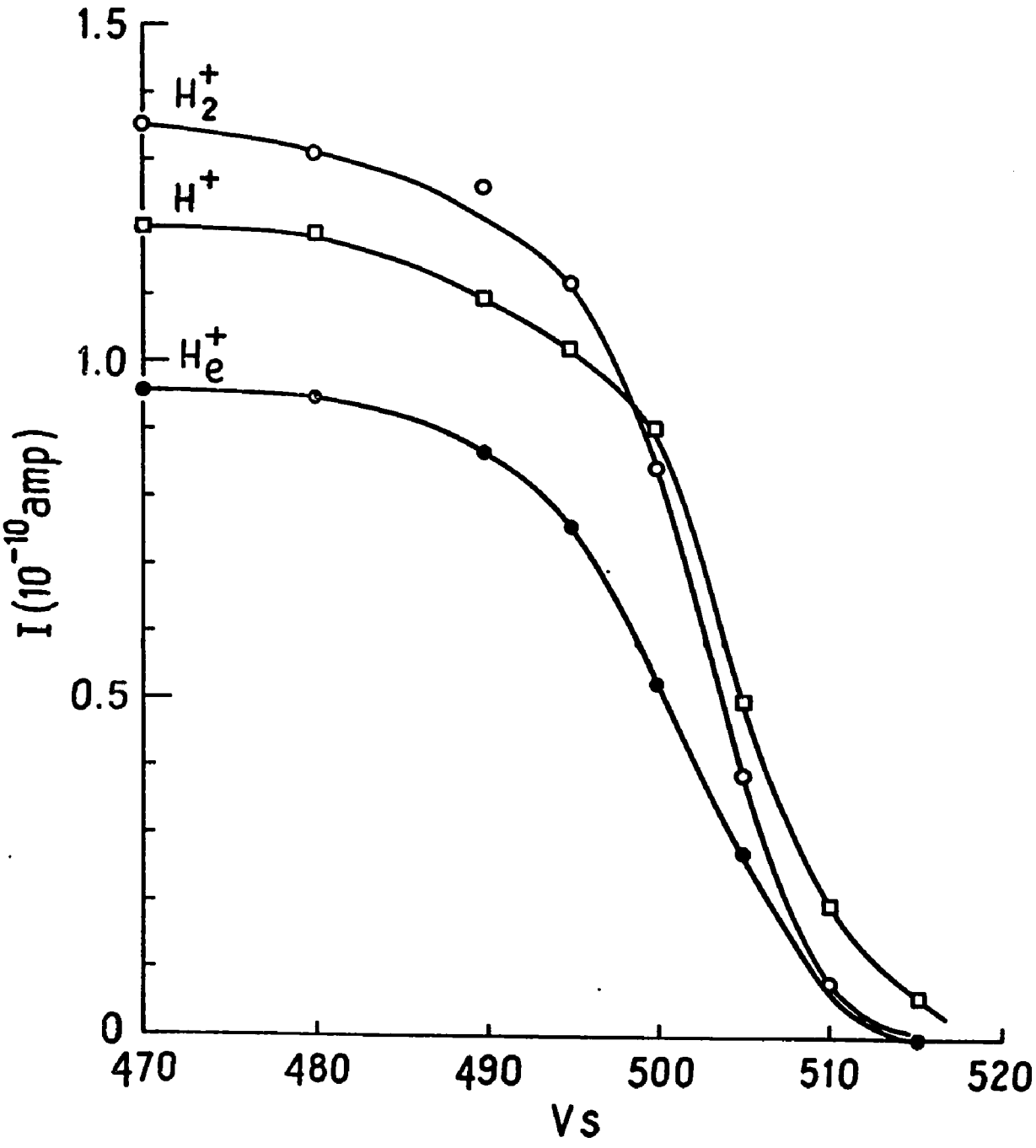

FIG. 22 ENERGY DISTRIBUTIONS FOR SEVERAL IONS LEAVING THE SOURCE SIMULTANEOUSLY.

this can only be done by observing the amplitudes of their cyclotron resonances, since this is the only time when the two ions are experimentally distinct in the apparatus. One interesting byproduct of the gas mixing is the mass 3 ion presumed to be HD^+ which is observed in the source output when the gases H_2 and D_2 are mixed.

The extraction voltage V is obtained from a conventional full-wave doubler power supply furnished by Ortec followed by additional filtering to reduce the ripple to 0.1 percent. This supply was operated from a Variac and an ac line regulator was used to obtain a stable dc output.

Einzel Lens

The Einzel lens immediately follows the source and consists of three cylindrical segments (Fig. 23), the outer two of which are grounded, while the inner one is connected to a dc voltage source. Since the beam enters and leaves at ground potential, there is no net change in the energy of the particles. The dc voltage supply was identical to that described for the ion source extraction voltage.

A beam of divergent ions with a 3 degree angular dispersion is produced by the canal tip geometry of the source (0.33 mm dia. x 12.7 mm) and is then focused by the Einzel lens to an image about 1.2 m away. The focal length of the lens is a function of the voltage applied and in normal operation the focal length is about 3.5 cm with image distance of about 5 cm and object distance 1.2 m as measured from the center of the lens. This results in a magnification of about 24 and a final spot size of 0.8 cm (Liebmann, 1927). The Einzel lens also produces

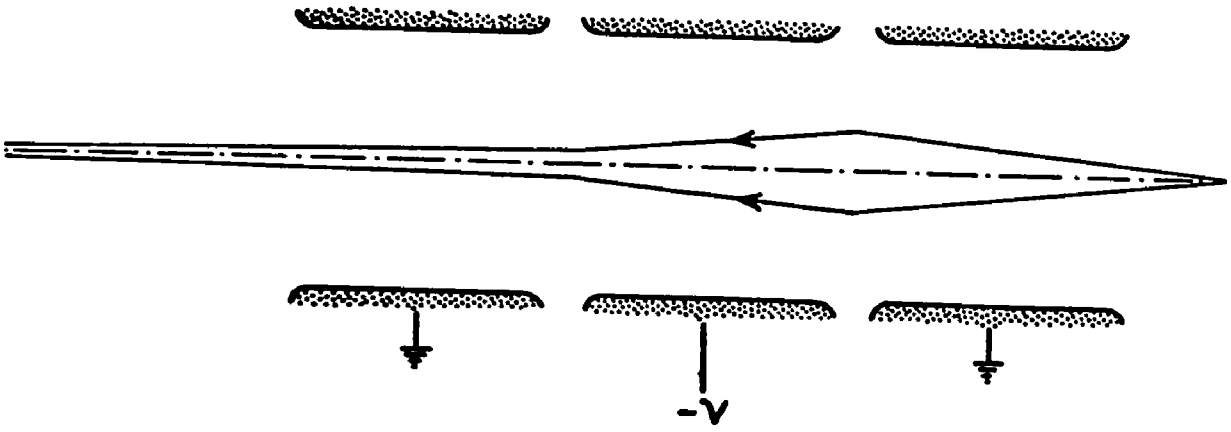

FIG. 23 FOCUSING BY AN EINZEL LENS. (BEAM DIVERGENCE EXAGGERATED.)

aberrations in the image which are dependent on the distance of the ions in the beam from the center line of the lens. This in turn is determined by the canal tip geometry and the distance from the canal tip to the center of the lens. The lens was operated with the central electrode negative in order to minimize these aberrations. In normal operation, the lens voltage was negative and about six times the accelerating voltage V. Under these conditions the actual spot size is about 20 percent larger than the expected image size.

Thus, when the beam reaches the entrance to the small beam tube it is already focused to a spot size approximately equal to the maximum aperture of the beam tube (0.8 cm). A larger canal tip could be chosen (up to 1.6 mm) to produce more gross current output from the bottle, but this current would be focused into a correspondingly larger spot size. Aberrations immediately become a serious problem as the spot size becomes four times the image size for the 1.6 mm canal tip. Thus while there is more gross beam output from the source, very little of it enters the small beam tube, but rather it scatters off of the inside of the beam tube and the electrodes. Furthermore, the larger canal tip allows more unionized gas to escape from the plasma bottle since the conductance is proportional to d^3/L (Spangenberg). This seriously increases the problems of differential pumping and gas supply. Similarly, the magnification of the lens could be decreased by moving the bottle further back behind the lens, but this would result in rapidly increasing aberration and no net increase in usable beam.

Beam Deflection System

Once the ions leave the ion source, they would immediately begin to execute cyclotron motion due to the external field of the solenoid if there were no electric fields present. As is well known, the force on a particle in electric and magnetic fields is given by $\vec{F} = m\vec{a} = q(\vec{E} + \vec{v} \times \vec{B}/c)$. If we require that the force on the ion be zero, we get $\vec{E} = -\vec{v} \times \vec{B}/c$. That is, an electric field orthogonal to the magnetic field and the velocity, will produce a cancellation of the magnetic force and the particle will move in a straight line. This electric field is established by a series of electric plates (Fig. 21) made of brass and separated a distance d with each operating at a potential $\pm U_i/2$, where $U_i = E_i d = vB_i d/c$. Since the magnetic field is not constant, the plates are bent and set at an angle to obtain a better approximation to the required field. Any magnetic field component along the direction of motion does not affect the motion, and the transverse magnetic field is essentially horizontal. These plates are driven by equal and opposite voltages so that the central beam experiences no net energy change due to the electric field of the plates. The required voltage are obtained from the circuit shown in Fig. 24. The voltage for the negative plates is obtained from a variable negative supply through a ten-turn potentiometer. The voltage on the positive plate is then determined by a comparator circuit which sets the positive voltage equal and opposite to the negative voltage. The negative supply voltage is varied by another ten-turn

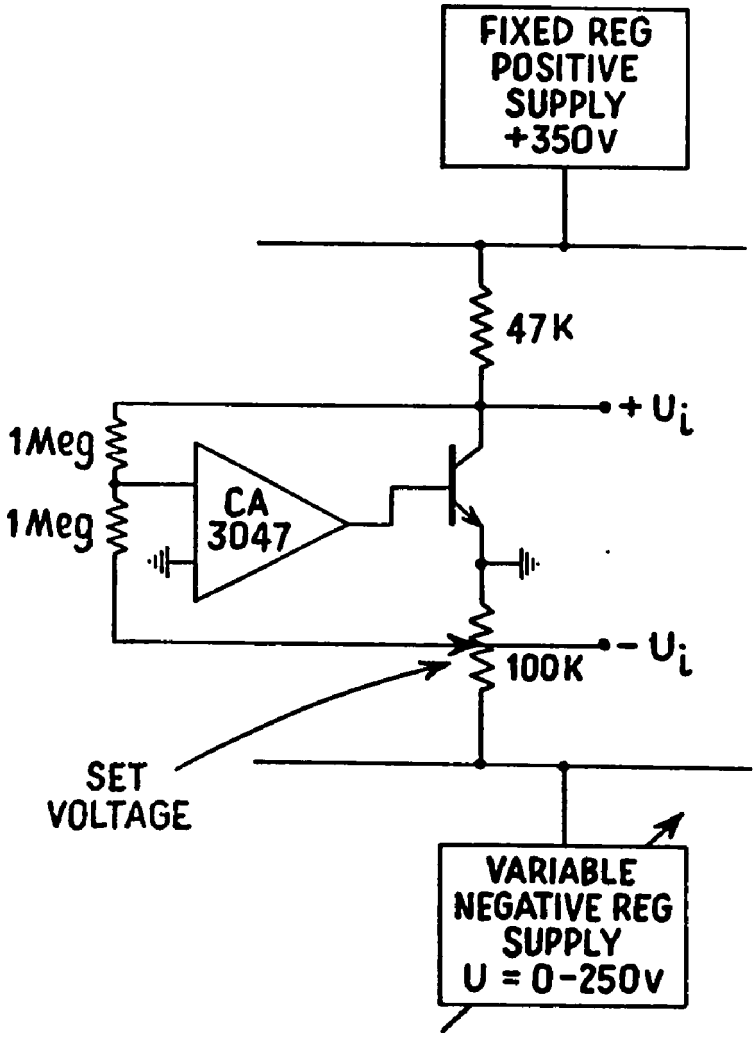

FIG. 24 DEFLECTION PLATE VOLTAGE SUPPLY.

potentiometer so that the electric field for the entire system may be scaled for different ion velocities. This system was voltage regulated to 0.01 percent.

In addition, two sets of horizontal control plates are used; the first (Fig. 21a) just beyond the Einzel lens, and the second (Fig. 21b) at the entrance to the small beam tube. These plates are also driven by voltage comparators, but their negative supplies are fixed.

Since magnetic field cancelling electrodes cannot be inserted into the interior of the Einzel lens, the source assembly is tilted slightly so that the ion path is more or less tangent to the beam (Fig. 21a). Most of the plates and surfaces in the large beam tube are coated with Aerodag G graphite spray which helps to produce a more stable beam.

A small Faraday cup can be inserted into the beam line just before the entrance to the small beam tube. This Faraday cup is equipped with a grounded guard plate and a stopping plate. The holes in both of these plates are screened with 100 mesh copper screening etched in acid to about 90 percent transparency. By applying a variable positive voltage to the stopping electrode and increasing it until the current measured at the Faraday cup begins to decrease, the mean energy and energy distribution of the beam can be determined.

The process of balancing the magnetic force with an electric force discussed above takes place for only one particular ion velocity. Since the energy of the ions coming out of the bottle is independent of mass, only the ions of one mass number are selected. All other ions

are deflected out of the beam line and strike the electrodes and vacuum system walls.

Attaining a dc Beam

Within the philosophy of treating the beam system as a source of ions at the injection point, both the adjustment of the beam system and some of its operating parameters will be discussed here. To align and test the beam system, it is placed in its normal operating position without the main vacuum tank in place but with a vacuum sealed cap over the output end. This cap serves to support a 0.125 inch diameter electrometer probe which can be extended over the entire length of the small tube. To align the dc beam, the probe is extended all the way forward to the mouth of the small beam tube. A value is then estimated for the negative supply voltage U and the U_i, and the voltage on the first set of plates U_1 is set along with the horizontal steering plates and the Einzel lens focusing to give the maximum current into the probe. The probe is then moved back to the end of the next set of plates and U_2 along with the horizontal deflection voltage is set. This procedure is repeated for each set of plates.

Once the U_i's have been determined, the velocity may be changed by either changing the energy of the ion or by changing the ion mass and readjusting the negative supply voltage U according to the relation $U(2)/U(1) = v(2)/v(1)$. The horizontal deflection voltage and all of the U_i's required a slight repeaking.

Ion Source Output Parameters

The ion source output can be characterized by three parameters; the mean energy T of the ion, the energy distribution about the mean, and the ion current. The output is dependent on three parameters; the extraction voltage, the ion being used, and the gas pressure. The extraction voltage V is given by $V = V^* - IR$ where V^* is the applied voltage, I is the current drawn, and R is the 25K resistor connected at the source to stabilize its operation. The IR drop is at most 15 V.

The energy of the ions entering the cyclotron apparatus is restricted by the relation $T \propto M^{-1}$ (Eq.(2.3))(typically $T \cong 500$ eV for H^+, and 125 eV for He^+. The spread in the energy of those ions which can be usefully trapped is determined by the annulus and the crossed field selection process of the deflection system, and is considerably less than the energy spread of the bottle output. However, the energy distribution of the output of the bottle is important as it determines what fraction of the total output current can be used for a given ion specie. The usable energy spread of the ions in the well is proportional to the energy of the ion.

The source parameters can be measured with the Faraday cup at the entrance to the small beam tube which is described above. If the current due to an ion is measured as a function of the stopping voltage V_s, a plot such as that shown in Fig. 22 is obtained. If it is assumed that an ion with energy qV will get past the stopping plate only if $V > V_s$, (see also Simpson, 1961) then the energy distribution of these ions may be obtained by differentiating the plot of I vs. V_s and

plotting $-dI/dV_s$ vs. V_s. The center of this distribution is then the mean energy. The absolute accuracy of the Faraday cup is not as good as might be expected. When ions with mean energies of 475 ± 7 eV (as determined by the annulus dimensions and the magnetic field) are being injected into the main apparatus, the Faraday cup determination of their mean energy is 500 ± 10 eV (see Simpson, 1961).

The mean energy is largely determined by the extraction voltage V_{Ex}, but is not exactly equal to it. The mean energy has been observed to be both above and below the extraction voltage on various occasions and the variation appears to be due to conditions within the bottle. Once the minimum gas pressure for a stable discharge has been attained in the bottle, the output falls off with increased gas pressure due to the decreasing mean free path of the ion in the residual gas of the bottle.

The distribution of the ion energies about the mean is proportional to the mean energy for the energies used. The energy spread ranges from approximately 14 eV at T = 500 eV to 4 eV at T = 100 eV. This is contrary to the constant energy spread of 65 eV quoted by Ortec. The fact that the energy spread is proportional to the energy is very advantageous as it allows more of the available ion output at lower energies to be used than was expected from the Ortec predictions. The mean energy and distribution was essentially identical for all ions comming from the bottle at the same time (e.g., H^+, H_2^+) as is shown in Fig. 22. From this, it is inferred that the distributions for mass doublets which cannot be resolved by our system, such as H_2^+–D^+, are

also the same. This is critical to establishing a beam of both ions for mass difference measurements on closely spaced doublets.

The source output current decreases with decreasing energy, and for constant energy it is proportional to $M^{-1/2}$. Since the apparatus requires lower energies for higher masses, the problem of getting sufficient beam current with higher mass ions quickly multiplies.

The overall stability of the source was more than sufficient for the present experiment. It should be noted that variations in the energy distribution of appreciably less than the distribution width do not affect the output as this variation has the effect of sweeping the relatively flat central portion of the distribution peak across the narrow energy band accepted by the annulus. The source tended to be unstable when first turned on or when large excursions in the gas pressure or extraction voltage were made. After the source settled down, it was not unusual for it to require no adjustment for a day or longer. The strength of the external field of the solenoid is about 10 gauss at the bottle in a direction transverse to the bottle axis and did not significantly affect the operation of the source.

Source System Output

The beam deflection system also functions as a crossed field velocity selector. If we approximate the system as two parallel plates of length L = 40 cm and separation of d ≐ 0.8 cm in a magnetic field of 800 gauss, we may calculate the expected resolution $\Delta v/v = 2r_o d/L^2 = \pm 0.002$, where $r_o = cMv/eB$ is the cyclotron radius.

For a given mass M and energy $T = 1/2\ Mv^2$ the energy resolution is $\Delta T/T = 2(\Delta v/v) = 0.004$. This also causes a difference in the cyclotron radius of these ions as they enter the trapping region of $\Delta r/r_o = \Delta v/v = 0.002$.

An attempt was made to measure the energy distribution of the ions at the end of the small beam tube using the Faraday cup shown at the left in Fig. 21(b). The observed energy spread was $\Delta T/T = 0.04$ (FWHM)--a factor of ten worse than predicted. This is apparently the limit of resolution of the Faraday cup. It is probably unreasonable to expect this Faraday cup to provide the resolution required for this measurement (Simpson, 1961).

Two ions with masses M_1 and M_2 differing by ΔM, $M_2 = M_1 + \Delta M$, will both leave the velocity selector with the same mean velocity, but their mean energies will differ by $\Delta T/T = \Delta M/M$. Their cyclotron radii are given by r_o and $r_o + \delta r$, where $\delta r/r_o = \Delta M/M$. Thus their cyclotron radii are distributed about their means with $\Delta r/r_o = \Delta v/v$ while their means are separated by $\delta r/r_o = \Delta M/M$. This results in a final distribution with characteristic width $\Delta r + \delta r$.

The defining annulus for the beam has an aperture $\Delta R/R = \pm 0.01$ which defines the energy to $\Delta T/T = \pm 0.02$. Since the beam through the annulus is optimized for maximum current, it is reasonable to assume $r_o \cong R$. In general, $\Delta R/R \gg \delta r/r_o + r/r_o$ for closely spaced mass doublets ($0.01 \gg 0.002 + 0.0008$ for H_2–D), so that both distributions are assumed to be present in the trap with mean radii which differ

by $\delta r/r = \Delta M/M$. Thus while the absolute radius of the ions orbit is only known to $\Delta R/R = 0.01$, the radii of two ions of slightly different mass are separated by $\delta r/r_o = \Delta M/M$ (= 0.0008 for H_2-D).

3.5 The Main Vaccum System

The minimum vacuum required to allow the trapping of ions for 10000 μsec may be estimated from one-dimensional multiple scattering theory (Fermi, 1950). In order to leave the well, an ion must be scattered through an angle α in the axial direction, where α is to a first approximation the pitch angle of an ion at the highest level in the well. Thus we have $\alpha = v_z(max)/v$. If we substitute from Eq. 2.9, this becomes $\alpha = (\Delta B(max)/B)^{1/2}$ where $\Delta B(max)$ is the well depth for the highest level in the well. Since $\Delta B(max)/B \cong 100$ ppm, we have $\alpha \cong 0.01$. Combining this value of α with a desired trapping time of 10,000 μsec, the minimum required pressure was estimated to be $\sim 10^{-8}$ Torr. Thus the vacuum system was designed to attain an ultimate pressure of 10^{-9} Torr.

The main vacuum tank (Fig. 17) was constructed entirely of aluminum and Viton O-ring seals were used throughout. The vacuum system is mounted on rollers so that it may be easily removed from the solenoid for access and baking.

The main vacuum pump is an NRC model VHS-6 diffusion pump with Dow-Corning DC-705 fluid. Directly above the diffusion pump is a cold cap kept at -40°C by a closed circuit freon refrigeration system. It was found that this freon system was as effective as more conventional liquid nitrogen cooling and much more convenient to use. The valve

plate and elbow provide additional baffling against backstreaming oil. A titanium sublimator located in the elbow provides an additional factor of ten in pumping speed. The vacuum is monitored with a Veeco type RG-75P ion gauge and type RG-31A gauge control unit.

In normal operation, the main vacuum system is first baked out at 200°C outside of the solenoid with the NMR mapping assembly and regulator probe removed. The system is then let down with helium and rolled into the solenoid where the mapping assembly and the beam system are inserted and the system is immediately pumped down again. In this manner and ultimate pressure of better than 1.0×10^{-9} can be attained. A series of tests were run with an additional gauge tube in the mapper port on the faceplate where it sensed the vacuum in the interior of the C's. These tests established that: (a) the vacuum gauge in the elbow is a good indicator of the vacuum in the entire system, (b) the pressure in the main vacuum system was not affected by the pressure in the beam system as long as the pressure in the latter was less than 5.0×10^{-7} Torr--a condition which was always satisfied.

3.6 Trapping and RF Assembly

Introduction

The trapping and RF assembly constitutes the main experimental area and are shown in Fig. 25. The electrode configuration is supported by ceramic insulators from two long rails fastened to the faceplate of the vacuum system and all of the electrical connections are made at the faceplate. This allows the entire assembly to be rolled out of the vacuum system for easy access. Construction is largely

of brass with an overall outside diameter of 12 cm, and an initial ion radius of 4.05 cm. These dimensions are a compromise between maintaining a reasonable RF efficiency at odd harmonics (see Eq. 2.37) and the desire to keep the ions a reasonable distance from the surfaces where they might experience high potential variations. All of the parts used were checked for magnetic contamination by bringing them up to an NMR probe and looking for significant shifts in the resonance frequency. These shifts were not more than a few ppm, for the largest pieces. This is not as important as it might be in other experiments since the NMR field map is made with the apparatus in place.

The parts are carefully cleaned before assembly and those parts which face the ions are sprayed with a very uniform coat of Aerodag G collodial graphite suspension in isopropyl alcohol. The use of the graphite coating to minimize stray electric fields follows the work of Parker and Warren (1962). This assembly is then mechanically aligned to an accuracy of 1 mm or better. Finally, the system is baked out at 200°C prior to use.

Deflection Disk

The ions must have enough pitch on their first revolution after leaving the beam tube to clear the tube walls. This pitch is provided by a positive voltage pulse on the deflection disk. The voltage required is usually from 100 to 150 V although the beam experiences an effective potential difference of only about 10 V. The beam arriving at the trapping region has a mean axial energy of about 9 eV with an energy spread of about 2 eV. When the ions are not pulsed into the well region, they strike the deflection disk.

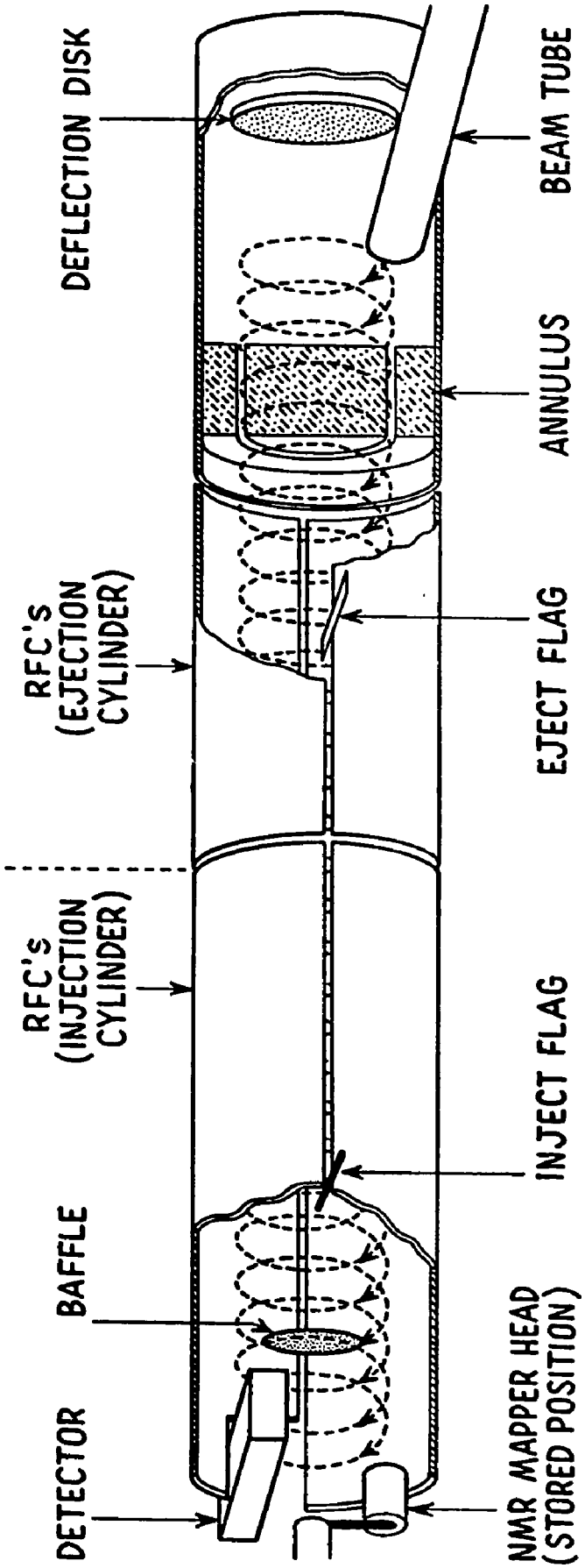

FIG. 25 TRAPPING REGION.

Annulus

The annulus defines both the mean radius and the spread in radius which the ions entering the trapping region will have and shields the trapping region from the electric fields of the beam system. To be effective, the annulus must have a length at least as long as the pitch length of the helical motion of the ions. Since the ions at this point have considerable pitch, the length of the annulus is 5.0 cm. The inner radius of the annulus is 4.00 cm and the outer radius is 4.10 cm. However, the magnetic field changes slightly over the length of the annulus and this results in a change in the radius of the ions cyclotron motion. Since the radius of the annulus is constant, this results in a reduction of the effective aperture of the annulus by 0.2 mm. Experimentally it is observed that the radial distribution of the dc beam has a FWHM width of 0.4 mm and a maximum width of 0.8 mm. The mean radius of the annulus is taken to be 4.04 ± 0.02 cm.

C's

The C's must function as a pair of axial cylinders when injecting and ejecting the ions and as C's when the RF field is being applied. The existence of a finite gap between the C's is a deviation from the assumption of an infinitesimal gap used for calculations. This is further complicated by the fact that this gap is not uniform. However, it can be shown that as long as the ion orbits are at least ten gap separations away from the gap, the effect of the gap is negligible. Electrolytic tank tests were carried out to determine the effect of varying the gap spacing on the dc potential distribution. These tests showed that for C's of 6.0 cm radius a typical gap width of 2.0 mm caused a reduction in the field at the ion

radius (4.0 cm) by about 1.0 percent and was approximately linear. Thus typical variations in the gap width are judged to produce longitudinal variations in the RF electric field at the ions orbit of no more than 1.0 percent and these are judged to be insignificant. The conditions seen by a resonant ion which might move out to a radius as large as 4.5 cm are not significantly different than those discussed above.

In order to maintain RF balance as discussed below, the ejection C's are electrically connected to the faceplate feedthrough with a section of vacuum coax terminated in 50 ohms near the C's.

Flags

The flags serve to limit the upper level of ions in the well by acting as a mechanical stop for their pitch motion. The width of the flag extending into the ejection cylinder (eject flag) is 5.0 mm and all of the ions trapped in the well strike it if the amplitude of their axial motion carries them beyond its axial position. However, the ion beam has considerably more pitch on injection so that the ions pass over the eject flag with only a few percent loss. The eject flag can be positioned from outside the vacuum system over the range z = 50 cm to z = 72 cm (see Fig. 31). The flag extending into the injection cylinder (inject flag) nas a diameter of 0.5 mm. This flag is generally used in conjunction with the eject flag to define both ends of the well. Thus, while it is wide enough to perform this function, most of the ions can pass over it in a normal ejection. The inject flag has a range of z = 0 to z = 31.5 cm. The flags extend radially from the edge of the C's into r = 3.0 cm.

The flags are normally grounded but the eject flag is driven along with the ejection cylinder during the ejection sequence. The flags do not interfere with the RF process since the centerline between the C's is the ground equipotential for the RF field. This was checked independently by observing the voltage on the flag with the RF voltage applied to the C's. The voltage on the flag was observed to be less than one percent of the RF voltage.

Baffle

The baffle (Fig. 20) which is mounted on the end of the NMR mapping probe, helps to shield the trapping region from any electric fields from the detector. This baffle is pulsed positive during the injection cycle to protect the detector from the direct dc beam. The electrical connection is made through the sweep connector with a 600 ohm resistor for isolation.

3.7 Electronic Equipment: Trapping and Cyclotron Resonance Timing Control Unit

The electronic control circuits for the machine cycle and data acquisitions are shown in the center section of Fig. 26. The basic timing sequence of the apparatus is provided by the timing control unit (TCU). This unit provides the pulses necessary for deflection, injection, RF control, ejection, and the detector gate. The signals as they appear on the electrodes of the apparatus are shown in Fig. 27. The TCU also provides synchronous pulses for the population and frequency stepping programs. The TCU operates from a crystal controlled time base with a basic time unit of 1.0 μs, an absolute accuracy of 100 ppm, and a reproducibility of 10 ppm. Since the period of an ion in the well is proportional to its mass, there

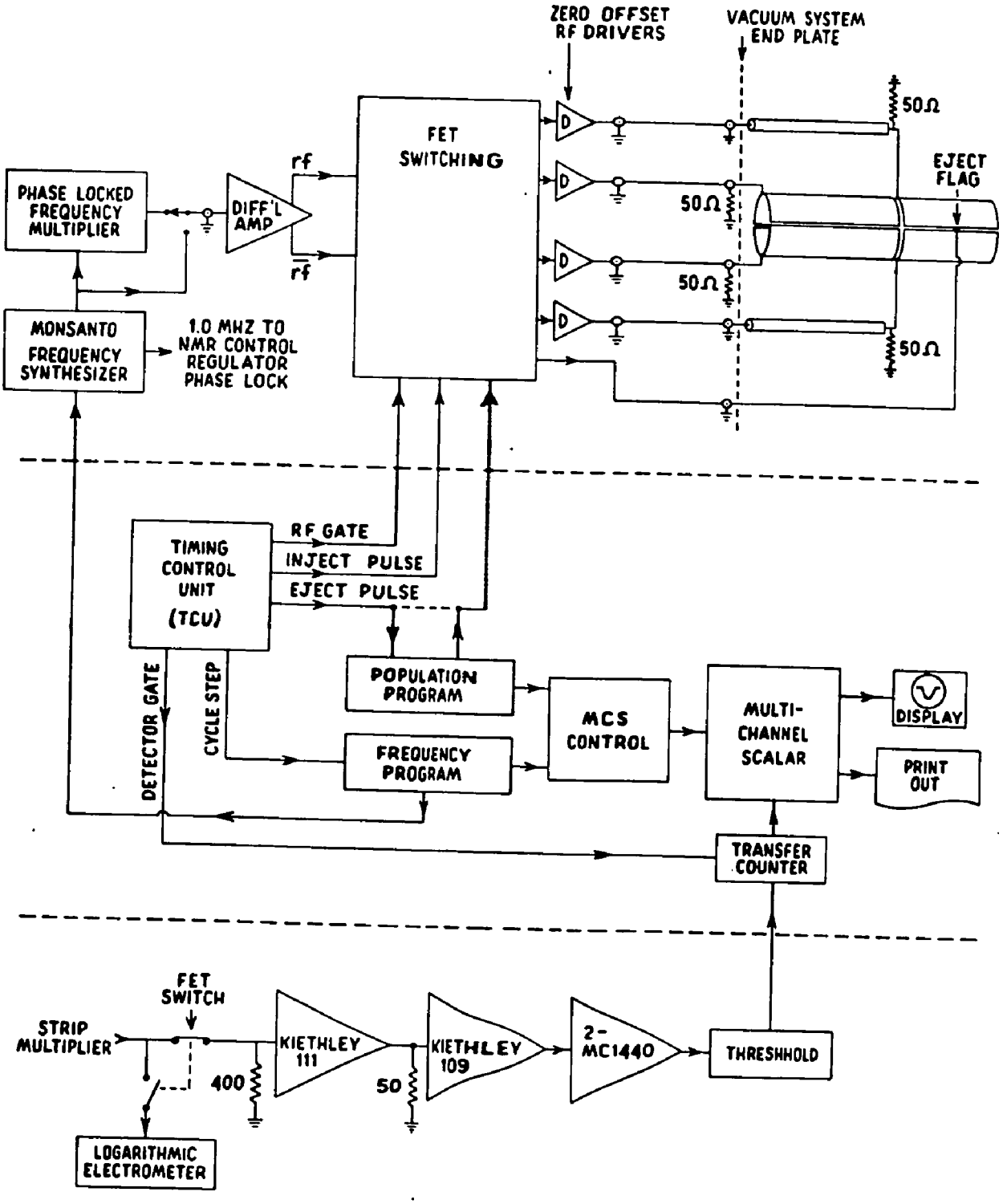

FIG. 26 ELECTRONICS FOR TRAPPING IONS AND OBSERVING CYCLOTRON RESONANCE.

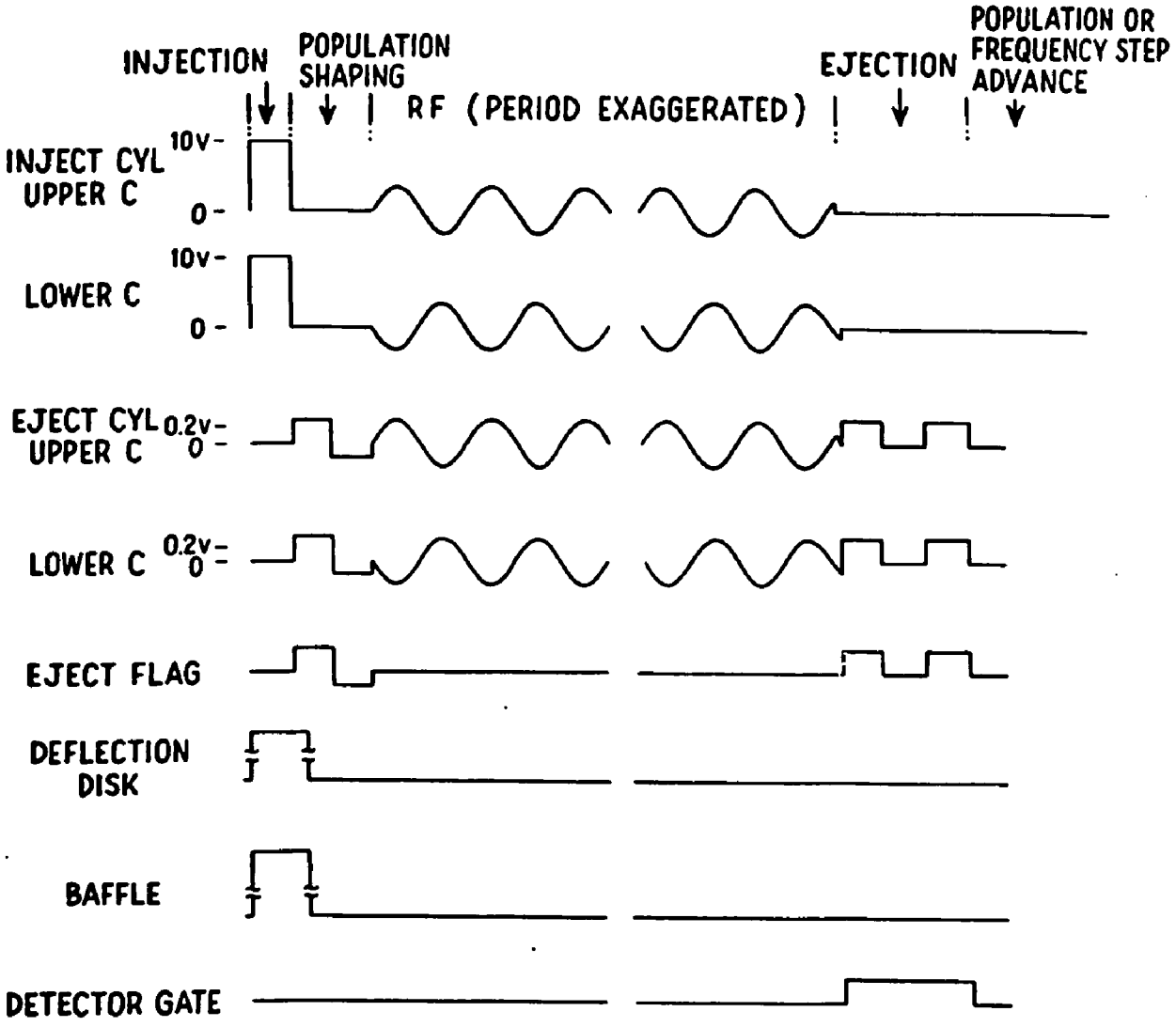

FIG. 27 ELECTRICAL SIGNALS APPEARING ON VARIOUS ELECTRODES.

is a time unit multiplier which allows the basic time unit of the system to be scaled according to the mass of the ion. The injection, population shifting, and ejection pulses closely approximate ideal square pulses and their amplitudes can be continuously varied. The TCU also provides for variation of the overall length of each machine cycle, the grouping of machine cycles, and delay between cycle groups to allow the frequency programming to advance one step.

Population Programmer

In order to determine the distribution of the proton in the well a series of eject pulses of progressively increasing voltage must be applied to the ejection cylinder on successive machine cycles as discussed in Section 2.1. This function is provided by a staircase pulse generator which advances once every machine cycle for a total of 16 to 256 steps. This pulser is controlled by the ejection pulse from the TCU and the output of the population pulser replaces the normal ejection pulse when it is used. The output pulse sequence had a linearity of better than one percent and noise levels of less than 1.0 mV peak-to-peak. In order to remove the effect of slow drifting in the trapping rate and other machine parameters on the population distribution, the pulse series is repeated many times and the data is collected in the multichannel scaler (MCS). The population generator provides the required synchronous pulses to control the routing of the detector output to the appropriate channel of the MCS.

RF System

The complete system for generating the RF voltages and applying them to the C's is shown in the top section of Fig. 26. The heart of this system is the Monsanto 3100A programmable frequency synthesizer. The frequency of the synthesizer is controlled by the frequency programmer. The synthesizer output is multiplied up to the desired harmonic by the phase-locked frequency multiplier and fed to the differential amplifier which produces two complimentary RF signals for application to the C's. These signals are then fed to the appropriate C's by the FET switching circuits and the RF drivers.

Frequency Synthesizer

The basic RF frequencies for the cyclotron resonance process are generated by a Monsanto 3100A frequency synthesizer which generates frequencies from 0 to 1.2 MHz in steps of 0.01 Hz. The output frequency of the synthesizer is controlled by the frequency programmer, and the output may be multiplied up to 15 MHz by the phase locked harmonic generator. Since the lineshape is only weakly dependent on the RF amplitude (Section 2.3), only moderate amplitude stability is required. The 1.0 MHz time base of the synthesizer is used as the reference for the NMR field regulator and the frequency counter time base so that all frequency measurements are related to the same base.

Frequency Programmer

The frequency programmer provides incremental stepping of the applied RF frequency synchronous with the machine cycle. This programming

can be done in steps of 0.01 Hz to 5.00 Hz with 16 to 256 steps per sweep. The stepping is begun at any switch selected eight digit base frequency. There are two independent frequency bases which can be alternated with the corresponding data stored in different sections of the MCS. This allows the simultaneous collection of data from both lines of a mass doublet without sweeping the dead area between the lines. The frequency programmer also provides synchronous pulses to control the routing of the detector output to the proper channel of the MCS.

Harmonic Generator

The harmonic generator is a stable tuned oscillator operating in the range of 1.0 to 15.0 MHz which is phase-locked to the RF frequency synthesizer. This allows the selection of any multiple of the synthesizer output frequency from 3 to 17 without changing the programming of the synthesizer. The lock range is approximately 1.0 percent of the output frequency so that the output of the harmonic generator tracks the synthesizer when the frequency is being swept by the programmer. This range is also large enough to allow both lines of a close mass doublet to be swept without retuning.

C-Switching and Drivers

The C-switching and drive unit provides for the separate control of the signals on each C and an individual emitter follower driver for each C. The RF signal from the synthesizer or harmonic generator is fed to a differential amplifier which provides two signals 180 degrees out of phase for the upper and lower C's respectively. A set of matched

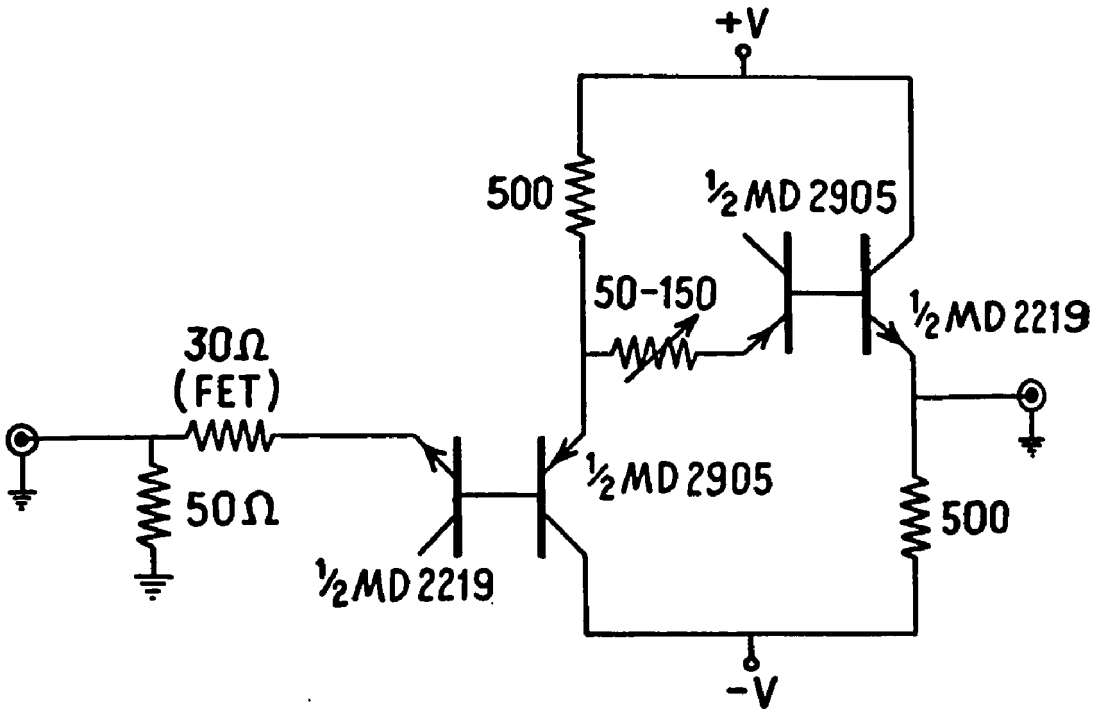

FIG. 28 ZERO OFFSET RF DRIVER.

THE MD2905 AND MD2219 EACH CONTAIN TWO TRANSISTORS ON A SINGLE CHIP. THEY ARE SOLDERED INTO A COMMON HEAT SINK.

FET switches are controlled by the RF gate and select alternately either an inject/eject pulse or the RF voltage to be applied to the C. The switching circuits are followed by balanced dc drivers shown in Fig. 28 which are designed to handle both pulses up to +10 volts and 20 MHz RF while maintaining a net dc offset of 0.0 $\pm$ 0.1 mV over a period of several days. The corresponding output amplitudes of the four drivers are matched to better than 1.0 percent, and at 20 MHz the phase relationships are held to better than 1.0 percent. These specifications are more than sufficient as is indicated by the RF balance tests discussed in Section 5.1.

Overall Performance

The final signal as it appeared on the individual C's was observed using differential oscilloscope techniques and found to be balanced in amplitude and phase to 1.0 percent at 1.0 MHz and 4.0 percent at 20.0 MHz which was the limit of the capability of the oscilloscope used to make the measurements. The rms noise is below 1 mV and most of this is common mode (i.e., identical on all four C's) so that it does not affect the motion of the ions.

3.8 Detection System

The Detector

The detector is a conventional magnetic strip multiplier of the type developed by Goodrich and Wiley (1961). The design of the detector was based on the observation that the detector of Goodrich and Wiley, which was designed to operate in a field of 400 G, could be made to operate in stronger magnetic fields by simply

scaling its size down proportionally and using the same operating voltages. In this manner the parameters calculated by Goodrich and Wiley remain unchanged. The detector (Fig. 29(b)) was constructed from nonmagnetic materials and mounted in a brass box to shield the rest of the experiment from its electric field. The plates were provided by the Bendix Corporation. The operating voltages were supplied by a single Northeast Scientific Corporation regulated high voltage supply and a Zener stabilized voltage divider network. The high voltage supply was interlocked with the vacuum safety to prevent damage to the detector due to vacuum failure.

The output of the detector is dependent on all three of the voltages shown. In operation, the gain of the detector is determined by the dynode voltage, and the bias and field voltages are set to optimize the output. There are two basic modes of operation, pulse and current. Due to the cyclic operation of the experiment itself, all of the data taken on a trapped beam used the detector in the pulse mode. The output pulses as observed on a Tektronix 661 sampling oscilloscope were always approximately 2.0 ns wide at their base when terminated into 50 ohms. This is somewhat smaller than the width reported by others (Heroux and Hinteregger, 1960), and is probably due to the physically smaller size of the detector. Typical peak output pulses (into 50 ohms) as a function of dynode voltage are shown in Fig. 30(b). The majority of the pulses are considerably smaller than the peak pulses as can be seen from the fact that for a given dynode voltage the charge gain for the peak pulses is more than ten times

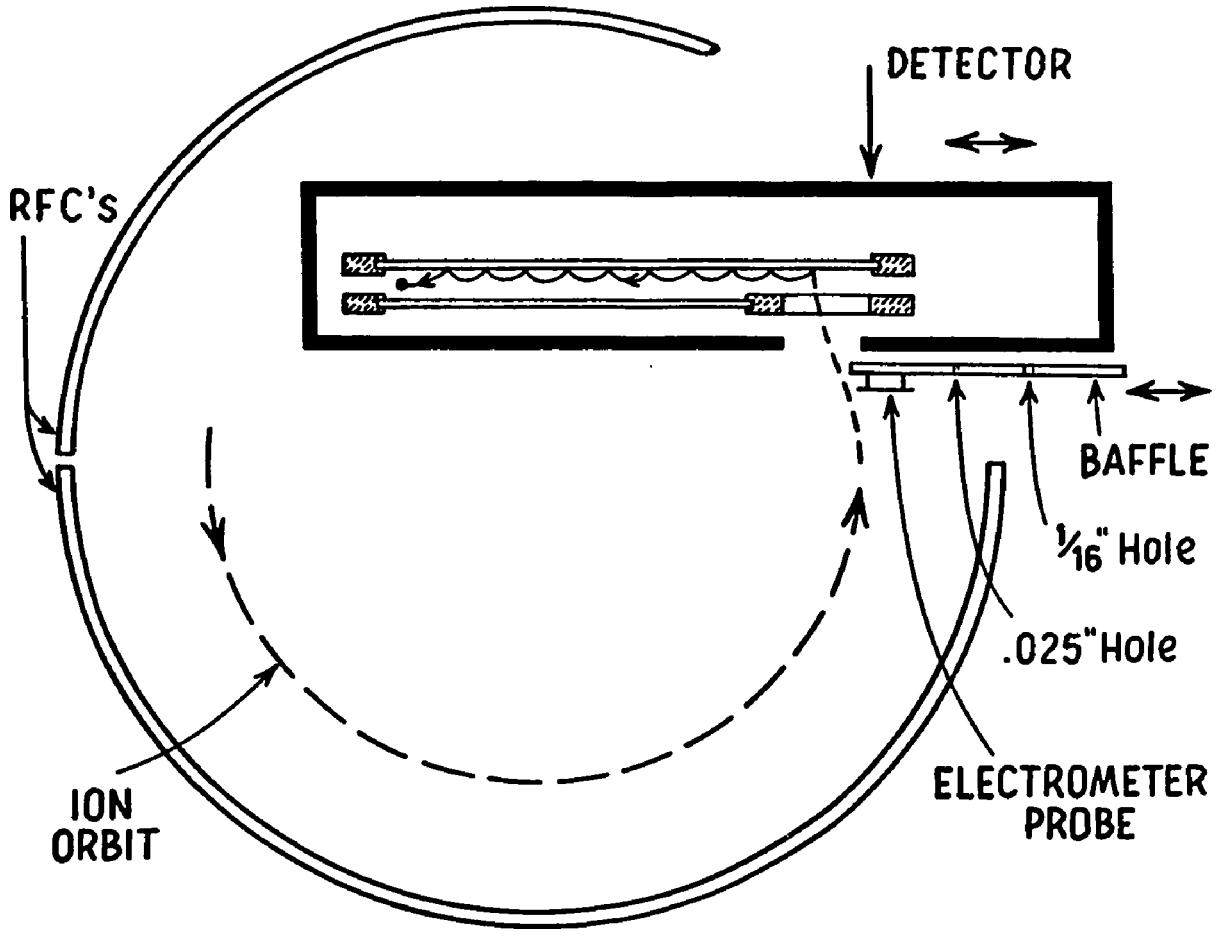

A. DETECTOR LOCATION

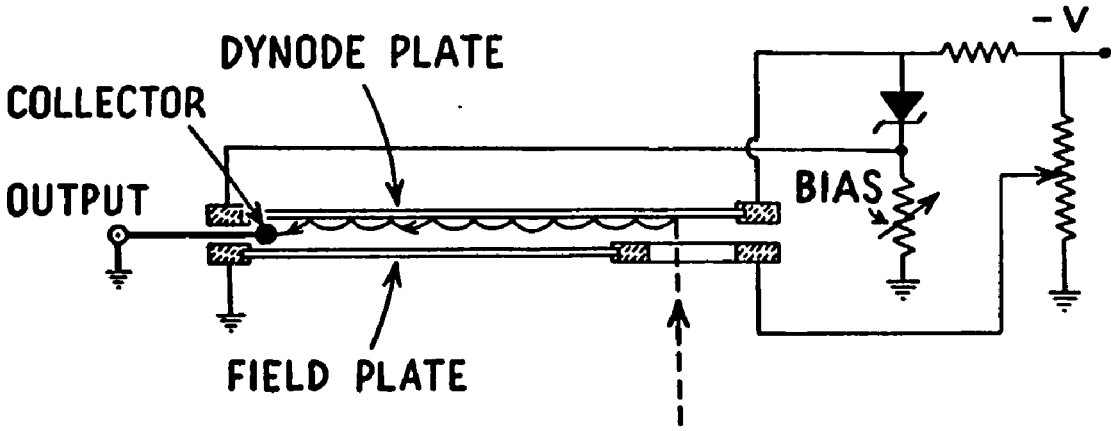

B. DETECTOR DETAIL

FIG. 29 THE DETECTOR.

larger than the current gain. The charge gain is determined by calculating the total area under the current pulse $\Delta Q = I\Delta t$ where I is given by $I = V/R$, V is the observed output voltage, and R is the terminating resistance. If we take $\Delta Q = Ne$ where e is the charge of the electron, then N, the number of electrons in the pulse, is also the change gain of the pulse. For a 1.0 volt pulse into 50 ohms, the charge gain is 1.5×10^8. The output of the unterminated multiplier may be fed into an electrometer where it is integrated into a current. The detector was used in this manner for certain dc beam tests. The current gain as a function of dynode voltage is shown in Fig. 30(a). The current output was kept below 10^{-7} amp to avoid damaging the plates.

The detector is mounted on the faceplate of the vacuum system in the position indicated in Fig. 29(a). The entrance window to the detector is 1.0 cm wide in the transverse plane by 2.1 cm long axially. The axial position of the detector is such that the pitch of the ions as they arrive from the trapping region is approximately equal to the window length. The entire detector can be moved back and forth in a plane transverse to the magnetic field by means of a rack and pinion drive controlled from outside the vacuum system. This system allows the detector to be positioned over a range of radii from 2.9 cm to 6.3 cm with an accuracy of $\pm$ 0.1 mm. The motion is controlled by a knob which is calibrated in units of 0.33 mm. The detector is mounted off center to allow clearance for the center shaft of the NMR mapper.

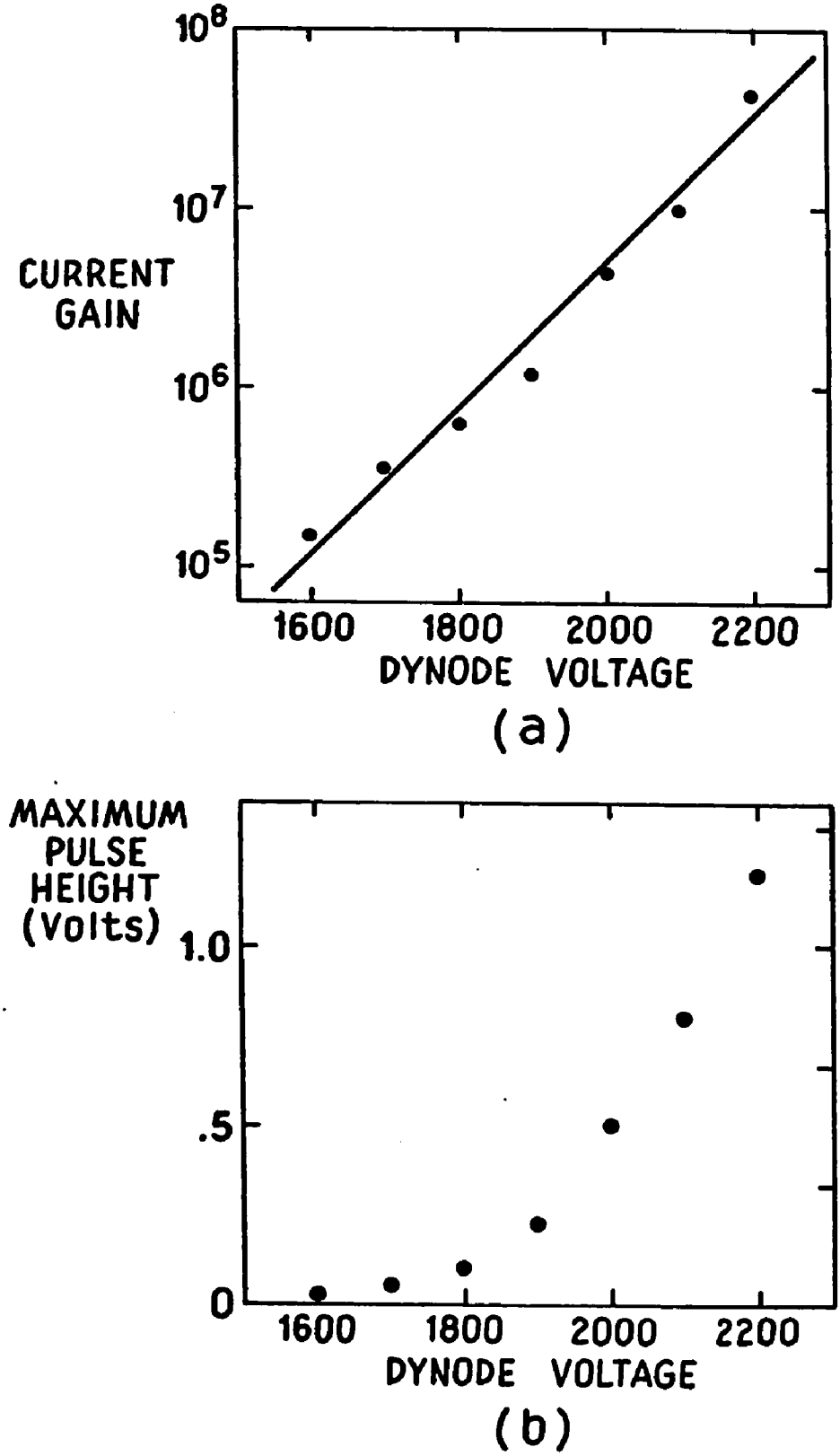

FIG. 30 DETECTOR GAIN VS. DYNODE VOLTAGE.

The detector is equipped with a moving baffle which can be adjusted to cover all or part of the detector window at any detector position. The baffle is driven by a rack and pinion drive similar to that used for the detector motion and also has a setting accuracy of ± 0.1 mm. The baffle has two holes in it with diameters of 1.6 mm and 0.5 mm which were used to limit the input current for certain dc beam studies. The baffle was also fitted with an electrometer probe which is used to align the dc beam.

Electronics

The electronics used with the detector are shown at the bottom of Fig. 26. The multiplier is connected to the first amplifier by a short piece of special low capacitance coax. At the first amplifier a FET switch selects either the amplifier or a direct input to a logarithmic electrometer to monitor the current output. The first amplifier is a Keithley model 111 pulse amplifier with a rise time of 3 ns, voltage gain of 1.0 V, output impedance of 50 ohms, and input impedance of 10 megohms. The input is shunted with a 400 ohm resistor which when combined with the stray capacitance of the input produces the maximum voltage pulse from the charge output of the multiplier within the rise time of the amplifier. Thus the amplifier is used as an impedance converter and provides an effective gain of 8 when compared to a 50 ohm input. This optimizes the signal to noise ratio of the amplifier without sacrificing maximum counting rate. This signal is further amplified and then fed into an MC1440 amplifier/threshold detector where the signal is converted into a DTL logic signal to be used in the data accumulation.

Operation

The detector was normally operated with 1800 to 2000 volts on the dynode. This gave a counting efficiency of about 50 to 90 percent of the particles striking the detector. It should be noted that the configuration of the plates accelerates any positive ion through the dynode potential before it strikes the plate. The non-ion related background was generally less than 100 counts per second. This corresponds to less than 0.1 count per machine cycle since the output is only gated into the counter during the ejection period, and can be compared with data rates of at least 1 count per cycle. The current gain varies across the window by a factor of two since those pulses which travel the greatest length in the detector have the greatest gain. This effect also produced variations in the average counting rate. Since only a small portion ($\leq$ 2.0 mm) of the window was used in taking the resonance data, the effect of this variation was negligible. In order to protect the detector from the full dc beam during the injection period, the baffle mounted on the NMR mapper shaft (Figs. 20 and 25) was pulsed positive. This allowed the detector to be run at higher gain without exceeding its average current rating of 10^{-7} amp.

3.8 Data Acquisition

The acquisition of data consists of transferring output probes from the detector to the MCS channel which corresponds to the frequency or population step being used (Fig. 26). Useful output is available only during the ejection process and the pulses are collected only during a period of approximately 500 μs after the beginning of the

ejection sequence. Due to the slow counting rate of the MCS (100 kHz), data is first collected in a 20 MHz transfer counter during the detector gate period and then regenerated with a slow oscillator and transferred into the MCS during the rest of the cycle.

The data is collected in a Nuclear Data model 1100 multichannel scaler (MCS). The channel of the MCS in which data is stored is advanced sequentially by a signal from either the population or frequency stepping programs. The collection of data begins and ends on a sweep cycle so that only whole sweep cycles are used. The data from frequency sweeps can be stored in each of the two memory halves alternately when determining mass doublets.

The data is a readout on a typewriter using a special data sheet (Appendix V) designed to insure that all of the relevant parameters are recorded. Generally, the data is also displayed on an oscilloscope and a photographic record made.

CHAPTER IV. EXPERIMENTAL PROCEDURE

This chapter discusses the basic procedures used in the operation of the apparatus. A summary of some of the experimental parameters is given in Table IV of Section 5.5. A typical data sheet is shown in Appendix V.

4.1 The Dc Beam in the Trapping Region

The dc beam from the source system (see Section 3.4) must be extracted through the annulus and down to the detector where it is observed as a current with the electrometer probe mounted on the detector baffle (Fig. 29(a)). The beam is extracted by observing the probe current while varying the ion energy T and the main deflection voltage U along with the voltage on the last set of plates. It is generally desirable to peak up most of the other source system parameters. The ion beam enters the trapping region with an axial energy of about 9 eV and an axial energy spread of 2 eV (FWHM). The high axial energy is due to the requirement that the ions have sufficient pitch on their first cyclotron revolution to clear the beam tube. It is interesting to note that the beam retains sufficient helical coherence that it either completely misses the wider eject flag or it can strike the flag and be lost completely. Thus, some optimization of the deflection voltage is necessary to keep the beam from striking the flag. Typical dc beam currents at the probe are 1.0 to 5.0 x 10^{-11} amp. Beams of ions of mass number 1 to 4 have been obtained in the well region.

Once the ion source has stabilized, the stability of the dc beam was good, often varying less than 20 percent in 24 hours.

4.2 Ion Trapping

Procedure

The procedure for setting the detector position is as follows: The detector aperture is formed by one edge of the detector window and one edge of the baffle. The detector is center on the initial beam radius by monitoring the output current of the detector (pulsing the deflection disk to limit the average current) and moving the edge of the detector baffle into the beam until the output current drops to one half of the initial value. This procedure is then repeated for the edge of the window. These positions are then taken as corresponding to the detector being centered on the beam. This is checked by observing that there is no detector output when both edges are returned to these positions thus closing the detector aperture. The aperture is then normally set for $\pm$ 1.0 mm about the beam radius.

Next, the injection pulse is turned on and the amplitude is set to reduce the detector output by one half. This sets the injection voltage at about the mean axial energy of the ions (see Fig. 6). The detector output is then switched to the amplifier and counting circuits so that the trapping rate can be observed on a counting rate meter. The transverse gradient position and strength (coil current) is then varied to obtain the maximum counting rate. At this point it is also necessary to optimize the injection voltage for maximum trapping. The amplitude of the ejection pulse is not critical as long as it is sufficient to eject

all of the ions. It was generally set at 0.4 volts. The machine is now ready to be given over to the RF or population programs for automatic data collection with the MCS.

Protons were usually trapped for 9000 μs as a best compromise between the RF linewidth, the number of ions that could be trapped, and the total running time. At this trapping time, the loss of ions due to background gas scattering is first noticeable at vacuum system pressures of about 1.0×10^{-8} Torr. This is appreciably higher than our normal operating pressures of 2.0×10^{-9} Torr. The typical trapping rates at 9000 μs ranged from a few hundred ions per cycle using the full well to one ion per cycle or less when the ions are limited by the flags for the narrowest resonances (see Fig. 31). Trapping has been observed at 39,000 μs with one-tenth the trapping rate seen at 9000 μs. Some trapping has been observed out to 100,000 μs. Trapping for times longer than 9,000 μs and the usefulness of ions trapped for this length of time is limited by the Ω-motion smearing (Section 4.3) which results in fewer ions getting to the detector. This already presents a problem at 9000 μs.

Ions of mass number 2 were usually trapped for 18,000 μs (thus holding N constant). Due to the fact that their total energy is only one-half that of protons, the effect of stray electric fields was increased and trapping was more difficult. The trapping of ions of mass number 3 or 4 has not been attempted to date.

The stability of the trapping was related to the stability of the dc beam, and the trapping rate changed less than 30 percent in 24 hours once the dc beam and source system stabilized.

Transverse Drifting of the Trapped Ions

The slow drift of the ion orbit centers in the plane perpendicular to the magnetic axis is discussed in Appendix III. These drifts are caused by transverse magnetic field gradients and transverse electric fields. To trap the ions, the external transverse magnetic field gradient is adjusted in strength and direction so that the net drift of the ion orbit centers is zero. This is done by adjusting for maximum counting rate into the detector which is set at the radius of the initial dc beam as discussed at the beginning of this section. An external gradient of about $4M/M_p$ ppm/cm was necessary to trap the ions. The required gradient was always nearly perpendicular to the plane of the RF gap (vertical).

One possible reason for the high magnitude of this gradient is that part of it is required to counteract a transverse electric field in the trapping region caused by stray potential variations between the C's. Comparing Eqs. (III.1) and (III.2) it can be seen that a gradient $\vec{\nabla}B/B_o$ of magnitude 2 ppm/cm has the same effect on the orbit center as an electric field of about 1 mV/cm in the opposite direction. Thus an electric field of up to 2.0 mV/cm could be part of the reason for the high magnetic gradients required for trapping. Such an electric field would imply a potential difference on the C's of 20 mV (Eq. (I.2)). Potentials of this magnitude seem somewhat large but are consistent with the stray contribution to the south end of the well (~ 30 mV).

These potentials are very dependent on the surface conditions of the C's. On one occasion the Aquadag coating on one of the C's was

burnished lightly with a soft paper towel to remove some foreign particles and the apparatus was put back into use. The gradients required to trap the beam became much higher while remaining essentially vertical. This indicates that a very large stray electric potential was present on the C. When this wiping was repeated to make sure that the observed effect was not due to foreign particles, the required magnetic field gradients became even higher. The induced electric potential appeared to be about 400 mV--more than an order of magnitude larger than those estimated to be present under normal conditions. Yet, on visual inspection, the changes in the surface were barely discernible. These electric potentials were never observed to change in time so long as the surfaces were not disturbed.

Equations (III.7) and (III.8) show that the transverse magnetic gradients required to adjust the slow drift of the ions to zero should be independent of the ion mass in the absence of any transverse electric field. But, if an electric field is present, the conditions for zero drift become dependent on the ion mass through the factor $\beta = 2Mc^2/eBr_o^2$. Since the magnetic gradients required are nearly proportional to ion mass, we can conclude that they are serving largely to counteract an electric field.

Similarly, a transverse electric field can be deliberately induced to lower the magnitude of the required magnetic gradient, independent of whether there are any stray electric fields present. Since the required magnetic gradients are essentially vertical, this can be simply accomplished by offsetting the dc bias of the C's by equal

voltages of opposite sign, thus producing an average vertical electric field (Eq. (I.2)). (By keeping the voltages symmetric, the effective potentials of the flags and baffles remain unchanged.) Electric fields of 1.0 to 2.0 mV/cm have been used and the trapped ions behave as predicted.

One result of using these gradients to adjust the drift of the orbit center to zero is the phenomenon of Ω-motion smearing. The radial gradient of the Ω-motion is dependent on the depth of the ion in the well as is indicated in Eqs. (III.6) and (III.8). The result of this is a spreading out of the orbit centers of ions at different levels in the well along a line in the plane transverse to the magnetic field, (their radii remain constant). At the end of the trapping time T, this results in the ions at different levels in the well being smeared out over the detector aperture. Thus they might appear to have different radii. The rate of this smearing for protons is about 0.17 mm/meV or 0.08 mm/ppm of difference in well depth. This means that if a certain level in the well is centered on the detector, those ions 60 ppm higher in the well will have drifted 5 mm off center and will thus appear at a detector position corresponding to a radius which is 5 mm smaller. Experimentally, the effects of this Ω-motion smearing are reduced by using only the bottom of the well and by utilizing the removal resonances which are insensitive to a smearing of the ion beam so long as the ions remain within the detector aperture.

Z-Gradient

The z-gradient provides a means for moving the bottom of the well back and forth axially. Although the gap between the cylinders was

originally at the minimum of the well, various repairs to the solenoid resulted in the gap being off center. The z-gradient allows us to correct this if desired, although the relative position of the gap and the minimum of the magnetic well is not critical. The z-gradient also allows the position of the ion's axial motion within the electrode configuration to be varied, thus allowing the effects of stray potential distributions on the electrodes to be studied.

4.3 Data Collection

The data taken for either a resonance or a population distribution was accumulated in the MCS. This data was printed out on a fixed format data sheet (Appendix V) which insured that all data pertinent to the run was recorded. A Polaroid photograph of the MCS output on an oscilloscope was taken to provide a visual record and allow immediate comparison of various data sets. The field maps were recorded on separate data sheets.

4.4 The Axial Motion of the Ions in the Well

There are two observable quantities associated with the axial motion of the ions in the well: (1) the endpoints of the motion, (2) the frequency of axial oscillation. The first can be investigated using the flags in conjunction with the determination of the population distribution in the well. The second is determined using an axial resonance process.

Population Determinations and Use of the Flags

The method of determining the population density in the well is discussed in Section 2.1. This technique measures the depth of the

ions below the south peak of the well in energy units, (the south peak is kept purposely lower than the north peak). Unfortunately the peaks are not very well defined since the azimuthal asymmetries about the mechanical center increase substantially at the inflection points due to the relatively low length to diameter ratio of the solenoid. In order to better understand the population distribution, the flags were introduced to provide calibration points. Using the flags we were able to determine that there was a stray electric potential distribution present which lowered the south peak of the well by about 30 mV. Systematic studies have eliminated all possible causes of this potential other than surface and contact potential variations.

The flags also served to limit the population of the well to the very bottom where it produces a contribution of only a few ppm to a 20 ppm resonance line. Using the flags to limit the population in a relatively deep well is more satisfactory than trapping in a shallower well because ions filling a shallower well would not lend themselves to the approximations of Section 2.4, would tend to have severe Ω-motion problems (Appendix III), and the top of the well would still be poorly defined and subject to distortion by electric potentials. Using the flag, the population can be determined from the obvious starting point at the flag (see Fig. 32).

Axial Resonance

The axial motion of the ions in the well may be resonated much like the RF cyclotron resonance by applying an audio frequency voltage

to either the injection or ejection cylinder while the ions are confined in the well. When the applied frequency is equal to the axial frequency of the ions (~ 3 kHz), an ion can gain axial energy each time it passes through the trapping gap and eventually gain enough energy to strike the flag or leave the well. The width of this resonance process is given approximately by $\delta f/f \cong 1/N' \cong \tau/T$ (FWHM) where τ is the axial period of the ions and N' is the number of axial cycles in the trapping time T. For the usual values of T = 9000 μs, we have $\delta f/f = 0.03$. This is in good agreement with the experimental observations. With the flag limiting the population to the bottom of the well, less than 0.3 mV peak-to-peak audio voltage is required. The resolution can be further improved by using odd harmonics of the axial frequency. The third and eleventh harmonics have been used successfully.

The axial resonance process provides an experimental measurement of the period of the axial motion of the ions in the well which can be compared with the expected value calculated from the magnetic field maps using Eq. (2.15). This comparison gives us an indication of whether or not the ions experience the magnetic potential well.

4.5 Cyclotron Resonances

Cyclotron resonances were generally observed using removal resonances (Fig. 13) although inward and outward resonances were also used for systematic studies (Fig. 12). The resonant behavior of the ions was found to be in good agreement with the predictions of Section 2.3. Most of the resonance work was done using 9000 μs trapping times and the

eleventh harmonic of the cyclotron frequency (11 x 1.2 MHz). Thus we have N = 10,000 and $1/(2n + 1)N$ = 9 ppm. This resulted in removal resonance lines which were about 20 ppm wide (FWHM). Certain resonances (see Fig. 34) had sufficient resolution to show the sidebands indicated in Fig. 13. The shape of the removal resonance lines was more trapezoidal than predicted by the theory even when using a first harmonic resonance (150 ppm FWHM) with a population distribution which was only a few ppm wide. These shapes were found to be dependent only on the details of the ejection procedure. The resonances might have been made even narrower by increasing either the harmonic order or the number of cycles, but increasing the harmonic order significantly would require unreasonable RF voltages (see Fig. 15), and increasing the number of cyclotron revolutions would result in difficulties in trapping sufficient numbers of ions. The present linewidths allow the medians of the cyclotron resonance lines to be determined to sufficient accuracy so that the measurements of μ_p/μ_n are limited by other errors.

The RF field is applied to the ions only between the end of the injection pulse sequence and the beginning of the ejection pulse so that the observed cyclotron frequencies are not perturbed by the fields associated with these pulses.

It proved desirable to work with removal resonances as compared to other forms of observing resonance for several reasons: (1) The detector position is fixed allowing rapid repeaking of the trapping rate. (2) Reproducible resonances and proper settings of the transverse

magnetic gradient were much easier to establish (Section 5.1). (3) The average trapping rate is indicated by the shoulders of the resonance lineshape. (4) The resonance process is relatively insensitive to the radial distribution of the ions (Section 2.3), the RF amplitude, and other variables of the experiment. (5) Systematic shifts in the cyclotron frequency due to the change in radius are insigificant (Section 2.4). (6) The small change in radius which is symmetric about the initial radius is more consistent with the assumption in the theory that the radius of the ions is constant (Section 2.3).

The median $\tilde{\nu}$ of the resonance lines were generally determined by eye. The resonance lines had sufficient symmetry that this could be accomplished to within $\pm$ 0.4 ppm ($\pm$ 1/2 frequency step).

4.6 Determination of μ_p/μ_n

Field Mapping and Computation of $[\omega_s(z_1)]$

The magnetic field was mapped either just before or just after a determination of $\tilde{\nu}$ from a resonance line was made. This mapping was carried out within the apparatus while it was under vacuum using the NMR mapper probe. Thus a rapid mapping of the field could be carried out *in situ*. The mapper probe was moved in 1.0 cm steps along an axial scale. At each axial position, the mapper head was rotated to each of four azimuthal positions and a measurement of $\omega_s(z,\theta)$ was recorded. The resonance center was automatically locked-in and the frequency was read directly from the Hewlett-Packard frequency counter to the nearest Hz (at about 3.3 MHz). A complete field map took about one-half hour to complete. One such field map is graphed in Fig. 31.

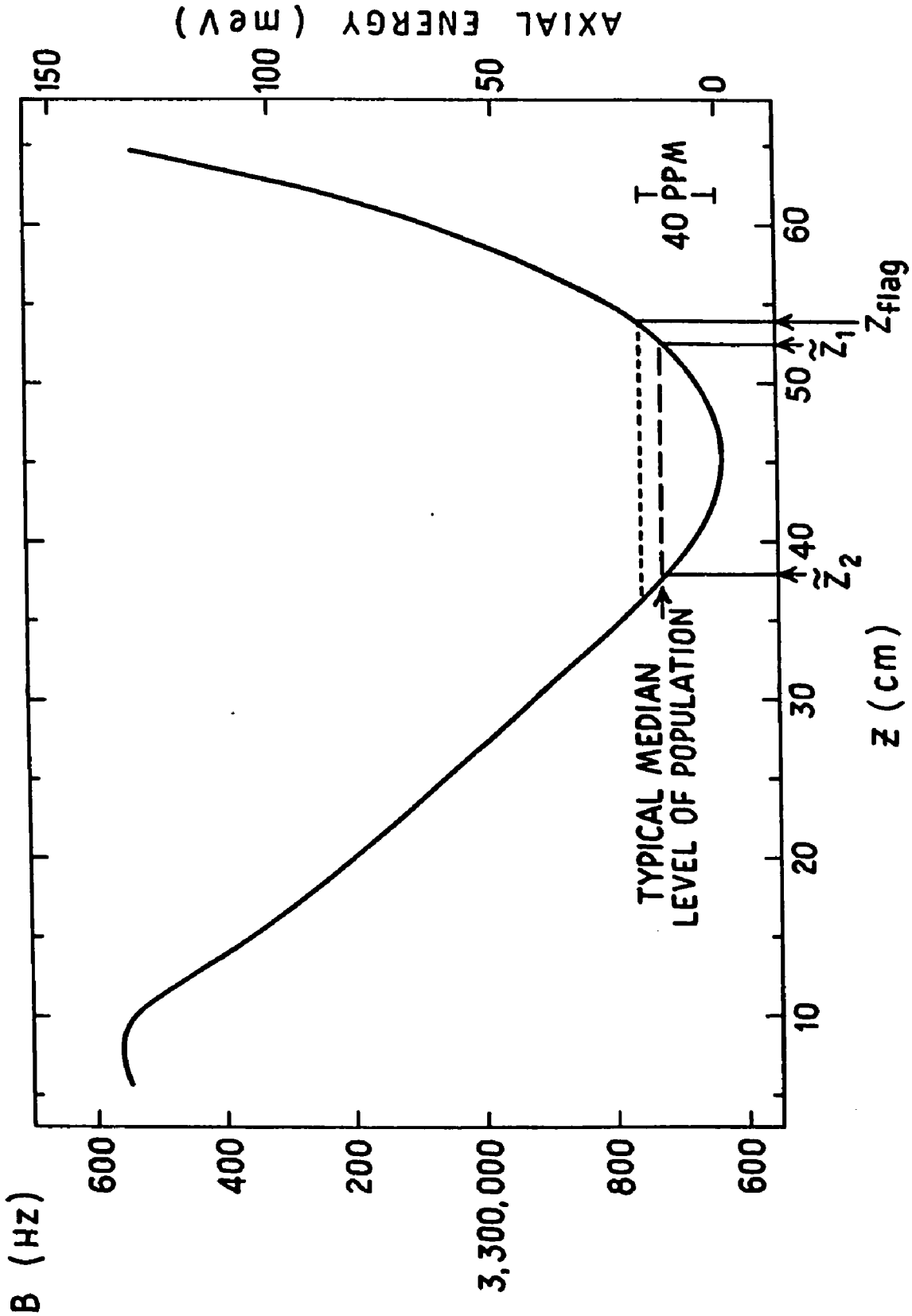

FIG. 31 THE MAGNETIC FIELD IN THE TRAPPING REGION.

The results of the map were used to compute the values of $[\omega_s(z_1)]$ and the period $\tau(z_1)$ for various levels in the well by numerical integration of Eqs. (2.18) and (2.15) respectively with the aid of a computer. The program first averaged the four azimuthal measurements at each axial position to obtain $\omega_s(z)$ (Eq. (2.13)).

Procedure for Determining $[\tilde{\omega}_s]$ in Data Runs

This section will specifically describe the steps used in determining $[\tilde{\omega}_s]$ from the population distribution and the field maps. These steps are summarized in Table 1. A typical population distribution used to obtain a resonance line is shown in Fig. 32. This is simply

$$N(V_e) = \int \rho(V_e)\, dV_e$$

as disucssed in Section 2.2. The voltage steps on the horizontal scale are controlled by the population programmer (Section 3.6), and are measured on an oscilloscope. The very sharp break in the curve at N_{min} corresponds to the position of the flag in the well. The point at which this break occurs is defined as $V_e(\text{flag})$. The median of the ejection voltage $\tilde{V}_e$ is defined by

$$N(\tilde{V}_e) = \frac{N_{max} + N_{min}}{2} . \qquad (2.16)$$

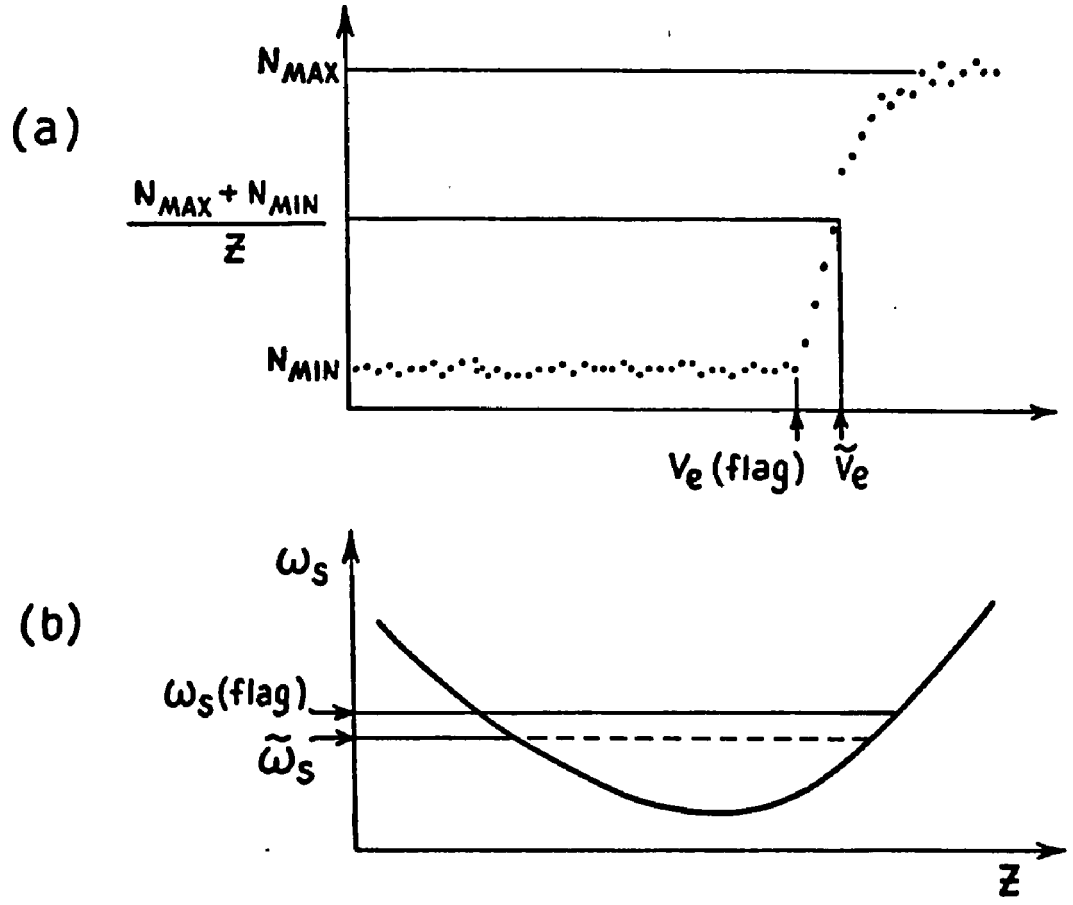

FIG. 32 A TYPICAL POPULATION AND MAGNETIC WELL.

Table I

Procedure for Determining $[\tilde{\omega}_s]$

1. Determine $\tilde{V}_e$ using $N(\tilde{V}_e) = (N_{max}-N_{min})/2$.
2. Determine $\Delta V_e = \tilde{V}_e - V_e(\text{flag})$ in units of the voltage step size.
3. Convert to a voltage by multiplying by the step size in volts.
4. Calculate $\Delta\omega_s = e\Delta V_e \omega_s/T_1$ (Eq. 2.4).
5. Determine $\omega_s(\text{flag})$ from the field map.
6. $\omega_s(\tilde{V}_e) = \omega_s(\text{flag}) - \Delta\omega_s$.
7. Compute $[\omega_s(\tilde{V}_e)]$ from the field map using Eq. (2.9).

Extrapolation

In order to determine μ_p'/μ_n, the observed value of $[\tilde{\omega}_s]/(\tilde{\nu}/2n + 1)(M/M_p)$ obtained for H^+ and H_2^+ ions was extrapolated as a function of mass to M = 0. It is important to insure that the value of $[E_r]$ experienced by the ions of both masses remains constant. Since $[E_r]$ is a function of the axial position of the ions in the well, the ions must be trapped at the same levels in the well with the same endpoints.

4.7 Measurements of Mass Differences

In order to establish a pair of resonances corresponding to a mass doublet, a removal resonance is first established with one of the species. Then, the second gas is simultaneously introduced into the ion source and the second resonance line is located. The mixture of the two gases is adjusted until the relative amplitudes of the two resonances are approximately equal. Since, when resonating one specie, the other remains in the well and is detected on ejection, the ideal minimum for each line of the doublet is 50 percent instead of zero as it is in a single removal resonance (see Fig. 13). Unfortunately, any change in the source gas results in changes in the source output energy distribution so that the source parameters must be readjusted, while trying to balance the gases.

Once suitable resonances are established and their centers estimated, each is collected in one of the 128 channel halves of the MCS memory.

These resonances are then compared using a fitting procedure which shifts their relative amplitude and position and fits their difference to a straight line. This assumes that the two lines have the same shape.

Again, the removal resonance is the logical choice. The relative insensitivity of the removal resonance to the other parameters is particularly desirable for avoiding systematic shifts. Although in principle the linewidth could be reduced as discussed in Section 4.5, the counting rates are already minimal, and a reasonable doublet with 128 points on each resonance line takes eight hours to collect.

CHAPTER V. ERRORS, RESULTS, AND CONCLUSIONS

In this chapter we discuss the errors in the observed quantities $[\tilde{\omega}_s]$ and $[\tilde{\omega}_c]$, and the final results for μ_p'/μ_n and the mass difference of the H_2^+–D^+ doublet. Finally the possibility of continuing these measurements both with the present apparatus and a new apparatus is discussed.

5.1 The Systematic Study of the Resonance Lines and the Error in $[\tilde{\omega}_c]$

There are two shifts in the observed frequency $\tilde{\nu}$. The relativistic shift due to γ which is small, and the electric field shift (Section 2.7). The latter point is considered in Section 5.3 since a knowledge of the spin frequency $[\tilde{\omega}_s]$ is required for our particular method of handling this.

This section consists of a discussion of the many systematic studies that were carried out. Other than those mentioned above, we never observed any systematic dependencies of $\tilde{\nu}$ on the apparatus parameters. There is no appreciable error in the frequency ν of the applied RF field. Since the NMR regulation is derived from the synthesizer frequency base, we only use the synthesizer to establish frequency ratios. This was accomplished to better than one part in 10^8. The only appreciable error in determining the median of the 20 ppm wide resonance lines is the error in visually splitting the line into two halves. This is taken as $\pm$ 0.4 ppm ($\pm$ 1/2 step). The resonance lines have very good symmetry and perhaps they could be split to even higher

accuracy, but it was not necessary for the present experiment. Once a resonance was established, there was never any shift noted at the 0.4 ppm level unless there was an obvious cause (i.e., power failure). Thus we conclude that for the removal resonances used, $[\tilde{\omega}_c] = \tilde{\nu}/(2n + 1)$, with an assigned error of ± 0.4 ppm.

Relativistic Correction

In order to account for the relativistic change in the cyclotron frequency ($\omega_o = \gamma\omega_c$) we must determine

$$\gamma = (1 - v^2/c^2)^{-1/2} \quad . \tag{5.1}$$

Since $v^2/c^2 \tilde{=} 10^{-6}$ we may write

$$\gamma = 1 + \frac{1}{2} v^2/c^2 \quad . \tag{5.2}$$

But, $v \tilde{=} r\omega_c$ so that this may be written

$$\gamma = 1 + \frac{1}{2} r^2\omega_c^2/c^2 \quad . \tag{5.3}$$

The cyclotron frequency is very well known from the resonance line, and the initial value of r is set by the annulus at 4.04 ± 0.02 cm (Section 3.6). Thus we find $\gamma(H^+) = 1 + 0.5$ ppm, and $\gamma(H_2^+) = 1 + 0.12$ ppm. Due to the small value of $\gamma - 1$ it is not necessary to correct it for the small change in r at resonance.

Systematic Shifts Due to the Change in Radius

One particularly instructive set of resonances is shown in Fig. 33.

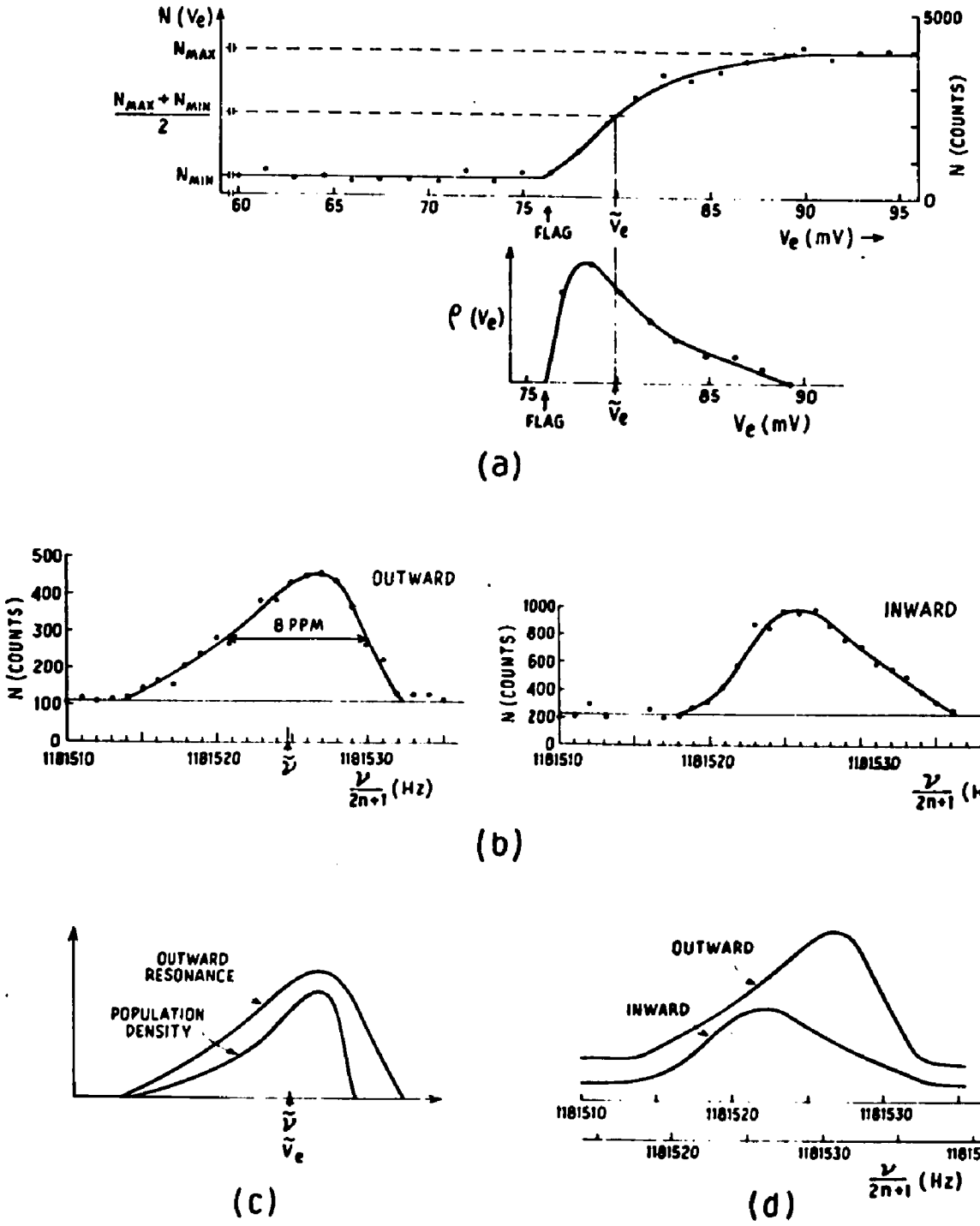

FIG. 33 INWARD AND OUTWARD RESONANCES. (a) POPULATION DISTRIBUTION (b) RESONANCES OBTAINED. (c) POPULATION FITTED TO THE OUTWARD RESONANCE. (d) INWARD RESONANCE SHIFTED TO ALIGN IT ON THE OUTWARD RESONANCE.

The figure shows a well population along with the inward resonances and outward resonances obtained from it. The population is limited by the north flag and has a width of only 6 meV (FWHM). This corresponds to a spread in $[\omega_s(z)]$ of 6 ppm. The detector is set for a 5.0 mm change in radius with an aperture ΔR = 2.0 mm. For an outward resonance, the resonant ions move to slightly lower levels in the well and experience a decreasing field since $[dB/dr] < 0$ (Section 2.4). Thus we expect a decrease in the observed cyclotron frequency or resonance.

For an inward resonance, these effects reverse, with the resonant ions moving to a higher level in the well and experiencing an upward shift in their cyclotron frequencies. However, when the ions move upward in the well those near the top strike the flag and are lost. This along with the details of the orbital and axial motion of the ions is the apparent cause of the slope on the right-hand side of the inward resonance.

The population is shown fitted to the outward resonance by matching the medians in Fig. 33(c). If we assume rms addition of the width σ_ρ of the density function $\rho(\omega_c)$ and the width σ_F of the RF lineshape $F(\nu)$, then the width σ_f of the expected lineshape $f(\nu)$ is given by

$$\sigma_f^2 = \sigma_\rho^2 + \sigma_F^2 .$$

Taking σ_f = 8 ppm and σ_ρ = 6 ppm, we have σ_F = 5 ppm which is in good agreement with the theory of Section 2.3 as may be easily seen from Fig. 12(c) with $r_1 \cong 1.25\ \Delta R$ and $1/(2n + 1)N$ = 9.0 ppm.

These resonances can be used to verify the approximations of Section 2.4. The two resonances are shown superimposed in Fig. 33(d) with their frequency scales shifted by 4.0 Hz or 3.4 ppm. This matches the points at which both resonances come out of the noise. The amplitudes are arbitrarily chosen so that the left-hand slopes are comparable. This is taken to indicate a net shift of each resonance by 1.7 ppm from the mean. From Section 2.4, we would expect a shift of 1.25 ppm due to the change in the axial motion of the ions while dB/dr is expected to produce an additional shift of 0.8 ppm. Thus we expect a net shift of 2.05 ppm from the mean. This is in reasonable agreement with the experimental measurement of 1.7 ppm. The typical removal resonance with only one-fifth of the change in radius would result in shifts of at most 0.3 ppm, but due to the symmetry of this resonance process the net result is only a slight broadening of the resonance line.

Detector Positioning and Transverse Gradient Setting

In order to properly adjust the drift motion of the trapped ions to zero, the detector must be correctly positioned and the transverse magnetic gradient adjusted to position the beam on the detector. It is possible to misalign the transverse magnetic gradient and detector position settings, but it was found that if the detector was correctly positioned and the gradient was not properly adjusted, the symmetry of the lineshape was lost and one shoulder of the line became higher than the other. Once the gradient and detector settings were established,

the detector could be moved ±0.3 mm without changing the lineshape or the line center (the normal reproducible setting accuracy is ±0.1 mm). Again, if the settings were varied beyond this, the lines became noticeably distorted. Thus, it is impossible to accidentally disrupt the settings without knowing it.

It is also possible to completely misalign the beam by incorrectly setting the detector aperture and then use the transverse gradient to align the ejected ions on it. It was found that with the detector displaced by an extreme distance of 5.0 mm, the net change in the determination of $[\tilde{\omega}_s]/[\tilde{\omega}_c]$ was only 3.0 ppm. Furthermore, the lineshape was not satisfactory. Thus it can be concluded that the normal setting accuracy of ±0.3 mm does not introduce an error in $[\tilde{\omega}_c]$. Increasing the detector aperture to ±2.0 mm did not cause any shift in $\tilde{\nu}$. No wider apertures were tried.

Slow Ion Drifts in the Field

One particularly important question is whether or not the ions are undergoing a slow drift in the magnetic field due to the various forces discussed in Appendix III. This might result in a slow drift in the value of the time-average magnetic field which the ion experiences during the time that the RF field is applied. To check for this, resonances at the 11th harmonic were run at both 5000 μs and 9000 μs with only the RF amplitude changed. If a slow drift were occurring, it should produce a frequency shift between the medians of

these two resonances, but no shift was observed at the 0.4 ppm level. This test is a positive indication of our understanding of the slow drifts of the ions in the field during the usual 9,000 μs trapping interval.

Details of the Trapping Cycle

On various occasions, resonances were observed as a function of the details of the ejection process (single ejection pulse, double ejection pulse, the timing of the pulses, etc.). These changes did not produce any observable changes in the value of $\tilde{\nu}$, but they did produce symmetric changes in the lineshape.

RF Amplitude

On several occasions the dependence of a removal resonance on the amplitude of the applied RF voltage was checked. The results of one such check is shown in Fig. 34(a). Note that for the lower RF voltages the lineshape shows some structure due to the population distribution of the well. This structure disappears as the RF amplitude is increased. However, the median value $\tilde{\nu}$ remains the same within the observed accuracy (0.4 ppm).

It is noted in Section 2.3 that even harmonics can be observed, but that they would not be as stable as the odd harmonics. In fact observed lines at the 10th harmonic exhibit a shift of 2 ppm over a 2:1 range of RF amplitude.

There is also the possibility of a time variation in the RF amplitude while the data for a given resonance line is being accumulated.

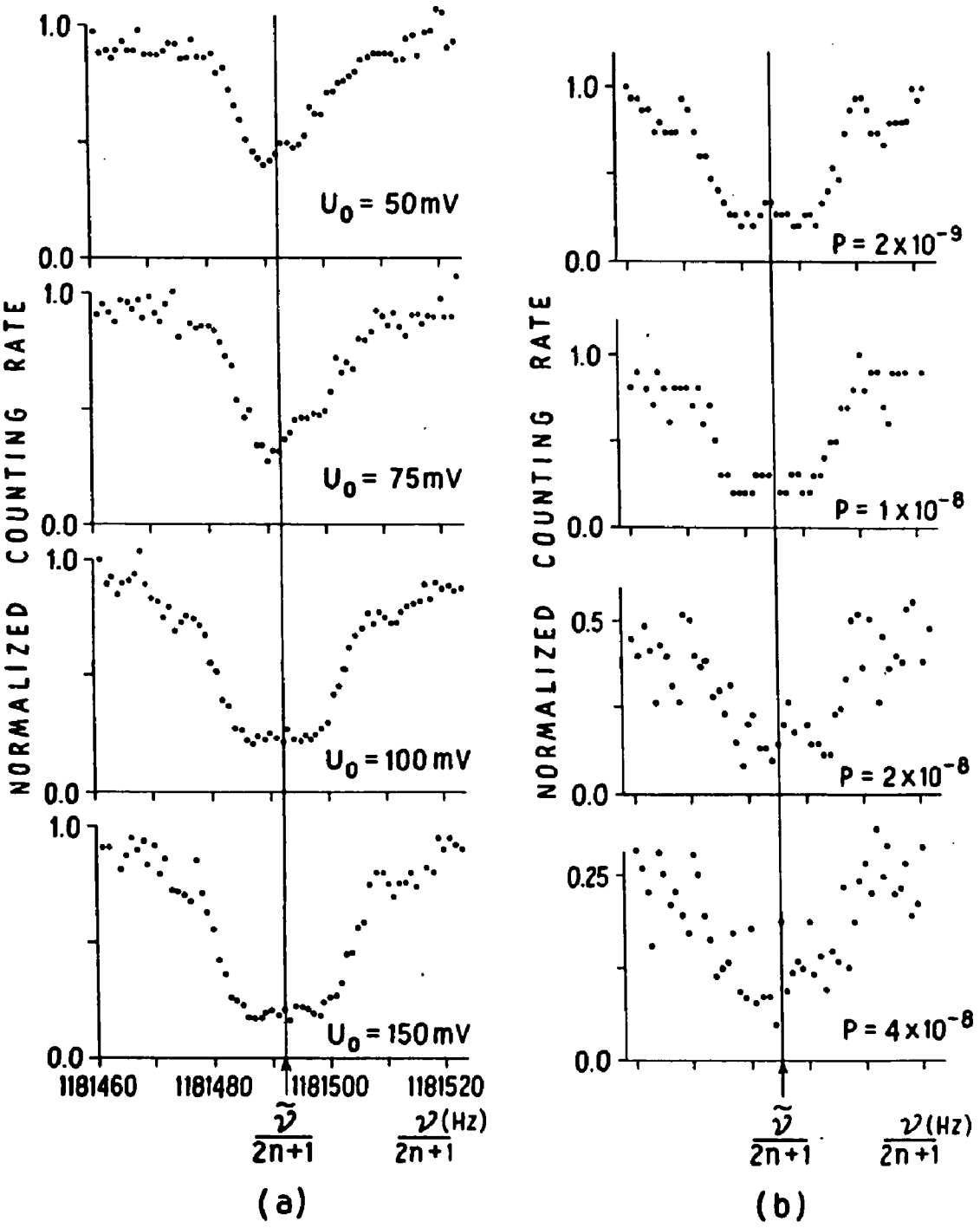

FIG. 34 REMOVAL RESONANCES. (a) AS A FUNCTION OF RF VOLTAGE. (b) AS A FUNCTION OF VACUUM SYSTEM PRESSURE.

The RF amplitude remained constant to at least one percent over the time it takes to obtain a resonance line. Since the removal resonance is insensitive to variations in RF amplitude and the resonance line is the total of approximately one hundred identical sweeps, it is concluded that any time variation of the RF amplitude should have negligible effect on the final resonance line.

RF Balance

Experimentally, the RF electric field of the four C's will not be that of two infinite half cylinders because they are both separately driven and mechanically imperfect. Thus, although the RF balance of the system was considered more than adequate, the effects of possible imbalances were experimentally investigated. For example, when the amplitude of the RF voltage on the ejection C's was increased 50 percent and the phase shifted by 18 degrees with respect to the injection C's or vice versa, there was no change in the line center at the 0.4 ppm level. Similarly, when the upper C's were shifted 20 percent in amplitude and 8 degrees in phase with respect to the lower C's or vice versa, no shift was observed in the resonance line. Since this last test was made with the flag in place and grounded, the flag was no longer on the RF zero equipotential. Thus this test also shows that some distortion of the RF field at the flag does not produce a shift in the resonance line center. When even greater imbalances were induced the lineshapes were noticeably distorted.

We conclude that the normal adjustment of the RF voltages on the C's to a few percent (Section 3.6) is more than sufficient for the accuracy of this experiment.

Background Vacuum System Pressure

In one run a typical resonance line was observed as a function of the vacuum system pressure. The eject flag was used to limit the level of the ions in the well to at most 40 ppm. The resonance lines obtained at various pressures are shown in Fig. 34(b). Notice that at 1.0×10^{-8} Torr the minor features of the lineshape are beginning to wash out although the trapping rate is just barely affected. At slightly greater pressures the trapping rate falls off and the resonance line is quickly obscured. However, there is no evidence of a shift in the line center due to the vacuum system pressure at the 0.4 ppm level.

5.2 Errors in Determining $[\omega_s(\tilde{z}_1)]$

In this section we will discuss the errors in computing the value of $[\omega_s(\tilde{z}_1)]$. This discussion can be divided into six categories:

(1) The systematic errors in determining the values of $\omega_s(z)$ with the NMR probe which correspond to the position of the trapped ions in the field.

(2) Errors in the computation of the time-average values $[\omega_s(z_1)]$ from $\omega_s(z)$ using Eq. (2.18).

(3) The errors in determining the position of the flag $z_1(\text{flag})$.

(4) The errors in determining $\omega_s(\tilde{z}_1)$ using the procedure outlined in Table I.

(5) Systematic study of the error in (4) above due to the deviation of the actual potential from the magnetic well potential.

(6) Calibration of the mapper probe to a standard spherical water sample.

Systematic Error in $\omega_s(z)$

There is no significant contribution to the error in $\omega_s(z)$ from attempting to set the mapper head radius equal to the ion radius. Measurements made with the mapper head at r_o = 3.45 cm along with the usual r_o = 4.05 cm showed dB/dr to be approximately 1 ppm/cm as predicted in Section 2.4 and verified by means of the resonance data in Section 5.1. This results in no appreciable error due to the radial positioning of the mapper head at the limit of the positioning error ($\pm$0.5 mm).

The transverse magnetic field gradient across the orbit could introduce a significant error in $\omega_s(z)$ if the mapper axis were displaced from the orbit center. In certain cases with mass 2 ions, these gradients, which are necessary in order to trap the ions, (see Section 4.2) are as large as 60 ppm across the diameter of the orbit or about 8 ppm/cm. The mapping assembly is centered within the C's to an accuracy of $\pm$1 mm. Thus an error as large as $\pm$1 ppm might occur with mass 2 ions. However, since the direction of these gradients is essentially constant and their magnitude proportional to the ion mass, this error is removed to a first approximation by the extrapolation.

Flag Position Calibration

The positions of the flags are calibrated by bringing them into ohmic contact with the front of the mapper head. The difference between the front of the mapper head and the center of the sample (1.10 cm) is then added to the mapper position to determine the flag position. The flag positions are then reproduced using a calibrated measuring rod. The overall error in determining the relative positions of the flag and mapper head is ± 0.5 mm or ± 0.5 ppm using $d[\omega_s]/dz = 5$ ppm/cm.

Errors in Computing $[\omega_s(z_1)]$

A complete field map consisted of four equally spaced azimuthal measurements (0, 90, 180, and 270 degrees, where 0 degrees is vertically upward) repeated in 1.0 cm steps in the z-direction over the effective length of the well. A complete set of measurements took about one-half hour to complete.

The θ positions are established by 8 equally spaced mechanical detents. No shift at the level of 1.0 Hz (0.3 ppm) was ever observed due to the azimuthal positioning by the detent. The sufficiency of 4 azimuthal measurements to determine $\omega_s(z)$ was tested on several occasions when measurements were made at all 8 positions. The values of $[\omega_s(z_1)]$ obtained from the data at 0, 90, 180, and 270 degrees were compared with those obtained from the data at 45, 135, 225, and 315 degrees. These results differed by a value of 0.1 ppm to 0.4 ppm.

The setting of the axial positions were reproducible to at least ± 0.5 mm. Since dB/dz is at most 10 ppm/cm in the regions of the well

used, this would result in a maximum error of ± 0.5 ppm. Since these errors are random, they would not contribute significantly to a given measurement of $[\tilde{\omega}_s]$. However, in determining the value of $\omega_s(z_1)$ corresponding to a certain flag position (step 5 in Table 1) the entire error appears, but it is essentially halved by the time-averaging.

The reproducibility of the values of $[\omega_s(z_1)]$ as computed using Eq. (2.18) is excellent. On several occasions, maps made from one hour to one day apart were compared and the values of $[\omega_s(z_1)]$ agreed to within 1.0 ppm although the agreement was usually much better. An error of ± 0.5 ppm is assigned as the rms error in the computation of $[\omega_s(z_1)]$.

Summary of the Errors in the Determination of $[\omega_s(\tilde{z}_1)]$

The effect of the preceding errors on the determination of $[\omega_s(\tilde{z}_1)]$ by the procedure outlined in Table I will be summarized by discussing each point of that table in turn.

(1,2) The number of voltage steps in ΔV_e is counted from a photograph. The error in this procedure is judged to be ± 0.5 step. This results in a final error in $[\tilde{\omega}_s]$ of less than 0.5 ppm. The presence of any ripple on the population pulser output can introduce an error in the determination of ΔV_e. On one occasion, a 3-mV peak-to-peak 120 Hz ac voltage was superposed on the population pulse signal fed to the ejection cylinder. This produces a broadening of the population density by about 2.4 mV. Thus while $\bar{V}_e$ remained the same, ΔV_e increased by 1.2 mV.

Since it is ΔV_e that is used, this would produce an error of 1.2 M/M_p ppm in the determination of $[\tilde{\omega}_s]$. The ripple was kept below 0.5 mV in order to keep this error negligible.

(3) The step size is determined to an accuracy of 2 percent by direct observation of the signal on the C's using an oscilloscope.

(4) Since ω_s is very well known from the field maps, the only additional error is due to $T_\perp$. The transverse energy is given by $T_\perp = 1/2\ Mv_\perp^2 = 1/2\ Mr_o^2\omega_c^2$. The only significant error is in r_o which is given by $r_o = 4.04 \pm 0.02$ cm (Section 3.6). This produces an error in $T_\perp$ of ± 1.0 percent, but introduces no significant additional error in the determination of $[\tilde{\omega}_s]$.

(5) The error in ω_s(flag) is given earlier in this section as ± 0.5 ppm.

(7) The direct error in the computation of $[\tilde{\omega}_s]$ is the sum of the random and systematic errors discussed at the beginning of this section and is 0.5 ppm.

The final error is given essentially by items (1), (5), and (7), so that the rms total is 0.9 ppm. We must add to this any error in the assumption that the potential well is given by the magnetic potential which is discussed in the next paragraph.

Error in Time-Averaging Due to Electric Potentials

The shape of the axial potential well is of extreme importance in averaging the spin frequency $[\omega_s(z_1)]$. The potential well is given by

$$U(z) = -\frac{T_\perp(z_1)}{\omega_s(z_1)}\{\omega_s(z_1) - \omega_s(z)\} + V(z) \qquad (2.11)$$

where the first term on the right describes the magnetic potential well and the second is any axial electric potentials which are present. For this experiment $T_\perp \cong 475\ M_p/M$ eV and $\{\omega_s(z_1) - \omega_s(z)\}/\omega_s(z_1)$ is 40 ppm or less when the ions are confined to the bottom of the well by the flags. If we assume $V(z)$ to be negligible, averaging over the magnetic potential well results in values of $[\omega_s(z_1)]$ which vary by only 22 ppm from the bottom of the well to the flag. This would allow us to assign an absolute error of ± 11 ppm to the determination of $[\omega_s(\tilde{z}_1)]$ with no knowledge at all of the population distribution in the well. The measurement of $\tilde{V}_e$ and thus $\tilde{z}_1$ (Section 4.6) should allow us to further reduce this error to below ± 1.0 ppm. However, the axial energy of protons just below the flag is only 20 meV while those lower in the well have proportionally lower energies. Thus axial electric potentials of the order of millivolts can cause significant changes in the axial motion of the ions. Yet, such small potentials can easily be caused by stray surface and contact potential differences. These electric potentials affect the average of $[\omega_s(z_1)]$ by changing the velocity $v_z(z)$, (Eq. (2.16)), and the endpoints z_1 and z_2, but the values of $\omega_s(z)$ over which the averaging is done remain the same. These problems did not affect previous Michigan g-factor experiments since $T_\perp$ was approximately two orders of magnitude larger than in this experiment.

The direct determination of the population distribution in the well using $N(V_e)$ (Section 2.2) indicated that the ions occupy only the top half of the available well below the flag. Eighty percent of the ions were in the top quarter of the well. This leads one to be suspicious of either the true distribution of the ions in the well or the shape of the well. The width of the ion distribution is confirmed by the resonance lineshapes (see Fig. 33), and a second population determining procedure which uses the flag as the measuring point rather than the top of the well. The relative position of the distribution was also verified by this last technique. The location of the ions just below the flag is further verified by the extremely small audio voltages necessary to cause the ions to strike the flag using the axial resonances. The final conclusion is that the function $N(V_e)$ accurately represents the position of the ions in the well.

There are indications of appreciable stray electric potentials in the well region. The south peak of the well was consistently about 30 mV lower than expected from the magnetic potential well. However, this would not necessarily cause an appreciable effect on the motion of the ions since they are at least 20 cm from the south peak and the effects of this potential would be negligible. The final extrapolation of the data to μ_p'/μ_n indicates a time-average radial electric field of (2.3 ± 1.1) mV/cm. This in turn implies at least local axial electric fields and of course an associated potential distribution. These potentials cannot be measured directly, but we can investigate the axial motion of the ions. This may be done in two ways:

(1) Determination of the endpoints of the motion using the flags.

(2) Measurement of the period of the axial motion using the axial resonance procedure (Section 4.4).

The functional form of the sides of the well can be determined by determining the highest level in the well which is filled V_e(flag) as a function of the flag position. Such tests showed that the shape of the potential well was given by the magnetic potential to a value within the experimental accuracy ($\pm$1.0 meV). Furthermore, the two endpoints of a given level agree to within $\pm$1.0 meV. This test cannot be extended to the bottom of the well as the presence of the flag would leave no population to be investigated. However, the endpoints are relatively more important than the bottom, as the ions spend proportionally more time near them.

The period of the axial motion of the ions in the well was measured on many occasions. The measured period and that calculated from the magnetic well shape agree to within 5 percent or better for protons.

Thus the motion of the ions in the well does not seem to be seriously disturbed by the stray electric potentials. Since $T_\perp$ is inversely proportional to the mass of the ion and the stray potentials presumably remain constant, certain changes in the potential well should produce effects which are to first order proprotional to the mass. If these effects were serious, the population distributions of ions of different mass would differ appreciably, but they do not. The effect

of electric potentials is considered to be no more than 10 percent of the available depth in the well for protons and proportional to ion mass. This results in an error assignment of ± 2.0 M/M_p ppm. It is interesting to note that any systematic dependence of these effects on the ion mass should be removed by the extrapolation procedure. Since only one exptrapolation is available at this writing, no attempt is made to use this.

Mapper Probe Calibration

The NMR mapper probe was calibrated against each of the three standard probes of J. Wesley (1970)(Section 3.3). The g-IV solenoid was used as it was more homogeneous than the solenoid used here. The probes were interchanged in the center of the field at a nominal frequency of 4.5 MHz. In order to verify the homogeneity of the field at the center, the larger standard probes were moved over a range of ± 2 cm in all directions. This resulted in a shift of ± 1 Hz or less. The results of 10 separate observations for each standard probe are:

Standard Probe	ω_s(mapper)-ω_s(standard) (Hz at 4.5 MHz)
1	+3.6
2	4.5
3	3.2
1(rotated 30 deg)	4.4
average	+3.9 = +0.87 ppm

Since, as in g-IV, there is no conclusive evidence of a difference between the probes at the level of ±1 Hz, the results are averaged with the final result:

$$\omega_s(\text{standard})/\omega_s(\text{mapper}) = 1 - (.87 \pm .20) \times 10^{-6} \quad .$$

The standard probe must be further corrected to a spherical water sample to remove the effect of the paramagnetic shielding of the Cu^{++} ions used to dope the water sample. For an infinite transverse cylinder containing 0.2 Molar $CuSO_4$, this correction is given by Dickenson (1950) as

$$\omega_s(\text{spherical})/\omega_s(\text{standard}) = 1 + (1.0 \pm 0.1) \times 10^{-6} \quad .$$

Thus the net correction of the mapper probe to a standard spherical water sample is

$$\frac{\omega_s(\text{spherical})}{\omega_s(\text{mapper})} = \frac{\omega_s(\text{spherical})}{\omega_s(\text{standard})} \frac{\omega_s(\text{standard})}{\omega_s(\text{mapper})}$$

$$= 1 + (0.13 \pm 0.22) \times 10^{-6} \quad .$$

This is negligible and will generally be ignored.

5.3 Final Results μ'_p/μ_n

Extrapolation

The extrapolation of the available data to μ'_p/μ_n is shown in Fig. 35, and the data is summarized in Table II. The value plotted at M = 1 is the average of six runs on H^+ ions taken over a period of a week under various operating conditions. These points have a standard deviation of $\pm$1.5 ppm. The value plotted at M = 2 is the average of two measurements on H_2^+ ions taken several days apart which differ by 2.5 ppm.

The error assignments are summarized in Table III. Although certain of these errors might more properly be assigned after the extrapolation, they represent only minor contributions to the final error at this writing and thus all errors are assigned before the extrapolation. The dispersion of the data points is consistent with the error assignments, but no attempt is made to statistically reduce the error bars due to the limited amount of data available, and because the data constitute only one extrapolation.

The final extrapolated value is determined by fitting a line of the form $y = ax + b$ to the two data points using standard statistical procedures (Wesley, 1970, Appendix E).

The data for M = 2 was taken two weeks after the data for M = 1, but the machine was in continuous operation during this period and the vacuum was maintained. The electric potential observed at the south end of the well remained constant, and the transverse magnetic gradient required to remove the slow drift of the ions also remained constant.

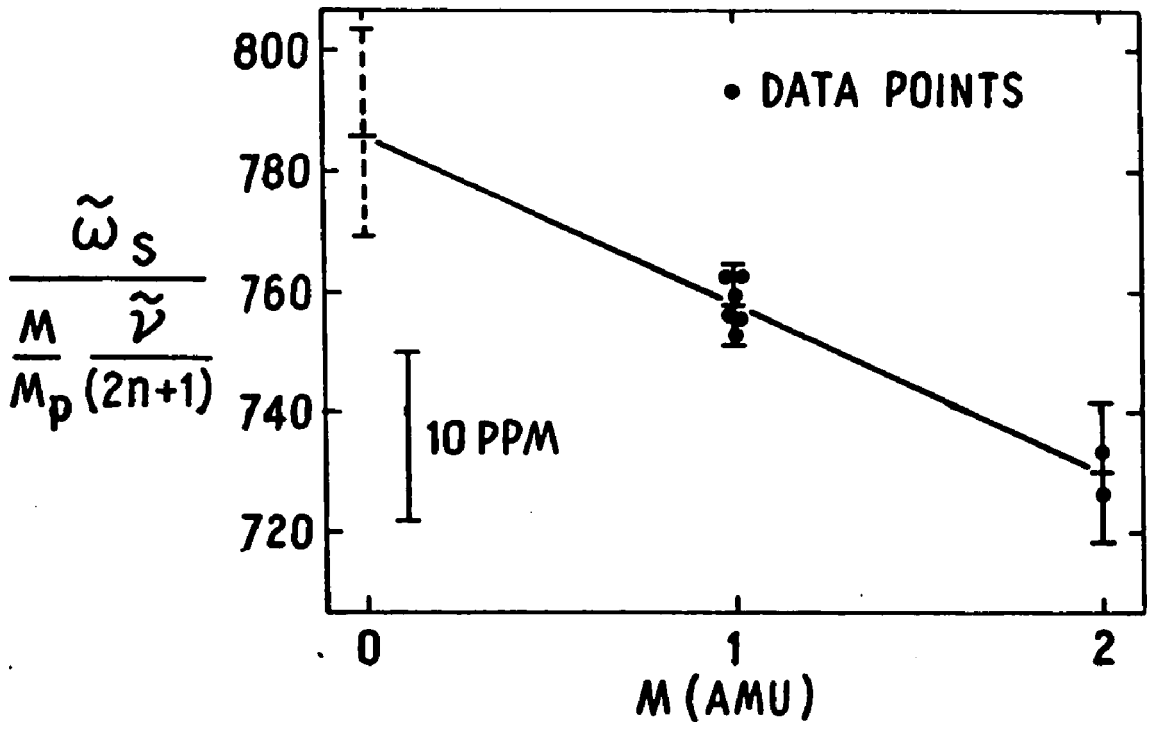

FIG. 35 EXTRAPOLATION TO ZERO MASS.

Table II, Summary of Data Runs.

RUN	MAP	$\tilde{\nu}$ (Hz)	ΔV_e (steps)	STEP SIZE	ΔV_e (mV)	$\Delta\omega_s$ (Hz)	ω_s (flag) (Hz)	$\tilde{\omega}_s$ (Hz)	$[\tilde{\omega}_s]$ (Hz)	$\frac{[\tilde{\omega}_s]}{\tilde{\nu}}\frac{M_p}{M}$
H^+ (M = 1.0072766 u)										
122	110	1 181 464	3.0	1.5	4.5	31	3299 671	3299 640	3299 537	2.792 753
123	110	1 181 446	2.0	1.5	3.0	21	3299 576	3299 555	3299 501	2.792 764
124	111	1 181 490	2.5	1.5	3.75	26	3299 696	3299 670	3299 615	2.792 757
126	113	1 181 491	4.0	1.44	5.7	40	3299 714	3299 674	3299 622	2.792 761
130	114	1 181 521	3.0	1.72	5.1	35	3299 787	3299 752	3299 700	2.792 756
131	114	1 181 520	2.0	1.72	3.5	24	3299 787	3299 763	3299 707	2.792 764
									Average	2.792 7592
									Relativistic Correction	- .000 0014
									Final Value (H^+)	2.792 7578
H_2^+ (M = 2.0151018 u)										
153	118	590 581	3.0	0.56	1.7	24	3299 615	3299 591	3299 568	2.792 733
140	117	590 576	3.0	0.70	2.1	29	3299 619	3299 590	3299 531	2.792 726
									Average	2.792 7295
									Relativistic Correction	- .000 0003
									Final Value (H_2^+)	2.792 7292

Table III

Summary of Errors

Source	Error (ppm)	
	M = 1	M = 2
Determination of $[\omega_s(\tilde{z}_1)]$	0.9	0.9
Possible variation in well potential	2.0	2.0
NMR probe calibration	0.3	0.3
NMR shielding correction	0.1	0.1
Determination of $\tilde{\nu}$	0.4	0.4
rms Total	2.3 ppm	4.2 ppm

This indicates that the stray axial and transverse electric fields in the well region remained constant during the measurements. The cyclotron resonances were not observed to drift as long as conditions remained the same. Stable resonances were observed for as long as 24 hours. Furthermore, the six measurements at M = 1 do not exhibit any slow time dependence. Thus it is reasonable to assume that $[E_r]$ remained constant during the time that the measurements were made.

The slope of the extrapolation indicates $[E_r] = (2.3 \pm 1.1)$ mV/cm. This may be compared with the magnitude of the transverse field estimated in Section 4.2 as 2.0 mV/cm. The axial electric fields may be estimated as 3.0 mV/cm from the observed change in the axial potential of about 30 mV and the characteristic length of the cylinder diameter (10 cm). Thus, the magnitude of the radial electric field is in agreement with the other electric fields observed in the apparatus.

Since only two points are used for one extrapolation, there can be no test for linearity. It is hoped that this test can be performed in future runs either by adding an additional point to the extrapolation or by varying the slope. The error in determining $[\tilde{\omega}_s]$ due to axial electric field should be dependent on the mass of the ion to first order and thus should be reduced by the extrapolation. This dependence was ignored when assigning the errors in $[\tilde{\omega}_s]$, and larger errors were assigned for mass 2. Thus the extrapolation could serve to reduce these systematic errors, but one is reluctant to apply this unless future extrapolations indicate that it is justified.

Final Result: μ_p'/μ_n, μ_p/μ_n

The final result of the extrapolation is

$$\mu_p'/\mu_n = 2.792\ 786 \pm 0.000\ 017\ (6.0\ \text{ppm})$$

for protons in a standard spherical water sample. If a correction of +26.0 ppm is made for the bulk diamagnetism of the water sample (Taylor et al. p. 53) this becomes

$$\mu_p/\mu_n = 2.792\ 859 \pm 0.000\ 017\ (6.0\ \text{ppm}) \quad .$$

This result is in agreement with other recent measurements (Fig. 1).

Continuation: μ_p/μ_n

It is hoped that continued work with the apparatus will result in an increase in accuracy to better than 2.0 ppm. In order to accomplish this, two points must be significantly improved. First, the extrapolation will have to be tested for linearity. This may be accomplished in three ways: (1) By the addition of another ion of mass number 3 or 4 to the extrapolation. The facilities for providing these ions (HD^+, D_2^+, and He^+) already exist, but the difficulties arise from the fact that the trapped ions have energies of 160 eV and 120 eV respectively. These low energies result in low output from the ion source and difficulties in trapping the ions. This is further aggravated by the fact that the trapping time increases with mass for constant N, so that the operating times are increased. However, the increased sensitivity of the higher mass ions to the stray electric potentials

affords us a better understanding of these potentials and thus should proprotionally increase our confidence in their effects on mass 1 ions. (2) By varying the magnetic field instead of the ion mass, and extrapolating as a function of B^{-2} to ω_o. The biggest disadvantage with this approach is the limited range over which it is feasible to carry out the extrapolation. If we are willing to let the energy of the trapped protons be reduced by a factor of two, B^{-2} would change by a factor of two. Thus we would be able to extrapolate over a 2:1 range and we would be no better off than we are now using two masses. (3) By varying the slope of the extrapolation. This would be done by introducing additional potentials on existing or additional electrodes. While at the present accuracy of the experiment, the electric field shift of 1.5 standard deviations is not excessive, an increase in accuracy without decreasing the radial electric fields would result in electric field shifts of several standard deviations. It would, in general, be desirable to avoid this situation.

Second, the effect of stray potentials on the axial motion of the ions in the well will have to be even more carefully investigated. This might be facilitated by improving the versatility of the population programmer and the axial resonance process.

5.4 Results H_2^+–D^+

Line Matching

The error in the determination of the H_2–D mass difference is the sum of the systematic errors and the error in matching the two

lineshapes. The final error at this writing is due almost entirely to the matching error because of the limited amount of data. The values of dB/dr and $[E_r]$ used to estimate the systematic shifts between the lines are verified in Sections 5.1 and 5.2, respectively. Thus with no further knowledge of the radial distribution of the ions than that given by the annulus, we can estimate that the systematic shifts between the two resonances do not exceed 100 ppb.

The two resonance lineshapes are matched by fitting their difference to a straight line. This is like the S-curve methods used with other mass spectrometers, (Stevens and Moreland, 1967, and Duckworth et al., 1967) but unfortunately it is not "on-line." The fitting process was carried out on a computer using a minimization program MINUIT to obtain both a least squares and a maximum likelihood fit. The adjustable parameters are the frequency shift and the amplitude ratio. It has been found that these lines can be fitted to a fraction of a frequency step even with relatively noisy data. The width (FWHM) of the likelihood function was one-eighth step of the frequency sweep, but the assigned error is $\pm$ one-half frequency step because of the limited amount of data available. It is felt that with more data, the accuracy to which this mass doublet is measured can be improved by a factor of ten. This would require further study of the shifts between the lines.

Final Result H_2^+-D^+

The final result of the mass doublet measurement is

$$\frac{\Delta M}{M(H_2^+)} = (768.31 \pm 0.10) \times 10^{-6} \quad .$$

If we take $M(H_2^+) = 2.0150$ u (Smith, 1971), we may write the mass difference

$$H_2^+ - D^+ = 1548.22 \pm 0.20 \text{ μu} \quad .$$

This result is in agreement with other measurements the most precise of which is that of Smith (1971): $H_2^+ - D^+ = 1548.287 \pm 0.004$ μu.

Extension of the Present Work with Mass Doublets

Although the preliminary results of this machine for the $H_2 - D$ doublet are fifty times less accurate than those of Smith (1971), and any final result will probably be about ten times less accurate, these results will hopefully provide a useful check of this measurement by an entirely different technique. The measurements of this doublet with the present apparatus are made on the doublet directly rather than being reduced from measurements made on a high mass molecular ion. In both the conventional deflection type spectrometers and the two revolution RF spectrometer of Smith, the resolution is determined by the separation of a slit. In the RF spectrometer this is more properly considered as defining the phase of the ions. In our machine, the detector aperture has little to do with the resolution, but rather the resolution is largely determined by the number of cyclotron revolutions which the ion makes in the field with some additional phase information being determined by the odd harmonics.

It should be possible to make a measurement of the D_2^+–He^+ doublet and possibly the HD^+–$^3He^+$ doublet if the operation of the apparatus can be successfully extended to higher mass ions. The D_2^+–He^+ doublet is of particular importance because of the role of the α-particle (He_4^{++}) in nuclear reactions and disintegrations.

5.5 A New Apparatus

In this section we shall discuss the feasibility of a new apparatus and its application to measurements of both μ_p/μ_n and the mass difference of low mass doublets. We will also discuss a new technique for the measurement of $\mu_p/\mu_n = \omega_s/\omega_o$ using a direct measurement on the spin motion of free protons along with the technique of this thesis for measuring ω_o. The relevant parameters of the present and proposed experiments are compared in Table 5.

μ_p/μ_n

This section will discuss the feasibility of a new apparatus for measuring μ_p/μ_n along with its characteristic parameters. In order to obtain a substantial increase in accuracy, it is necessary to increase the magnetic field by an order of magnitude to about 10 kG. It would also be necessary to improve both the stability and intrinsic magnetic field homogeneity by a similar amount. If this is to be attained over an experimental volume which is comparable to that of the present apparatus, it will probably require a super-conducting solenoid of about the size of the present one (2 ft dia by 5 ft or more long).

Table IV

Summary of the Parameters of the Present and Proposed Apparatus

Parameter	Present	Proposed
Magnetic field B	800 G	10000 G
Ion radius r_o	4 cm	1 cm
Ion energy $T_\perp$	500 eV	5000 eV
Trapping time	10000 μs	10000 μs
Cyclotron revolutions N	10^4	10^5
Well depth ΔB/B	40 ppm	4 ppm
(Energy units)	20×10^{-3} V	20×10^{-3} V
Spin frequency ω_s	3.3 MHz	42 MHz
Difference frequency ω_D		27 MHz
Cyclotron frequency ω_c	1.2 MHz	15 MHz
RF frequency (11th harmonic)	13 MHz	165 MHz
RF linewidth	20 ppm	2 ppm
Electric field shift for $[E_r] = 1$ mV/cm	4.3 ppm	0.15 ppm
Relativistic correction $(\gamma - 1)$	0.5 ppm	5 ppm
Error in $\gamma - 1$	±.005 ppm	±.05 ppm
Well period τ	350 μs	~350 μs
Trapping rate, counts/cycle	1	100
Accuracy of determination of $[\tilde{\omega}_s]$	1.0 ppm	0.1 ppm
Vacuum system pressure (Torr)	3×10^{-9}	1×10^{-10}

From the relation $r_o = c(2MT_\perp)^{1/2}/eB$ it can be seen by comparison to the present apparatus that an increase in the magnetic field strength B by a factor of ten would allow both the ion energy to be increased by a factor of ten and the ion radius to be reduced by a factor of three. Thus we would be able to use 5000 eV protons at an orbital radius of about 1.0 cm. The smaller radius would allow the size of the experimental region to be reduced and thus result in a significant improvement in the homogeneity of the field. This should allow the trapping to be extended out to 100,000 cyclotron revolutions--ten times the present number. The increased field results in a proportional increase in ω_c to about 15 MHz. Thus the tenfold increase in the number of cycles would be accomplished in the same total time as is presently used.

From Eq. (2.2) it can be seen that a tenfold increase in the ion energy would allow one tenth of the magnetic well depth to be used and still keep the resultant potential well at the same depth as it is now. The stray potentials in the well region should remain about the same as they are in the present apparatus. Thus, the tenfold increase in the number of cycles along with a tenfold decrease in the depth of the magnetic well should allow the resonance linewidth to be reduced by a factor of ten to about 1 ppm.

The relativistic change in the cyclotron frequency would increase to about 5 ppm. The quantity $\gamma - 1$ can presently be determined to an accuracy of 2 percent due to the absolute limits of the annulus aperture. This would allow γ to be calculated to an accuracy of 0.1 ppm.

A minimal determination of the distribution of the ions within the annulus aperture (as has been done with the present apparatus) would allow the error in the initial determination of relativistic correction to remain negligible. The change in radius on resonance results in a small change in γ. Using the removal resonance procedure the change is about 2 percent, and would result in a change in γ of about 0.2 ppm. However with the removal resonances, the net result to first order is a symmetric broadening of the resonance line and there is no net change in γ.

The electric field shift is given by

$$\omega_c' = \omega_c \left[1 - \frac{c^2[E_r]}{vB} \right] .$$

Since the velocity would be increased by a factor of $10^{1/2}$ over the present experiment and the field would be 10 times larger, the shift for a given electric field would be $10^{1.5}$ of what it is now. Thus, if we envision a tenfold increase in accuracy, the relative effect of the electric field shift would probably be about one-third of what it is now. It may be possible to further reduce the stray electric fields by a careful choice of materials.

The mean square scattering angle $\overline{\theta^2}$ of an ion in the well is given from Fermi (1950) by the proportionality $\overline{\theta^2} \propto vTP$, where v is the ion velocity, T is the trapping time, and P is the vacuum system pressure. As a criterion for the ions to be scattered out of the well, let us take $\overline{\theta^2} \propto \alpha_{max}^2$, where $\alpha_{max} = (\Delta B_{max}/B)^{1/2}$ is the maximum pitch angle an ion may have and still remain in the well. Thus we may compare the present

experiment to the proposed experiment using the proportionality $\Delta B_{max}/B \propto vTP$. If the well depth is reduced by a factor of 10 and the velocity increased by $10^{1/2}$ in the same total trapping time, then the vacuum would have to be improved by a factor of $10^{1.5}$. Thus a vacuum system with an ultimate pressure of 1×10^{-10} Torr would be required. This should be possible using modern techniques.

The increased energy of the ions would result in considerably greater ion source outputs than are now available. The present RF ion source would produce about 20 times the proton current with only a slight increase in energy spread. However, due to the increased magnetic field, the potential well in energy units would remain about the same as it is now so that a similar fraction of the beam can be used. Thus one would expect a tenfold increase in trapping rate. Furthermore, the present dc beam in the trapping region and trapping rates are considerably below those that are expected; thus it is felt that improved design of the beam system would result in even more of the ions being trapped. Therefore it does not seem unreasonable to predict trapping rates a hundred times greater than the present minimum working rates of one ion per machine cycle. The space charge due to these ions would not produce an appreciable electric field shift unless the trapping rate exceeded 10,000 per cycle.

The higher ion velocities along with the increased magnetic field would require that the electric fields in a deflection system similar to the one presently used to guide the

ions into the field center be increased by a factor of thirty to about 5 kV/cm. While this would not be impossible, it would certainly be more difficult to realize than the present system. Thus a new system for getting the ions into the field center might be desirable. Due to the amount of time required to change over from ions of one mass to ions of another, which is due to the time required for the beam system to stabilize, it might be desirable to install two beam systems.

The actual trapping of the ions should be no more difficult than it is in the present apparatus if there is a proportional improvement in the homogeneity of the magnetic field.

The biggest problem in the present apparatus is the Ω-motion smearing of the orbit centers of the ions in the orbital plane. This is essentially due to the orbit center not being at the field center of the apparatus, and should not be a problem with a new apparatus because of the increased homogeneity and smaller orbit diameter. The effect of the electric fields transverse to the magnetic field which have been very troublesome in the present experiment, is reduced by a factor of ten due to the increased magnetic field (Eq. III.1).

The increased cyclotron frequency would result in RF frequencies of about 150 MHz at the eleventh harmonic. This corresponds to a wavelength of about 2 meters; but due to the smaller physical size of the apparatus, there should be no relativistic phase shift problems. However, the driving and switching electronics would be considerably more difficult to develop than the circuits which are now in use.

There is at this time no obvious choice for a detector. The operation of the strip multiplier presently used is dependent on the magnetic field strength. While one might envision a scaling down of this detector by a factor of ten similar to the scaling down of a factor of two used for the present detector, this could be difficult and the results unpredictable. Such a scaling down would result in the electric fields along the strips being increased by a factor of ten to about 5000 V/cm. Furthermore, the small physical size required could result in a saturation effect due to the inability of the active surfaces to supply the required electrons.

In order to determine μ_p/μ_n, the value of $[\omega_s]$ must also be determined to a corresponding accuracy. Due to the higher field strength along with improved homogeneity and stability, the intrinsic measurement error in a local determination of ω_s should be improved sufficiently to allow it to be measured to an accuracy of better than 0.1 ppm. The shallower well should allow the averages to be obtained to a proportionally higher accuracy, and thus the time-averaging could be done to an accuracy of $\pm$0.1 ppm.

In conclusion, it is reasonable to predict that an extension of the present apparatus along more or less conventional lines would result in a measurement of μ_p'/μ_n which is a factor of ten more accurate than the results obtained with the present apparatus. This measurement would be made using cyclotron linewidths which are considerably narrower

than those obtained in other apparatus used to make this measurement. Thus, the measurement would require only a modest interpretation of the line center as in the present experiment. The electric field shift would remain relatively small and would probably result in a shift in the cyclotron frequency of protons of about one standard deviation. It should be possible to more readily extend the extrapolation to account for this shift to mass 4 u. Finally, the energy change of the resonant ions would remain small (about 2 percent).

Mass Doublets

The new apparatus discussed above could also be used to extend the work with mass doublets and improve the accuracy of our measurements. This apparatus has the advantage of allowing the low mass doublets to be measured directly rather than measuring the mass difference of a high mass molecular ion and deducing the value of the doublet. It would be desirable to extend the range of a new machine to include masses up to about mass 20 u. This would allow more direct comparisons of the results of this apparatus to the work of others.

The operational principles of this machine are quite different from those of the RF mass spectrometer of Smith (1971) and a similar instrument in the U.S.S.R. (Mamyrin and Frantsuzov, 1962) (also used by Mamyrin et al., 1965, 1971, to measure μ_p/μ_n). In these instruments, the cyclotron frequency is determined in one revolution and the resolution is determined by the aperture of sets of very narrow

slits. The limit in the resolution is ultimately determined by mechanical limitations of the slits. The apparatus suggested here is quite different in that the ions would make many (10^5) cyclotron revolutions in the field, and this along with the depth of the well used for trapping the ions determines the final resolution.

The characteristics of a new mass doublet apparatus will be presented in terms of the apparatus discussed above for measuring μ_p/μ_n in a field of 10 kG. The increased magnetic field would allow a resolution of about 10^6 for ions of mass 2 u. If we assume a line matching accuracy of 1:1000, the mass ratio of the H_2^+—D^+ doublet could be determined to 1.00 ppb or 1.2 μu. This compares to a resolution of 2×10^5 in the recent work of Smith along with a line matching accuracy of 1:2500 and a final accuracy of 4.0 ppb in the H_2—D doublet. These predictions are based on a conservative extension of the present work, and if further increases in either the resolution or line matching accuracy can be had, then the final accuracy would be further improved.

A new machine would still have the restriction of the present apparatus that once the cyclotron radius of the apparatus is fixed, the kinetic energy of an ion is inversely proportional to its mass. For instance, if an energy of 5000 eV in a field of 10 kG is chosen as optimum for protons as a reasonable compromise between the relativistc effects (γ) and the depth of the well in energy units (which determines the effects of stray fields), then at mass 4 u the ion energy is 1250 eV and the energy well is only one-fourth as deep so that stray

electric fields become a problem. Thus it becomes apparent that in any fixed configuration the reasonable range of masses for operating the machine is approximately 4:1. It is interesting to note that most, if not all, of the mass spectrometers currently in use seem to be limited to similar ranges. Thus an apparatus can be optimized for use with masses 1 to 4 u, 10 to 40 u, 20 to 80 u, etc.

The range of a new apparatus might be varied by increasing either the magnetic field strength or the ion radius. If we recall that the cyclotron radius is given by $r_o = mVc/eB = c\sqrt{2MT}/eB$, it can be seen that an increase in either B or r_o by $10^{1/2}$ allows the energy T of the ions to be increased by 10. Each of these possibilities has certain advantages and disadvantages. Increasing the ion radius would result in greater field inhomogeneities. Homogeneity is no longer required to make a determination of $[\omega_s]$ as is the case when measuring μ_p/μ_n but the increased inhomogeneity would eventually limit the confinement time of ions. Increasing the field strength would make the solenoid considerably more expensive and create mechanical difficulties, but it has the advantage of also increasing the cyclotron frequency. This would help to compensate for the normal decrease in cyclotron frequency with mass and the resultant increase in operating times. Thus one might envision the machine discussed in the last section for measuring μ_p/μ_n with either variable radius or field strength to allow its operation to be extended to ions of somewhat higher mass.

Since the electric field shift for a given radial electric field should be reduced by $10^{1.5}$ in a new apparatus as compared to the present apparatus, the differential electric field shift should be the cause of only small systematic errors. These errors could be effectively removed by performing an extrapolation as discussed for μ_p/μ_n and adjusting the slope to zero by introducing potentials on the appropriate electrodes.

In conclusion, a new apparatus would apparently allow us to make useful measurements of the mass differences of low mass doublets. This would also afford us the opportunity to further investigate the technique and could result in an even greater extension of its application.

Spin Resonance on Free Protons

Another interesting possibility is the direct measurement of μ_p/μ_n for free protons in a vacuum. A technique has recently been developed at our laboratory (Luxon et al., 1972) for the measurement of the difference frequency $\omega_D = \omega_s - \omega_c$ of polarized electrons in a magnetic well similar to the one used in this work. If this technique were applied to protons along with the present technique for measuring ω_c, we would be able to measure μ_p/μ_n by measuring the ratio $(\omega_D + \omega_c)/\omega_c = 1 + \omega_D/\omega_c$ for free protons in a vacuum. The ratio ω_D/ω_c would be determined by comparing two resonance lines from the same sample.

The method used to determine the difference frequency is based on a resonant perturbation of the spin motion of the proton in the

magnetic field. This motion can be summarized as follows: Consider a proton with velocity $\vec{v}$ and polarization $\vec{S}$(parallel to $\vec{\mu}_p$) undergoing planar cyclotron motion at frequency ω_c in a uniform magnetic field $\vec{B}_o = B_o\hat{z}$. $\vec{S}$ will then precess about $\vec{B}_o$ at frequency ω_s. Thus, the relative precession of $\vec{S}$ with respect to $\vec{v}$ will occur at the difference frequency $\omega_D = \omega_s - \omega_c$. Due to this precession, the helicity $\hat{S} \cdot \hat{v}$ varies as cos $\omega_D T$, where T is the time spent by the protons in the magetnic field.

The means of determining ω_D is illustrated in Fig. 36. A current carrying wire is placed at the center of the proton orbit parallel to $\vec{B}_o$ and generates an azimuthal field $\vec{B}_\theta$. If a proton is oriented with $\vec{S}$ perpendicular to both $\vec{v}$ and $\vec{B}_o$ at T = 0, then the torque $\vec{\mu} \times \vec{B}_\theta$ will tend to rotate $\vec{S}$ parallel to B_o. The component of $\vec{S}$ perpendicular to $\vec{B}_o$ will continue to precess about $\hat{z}$ at frequency ω_D with respect to $\vec{v}$. After half a period of ω_D ($T = \pi/\omega_D$), $\vec{S}$ will have rotated 180 degrees with respect to $\vec{v}$ (see Fig. 36). If $\vec{B}_\theta$ has also reversed direction, the resultant torque will continue to rotate $\vec{S}$ into the direction of $\vec{B}_o$. Thus if the θ-field oscillates at frequency $\omega = \omega_D$, the time-average torque experienced by the orbiting proton will rotate $\vec{S}$ toward $\vec{B}_o$. The resonance condition corresponds to the maximum decrease in the component of the polarization in the orbital plane, or conversely, the maximum increase in the component of $\vec{S}$ in the direction of $\vec{B}_o$. Similarly, the protons may be initially polarized parallel (or anti-parallel) to $\vec{B}_o$ and resonance observed as a decrease in the component of polarization in the direction of $\vec{B}_o$.

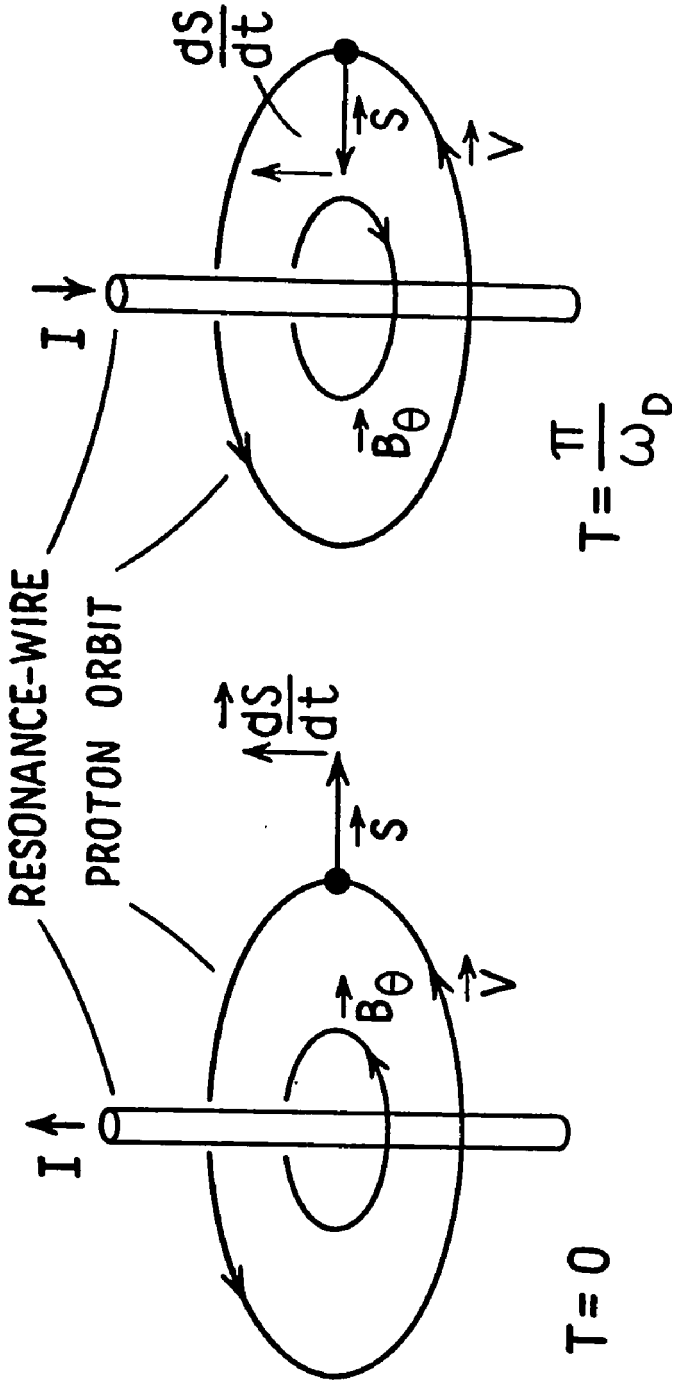

FIG. 36 SPIN ROTATION IN THE FIELD OF A WIRE.

The minimum θ-field necessary to rotate the spin through $\pi/2$ about $\vec{v}$, say from parallel to $\vec{B}_o$ to perpendicular, can be estimated by noting that $\vec{S}$ rotates about $\vec{v}$ at the "usual" NMR frequency $\omega_1 = (1/2)(\mu_p/\mu_n)(eB_1/\gamma M_p c)$. The factor of 1/2 is due to time-averaging. If we now require that $\vec{S}$ rotate through $\pi/2$ about $\vec{v}$ in the same time that it precesses $2\pi N_s$ revolutions about $\vec{B}_o$, we have

$$\frac{B_1/2}{B_o} = \frac{\pi/2}{2\pi N_s} .$$

or

$$B_1 = \frac{1}{2N_s} B_o .$$

Since $N_s = (\mu_p/\mu_n)N$, and taking $N = 10^5$ and $B_o = 10$ kG for a new apparatus, we have $B_1 = 0.02$ G. The width of the resonance line is expected to be approximately $1/N_D$(FWHM), where $N_D = N_s - N$. Using the parameters given above, the expected width is about 5 ppm.

The magnetic field of a wire is given by $B_1 = I/(cr_o)$ where I is the current in statamperes. If we take $r_o = 1$ cm, the required peak current is I = 0.2 amp. The required frequency would be about 27 MHz. This current can be readily obtained, but the associated RF electric field may cause difficulties. If we consider that the wire might have an inductive reactance of about 10 ohms, then with one end of the wire grounded an RF voltage of amplitude 2 volts would be present at the other end of the wire. However, the associated radial RF electric field oscillates at a frequency which is very high compared

to the frequency of axial oscillation of the ions in the well. A dc field of this magnitude would cause a shift in the cyclotron frequency of about 30 ppm; but any shift due to the RF field could be expected to be averaged to zero by the axial motion of the ions, their cyclotron motion, or by applying the RF with random phase. The associated RF electric field might be reduced by either increasing N_s, or by designing an electrode configuration which would minimize it. Furthermore, measurements of both ω_D and ω_c could be made with both of the RF fields present so that any shifts would be accounted for.

In order to implement this technique, a source of polarized protons would be required along with an analyzer to determine their final polarization. The techniques to accomplish this appear to be available, but their application to this experiment has not been carried out in detail. Polarized ion sources of suitable energy are in use at particle accelerators and the design of a suitable source seems feasible. Techniques are available for polarization analysis at these energies, but further studies are necessary to ascertain whether analysis can be carried out in the high field region or if the protons must be first extracted.

An extrapolation would still be necessary to account for any radial electric fields. This is probably still best accomplished as a function of ion mass. The extrapolation might be facilitated by using two ion source systems in order to have ions of different mass available at the same time. One fringe benefit of the wire at the

center of the orbit is that the apparatus could be electrically biased to vary the net radial electric field.

In conclusion, it may be possible to use a new apparatus to measure μ_p/μ_n by measuring both the spin and cyclotron frequencies of the same sample of free protons in a vacuum without having to relate the spin measurements to a water sample. This would seem to be the next logical step in the measurement of this constant.

APPENDIX I. THE dc ELECTRIC FIELD OF THE C's

The electric field of a longitudinally split infinite cylinder can be solved as a two-dimensional problem in complex variables (see for example, Churchill, 1960). Consider two semicircular segments on the two-dimensional unit circle, $r = 1$, with the segment $0 < \theta < \pi$ at potential $V = 1$ and the segment $\pi < \theta < 2\pi$ at potential $V = 0$ (see Fig. 37). The equipotentials inside the unit circle are given by

$$V = \frac{1}{\pi} \tan^{-1} \frac{1 - x^2 - y^2}{2y} .$$

This can be rewritten as

$$x^2 + y^2 + 2y \tan \pi V = 1 .$$

This represents a family of circles centered on the y-axis and passing through (1,0) and (-1,0). These are the equipotential lines and are shown as solid lines in Fig. 37. The field lines are given by the conjugate potential which is given by

$$U = \frac{1}{\pi} \log \frac{|1 - x - iy|}{|1 + x + iy|} .$$

This can be rewritten as

$$y^2 + (x - b)^2 = b^2 - 1 ,$$

where

$$b = \frac{1 + e^{2\pi U}}{1 - e^{2\pi U}} .$$

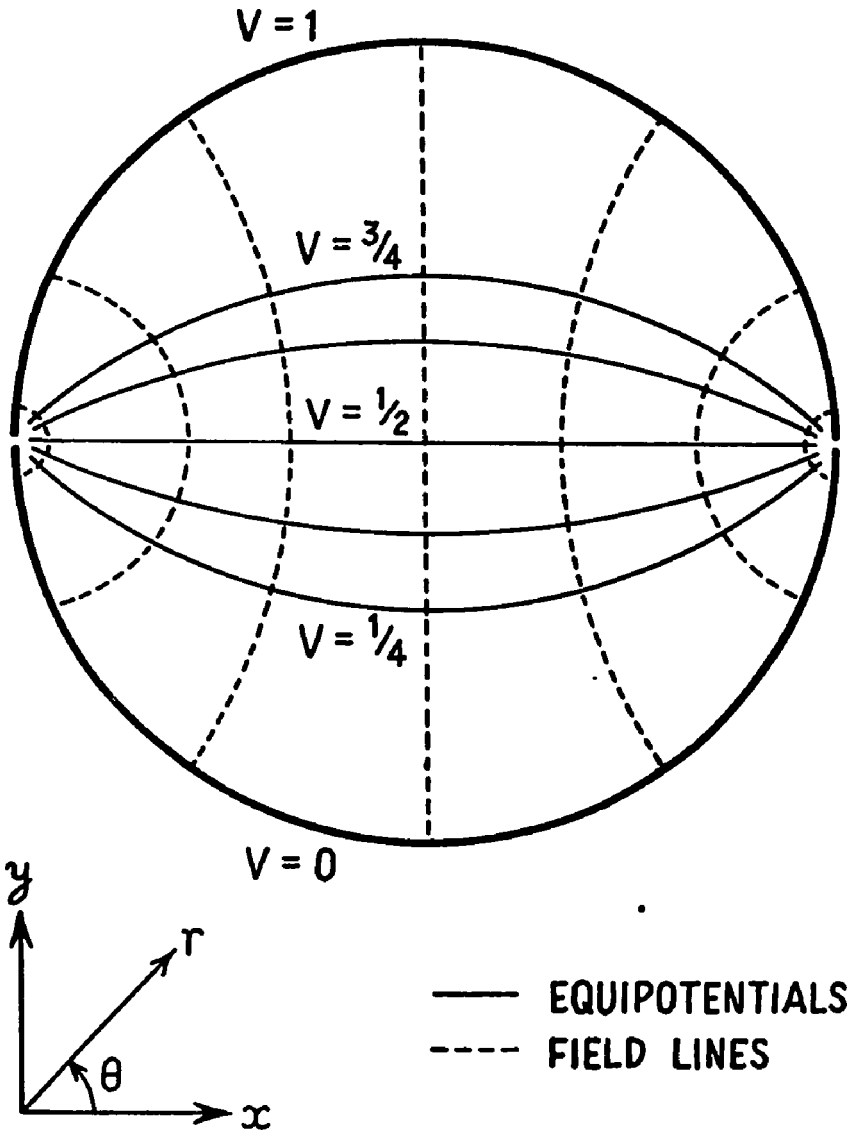

FIG. 37 THE ELECTRIC FIELD OF THE C's.

This represents a family of circles centered on the x-axis at $x = \pm b$, with $r = \sqrt{b^2 - 1}$. The field lines are shown as dotted lines in Fig. 37.

The electric field $\vec{E}$ is then given by

$$\vec{E} = -\frac{\partial V}{\partial x}\hat{x} - \frac{\partial V}{\partial y}\hat{y} \quad .$$

Performing this operation gives the result

$$\vec{E} = \frac{2}{\pi}\frac{xy\,\hat{x} + (y^2 - x^2 + 1)\,\hat{y}}{4y^2 + [1 - (x^2 + y^2)]^2} \quad .$$

If this is rewritten in complex form with $x = r/R_c \cos\theta$ and $y = r/R_c \sin\theta$ we have

$$E = \frac{2i}{\pi R_c}\frac{1}{1 - (r/R_c)^2\, e^{-2i\theta}} \quad .$$

For C's at potentials $\pm U_o$, this becomes

$$E = \frac{4iU_o}{\pi R_c}\frac{1}{1 - (r/R_c)^2\, e^{-2i\theta}} \quad . \qquad \text{(I.1)}$$

It is also useful to calculate the average DC electric field experienced by an ion in an orbit concentric with the C's. This is given by

$$\bar{E}_{dc} = \frac{1}{2\pi}\int_0^{2\pi} E(r,\theta)\, d\theta \quad .$$

For C's of radius R_c at potentials $\pm U_o$ (potential difference $2U_o$) this becomes

$$\bar{E}_{dc} = \frac{2iU_o}{\pi^2 R_c} \int_0^{2\pi} \frac{d\theta}{1 - r^2 e^{-2i\theta}} .$$

Thus we have the result

$$\bar{E}_{dc} = \frac{4U_o}{\pi R_c} i . \qquad (I.2)$$

This is independent of the ions' radius and is simply the value of the electric field at the origin.

APPENDIX II. THE GARREN WELL

The magnetic field of the solenoid in the well region can be approximated by an analytic function which was first suggested by Garren et al. (1958):

$$B = B_o[1 - \alpha I_o(\eta) \cos \xi] \hat{z} - \alpha B_o I_1(\eta) \sin \xi \ \hat{r} \ , \qquad \text{(II.1)}$$

where $\eta = 2\pi r/L$, $\xi = 2\pi z/L$, α is the characteristic depth, and L is the characteristic length. I_o and I_1 are Bessel functions of imaginary arguments. An actual fit of the Garren well to a field map is shown in Fig. 38 using $\alpha = 1.6 \times 10^{-4}$, L = 80 cm, and since $r_o = 4.0$ cm, we have $\eta \cong .32$. I_o and I_1 may be expanded so that Eq. II.1 gives us

$$B_z = B_o[1 - \alpha(1 + 1/2 \ \eta^2 + \ldots) \cos \xi] \ , \qquad \text{(II.2)}$$

and

$$B_r = -\alpha B_o(\eta/2 + \ldots) \sin \xi \ . \qquad \text{(II.3)}$$

Differentiating B_z with respect to r, we get the change in field with radius to a first approximation as

$$\frac{\partial B_z}{\partial r} = -2\pi^2 \frac{\alpha B_o}{L^2} r \cos \frac{2\pi z}{L} \ . \qquad \text{(II.4)}$$

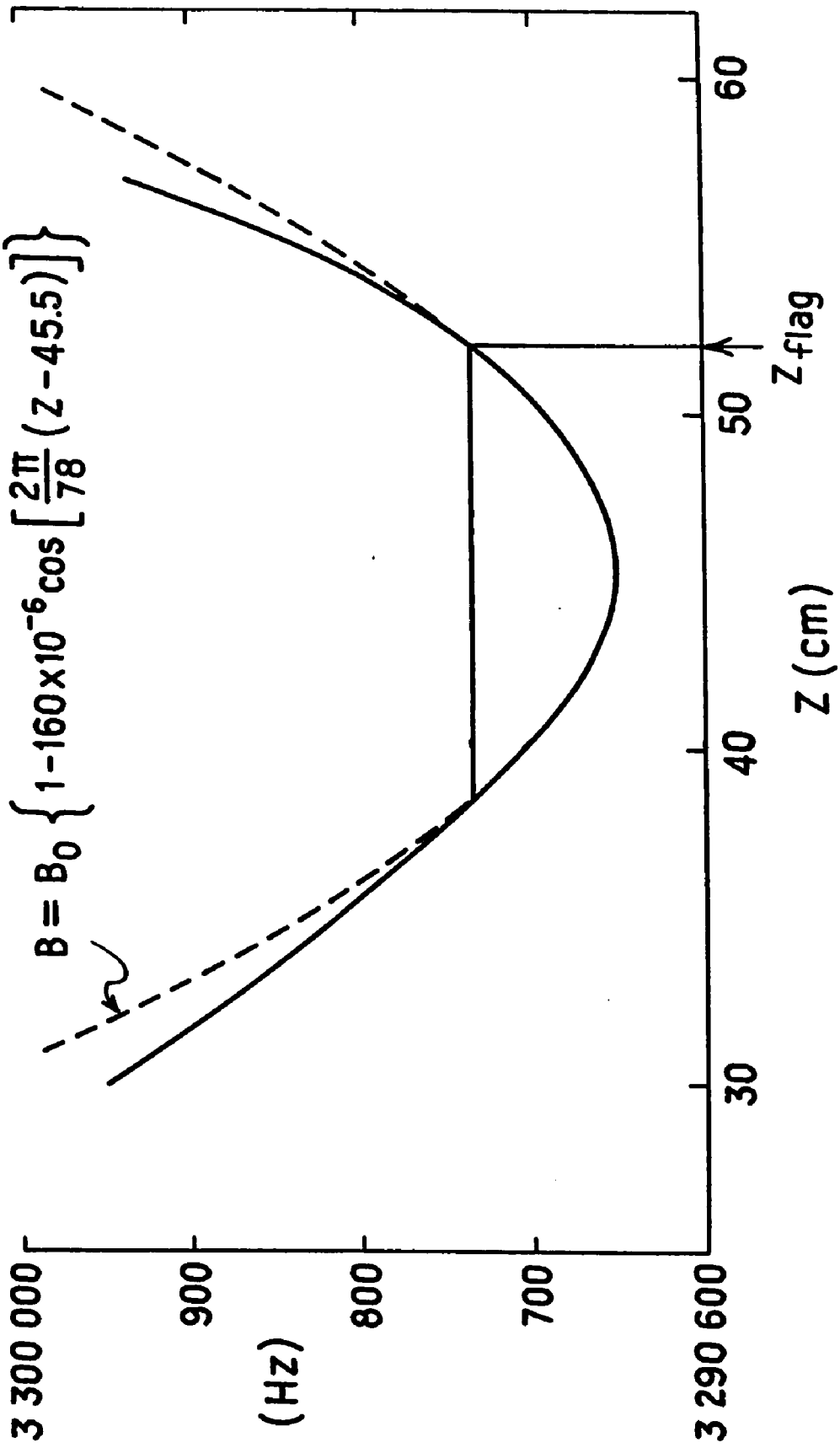

FIG. 38 THE FIT OF A GARREN WELL TO THE MAGNETIC WELL BELOW THE FLAG.

If we expand cos ξ, the axial field, to a first approximation in z, becomes

$$B_z = B_o[1 - \alpha I_o(\eta)(1 - \xi^2/2 + \ldots)] \quad . \tag{II.5}$$

Thus the bottom of the well can be approximated as a parabola. This parabolic field shape leads to a parabolic potential well and is equivalent to a one-dimensional harmonic oscillator, which is characterized by a constant period of oscillation.

APPENDIX III. SUMMARY OF ION ORBIT DRIFTS

Superposed on the cyclotron and axial motions of the ion in the well is a slow drift of the orbit center in the orbital plane due to several effects. These drifts are summarized here to the extent that they affect the experiment. For further discussion see Chandrasekhar (1960). In practice certain of these drifts are always present, but others may be experimentally introduced to produce zero net drift to first order.

The presence of a transverse electric field $\vec{E} = \vec{E}_\perp$ produces a drift with velocity

$$\vec{V}_E = c \frac{\vec{E}_\perp \times \vec{B}}{B^2} . \qquad \text{(III.1)}$$

For B = 800 gauss and $E_\perp$ = 1 mV/cm, we get V_E = 125 cm/s. From Eq. I.2 we see that a potential difference of 10 mV across the C's produces an average $\bar{E}_{dc} \cong 1$ mV/cm. The effect of such a field has been experimentally verified by observing the drift of the beam as a function of the offset voltage applied to the C's.

Similarly, other external forces on the particle such as gravity produce a drift. However, the gravitational drift is only 10^{-4} cm/s and no other external forces are known to us at this time.

If there is a magnetic field gradient $\vec{\nabla}B$ transverse to the principle field direction, $\vec{\nabla}B \cdot \hat{z} = 0$, then there is a drift of the orbit center with velocity

$$\vec{v}_g = \frac{cT_\perp}{eB} \frac{\vec{B} \times \vec{\nabla B}}{B^2} = \frac{1}{2} r_o^2 \omega_c \frac{\vec{B} \times \vec{\nabla B}}{B^2} \quad . \tag{III.2}$$

If we take $r_o = 4.0$ cm, and $\omega_c = 2\pi \times 1.2$ MHz then a linear gradient of 1.0 ppm/cm produces a drift $V_g = 60$ cm/s. While there are gradients of about 1 ppm/cm present due to inhomogeneities in the field of the solenoid, gradients of up to 10 ppm/cm may also be introduced by the external gradient coils described in Section 3.1.

One special case of the gradient drift is due to the radial gradient $(\vec{\nabla B})_r$ inherent in a magnetic field containing a well. For the Garren well model discussed in Appendix II, the radial gradient is given to first order by

$$(\vec{\nabla B})_r \cong \frac{\partial B_z}{\partial r} = -\frac{2\pi^2 \alpha B_o}{L^2} r \cos \frac{2\pi z}{L} \quad . \tag{III.3}$$

This gradient is directed radially inward and proportional to r. If the orbit center coincides with the field center there is no net drift. However, if the orbit center is displaced from the field center by an amount d, then it may be shown (Wesley, 1970) that the average gradient at the orbit center is directed toward the field center with magnitude

$$\langle (\vec{\nabla B})_r \rangle = \frac{2\pi^2 \alpha B_o}{L^2} d \cos \frac{2\pi z}{L} \quad , \tag{III.4}$$

where the average is over one orbit.

In order to determine the average radial gradient experienced by an ion, the results of Eq. (III.4) must be further averaged over the axial motion of the ion in the well. Thus we have

$$\vec{\nabla B}_G = [<(\vec{\nabla B})_r>] = \frac{2\pi^2 \alpha B_o d}{L^2} \frac{1}{\tau} \oint \cos \frac{2\pi z}{L} \frac{dz}{v_z} ,$$

where the integral is over the axial motion in the Garren well, and may be carried out using the techniques of Section 2.2. Since the result of the integral cannot be expressed in closed form, it will be denoted $G(z_1)$. The function $G(z_1)$ is graphed in Fig. 39(b), and ranges from -1.0 at the bottom of the well to +1.0 at the top. The gradient may now be written as

$$\vec{\nabla B}_G = \frac{2\pi^2 \alpha B_o}{L^2} d \; G(z) ,$$

where the range of $G(z_1)$ is from -1.0 to +1.0. Thus, the orbit center drifts orthogonal to $\hat{z}$ and $\hat{r}$ with velocity

$$\vec{v}_g = \frac{1}{2} r_o^2 \frac{\vec{\nabla B}_G}{B} \omega_c . \qquad \text{(III.5)}$$

This represents a circular precession of the orbit center about the field center at radius d. The frequency of this precession is given by $\Omega = v_g/d$ or

$$\Omega = \frac{\alpha \pi^2 r_o^2}{L^2} \omega_c |G(z_1)| . \qquad \text{(III.6)}$$

Using the values $\alpha = 160 \times 10^{-6}$, $r_o = 4.0$ cm, $L = 80$ cm and $\omega_c = 2\pi \times 1.2$ MHz, this frequency is $\Omega = 4.8|G(z_1)|$Hz. Note that $\Omega >> 1/\tau$ where τ is the period of the axial motion, so that the average

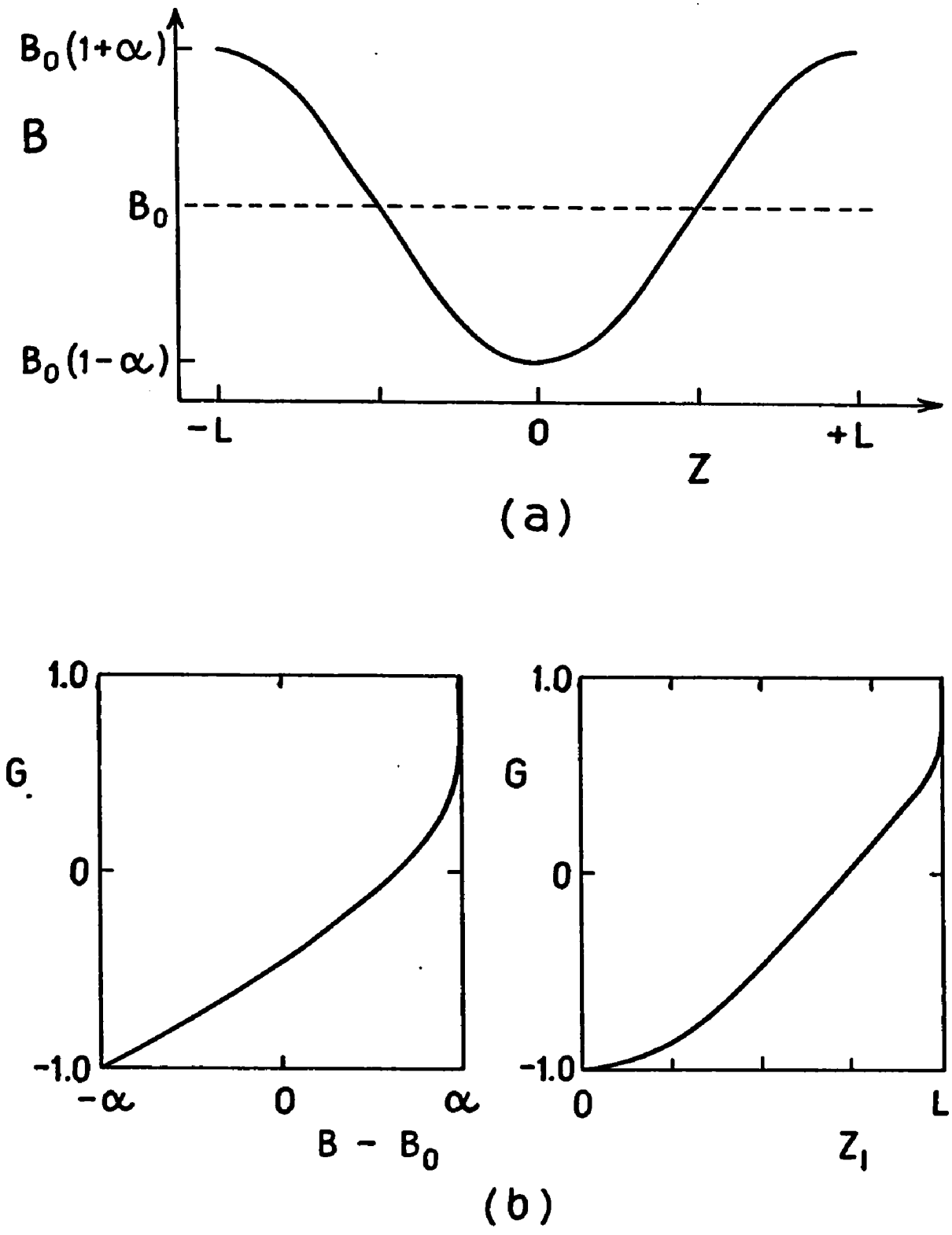

FIG. 39 THE FUNCTION $G(z_1)$.

(a) THE GARREN WELL (USED FOR AVERAGING).

(b) THE AVERAGE VALUE OF G AS A FUNCTION OF THE WELL PARAMETERS.

over the axial motion is both necessary and valid. There is a point high in the well for which $G(z_1) = 0$, and thus there is no Ω-motion.

The drift motion of the orbit center for ions in a Garren well with a transverse magnetic gradient superimposed has been discussed by Wesley (1970, Appendix C). He shows that the effect of a transverse gradient is to shift the field center and thus change the Ω-motion radius d. This may be extended to include a superimposed transverse electric field, and the variation of the shift with the depth in the well. The external field gradient can be represented by $\vec{\nabla}B = k_1 \hat{x}$ and the electric field by $\vec{E} = E_1 \hat{x} + E_2 \hat{y}$ where $E_1 = E \cos \lambda$ and $E_2 = E \sin \lambda$. The field center is taken as $(x,y) = (0,0)$. The Garren well gradient may then be written as

$$\vec{\nabla}B_G = (-kx)\,\hat{x} + (-ky)\,\hat{y} \quad ,$$

where $r^2 = x^2 + y^2$ and

$$k = \frac{2\pi^2 \alpha B_o}{L^2}\, G(z_1) \quad .$$

These may be combined to obtain the effective transverse gradient:

$$\vec{\nabla}B = (-kx + k_1 - \beta E_1)\,\hat{x} + (-ky - \beta E_2)\,\hat{y} \quad , \qquad \text{(III.7)}$$

where $\beta = 2c/r_o^2\omega_c$.

If we set $x' = x - k_1 - \beta E_1/k$ and $y' = y + \beta E_2/k$, we get

$$\vec{\nabla}B = (-kx')\,\hat{x} + (-ky')\,\hat{y} \quad .$$

This is a radial gradient about the center

$$x = \frac{k_1 - \beta E_1}{k} \quad , \quad y = -\frac{\beta E_2}{k} \quad . \tag{III.8}$$

Thus the Ω-motion will take place about this new center with only the radius of the motion d' being changed. Given $\vec{E}$, either stray or induced, along with any constant stray transverse gradients which happen to be present in the well, then the external field gradient may be adjusted in magnitude and direction to move the field center to the initial orbit center (d' = 0). Unfortunately this can only be done for one value of $k = (2\pi^2\alpha B_o/L^2)G(z_1)$ as k is dependent on the level in the well through $G(z_1)$.

The dependence of d' on the level of the ion in the well results in a transverse smearing of the levels in the well along the line from (0,0) to $(k_1 - E_1/k\ ,\ -E_2/k)$. If the orbit center is initially displaced from the field center, and k_1 is adjusted so that the ions at the bottom of the well ($G(z_1) = -1$) have their field center at their orbit center, then they will experience no Ω-motion. Ions higher in the well ($G(z_1) > -1$) will experience greater shifts and the field center will have moved beyond their orbit center. They will execute Ω-motion about their new field center $(k_1 - E_1/k\ ,\ -E_2/k)$ with a new radius d'. Those

ions with $G(z_1) = 0$ would not have experienced any Ω-motion initially and simply move under the linear gradients $k_1\vec{\nabla}B$ and $\beta\vec{E}$ (i.e., orbit center at ∞).

The Ω-motion smearing makes it impossible to align the field center on the orbit center for all ions in the well. In part, this problem is overcome by using the flag to limit the population of the well to the very bottom so that the variation is very small. The insensitivity of a removal resonance to slight shifts in the ion centering on the aperture can be used to advantage in handling this, whereas reproducible inward and outward resonances can be very difficult to establish with this smearing present.

Removal resonances were taken at the 11th harmonic using trapping times of 5000, and 9000 μs. No shift was seen between the 5000 and 9000 μs resonances.

APPENDIX IV. MEAN VALUES

The corresponding values of ω_s and ω_c for a sample of ions in the well can be determined rigorously by using the mean values of these quantities.

If we let $\rho(\omega_s)$ denote the density function of the ions in the well (Section 2.2) where $\int \rho(\omega_s)\, d\omega_s = 1$, then the mean value $\langle\omega_s\rangle$ is given by

$$\langle\omega_s\rangle = \int_0^\infty \rho(\omega_s)\, \omega_s\, d\omega_s \quad . \tag{IV.1}$$

If we assume $\omega_s = (\mu_p/\mu_n)\omega_c$, then we have

$$\langle\omega_s\rangle = \frac{\mu_p}{\mu_n} \int_0^\infty \rho(\omega_c)\, \omega_c\, d\omega_c \quad ,$$

or

$$\langle\omega_s\rangle = \frac{\mu_p}{\mu_n} \langle\omega_c\rangle \quad , \tag{IV.2}$$

where

$$\langle\omega_c\rangle = \int_0^\infty \rho(\omega_c)\, \omega_c\, d\omega_c \quad . \tag{IV.3}$$

The RF lineshape function is denoted $F(\nu - (2n + 1)\omega_c)$ and is discussed in Section 2.3. This is the probability that an ion with

cyclotron frequency ω_c will reach the detector when an RF field of frequency ν is applied. Thus we have

$$\int_0^\infty F(\nu - (2n + 1)\omega_c)\, d\nu = 1 \quad .$$

If $F(\nu - (2n + 1)\omega_c)$ is symmetric about $(2n + 1)\omega_c$, then its mean value is given by

$$\int_0^\infty F(\nu - (2n + 1)\omega_c)\nu\, d\nu = (2n + 1)\omega_c \quad . \qquad \text{(IV.4)}$$

The observed lineshape for a sample of ions with density function $\rho(\omega_c)$ is then given by

$$f(\nu) = \int_0^\infty F(\nu - (2n + 1)\omega_c)\rho(\omega_c)\, d\omega_c \quad . \qquad \text{(IV.5)}$$

The mean value of $f(\nu)$ is given by

$$\langle\nu\rangle = \int_0^\infty f(\nu)\, \nu\, d\nu \quad ,$$

or

$$\langle\nu\rangle = \int_0^\infty\int_0^\infty F(\nu - (2n + 1)\omega_c)\rho(\omega_c)\, d\omega_c\, \nu\, d\nu \quad . \qquad \text{(IV.6)}$$

If we perform the integration over ν first and substitute from Eq. (IV.4) into Eq. (IV.6), we get

$$\langle\nu\rangle = (2n + 1) \int_0^\infty \rho(\omega_c)\omega_c\, d\omega_c \quad .$$

Substituting from Eq. (IV.3), we have

$$\langle \nu \rangle = (2n + 1) \langle \omega_c \rangle \quad . \tag{IV.7}$$

If we combine this result with Eq. (IV.2) we have the result

$$\frac{\mu_p}{\mu_n} = \frac{\langle \omega_s \rangle}{\langle \nu \rangle / (2n + 1)} \quad . \tag{IV.8}$$

While this result is completely rigorous, the mean values have been replaced with their median values as a matter of experimental convenience. This approximation introduces negligible error in the results of the present experiment.

APPENDIX V: DATA SHEET

FUNCTION	V	TIME
INJ STOP	848	000 220
SHIFT 1		not used
SHIFT 2		not used
STOP		330
baffle		300
EJ START	945	9 000
STOP		170
START	945	340
STOP		600
CYCLE .01	MASS 1	

DATE _____ START _____ STOP _____

P_M 2 x 10^{-9} P_S 2 x 10^{-7} F x

REG FREQ 3.3 MAP REF 114 I 205 G 103

ION H^+ T 475 V not used

N FLAG 54 S FLAG out

DETECTOR 78 BAFFLE 82

RF FREQ 1 , 181 , 420 . 00 X HARM 11

2 , , . LEVEL 100 mV

STEP 1.0 RANGE 64

POP STEP SIZE 1.5 mV RANGE 64

TRAPPING RATE 1 DYNODE 1800

Z GRAD 0 C OFFSET 0

(See key on next page)

DATA SHEET KEY

The items in the box are the parameters of the Timing Control Unit. (See Figs. 26,27). The TCU cycle begins at 0 μs, and all times are in μs.

INJ STOP	*Time (μs) to the end of the injection pulse.*
STOP	*Begins the RF period.*
BAFFLE	*The end of the baffle pulse (less than STOP above)*
EJ START	*The end of the RF period, the beginning of the ejection pulse, and the beginning of the detector gate period.*
STOP	*The end of the first ejection pulse.*
START	*The beginning of the second ejection pulse.*
STOP	*The end of the second ejection pulse, and the end of the detector gate period.*
MASS	*The position of the MASS switch. The basic time unit is 1.0 μs multiplied by this number.*
CYCLE	*The length of the machine cycle (sec).*
V	*The level of the pulse indicated in potentiometer units.*
P_M	*Pressure in the main vacuum tank.*
P_S	*Pressure in the source vacuum tank.*
F	*Condition of the freon cooling system.*
REG FREQ	*Operating frequency of the NMR regulator.*
MAP REF	*Serial number of the relevant field map.*

I	*Current in the transverse gradient coils in dial units (≅ amp).*
G	*Azimuthal position of the transverse gradient (arbitrary units).*
ION	*Ion(s) used.*
T	*Approximate energy of the ions used (eV).*
N FLAG	*The axial position of the North flag (cm).*
S FLAG	*The axial position of the South flag (cm).*
DETECTOR	*Detector position (knob units).*
BAFFLE	*Baffle position (knob units).*
RF FREQ	*RF base frequency (ies) used (Hz).*
HARM	*RF frequency multiple.*
AMP	*RF amplitude (mV peak-to-peak).*
STEP	*RF frequency step size (Hz).*
RANGE	*Number of steps in RF sweep.*
POP STEP SIZE	*Difference between successive pulses in the population sequence (mV).*
RANGE	*Number of steps in population sweep.*
TRAPPING RATE	*Average number of output pulses per cycle.*
DYNODE	*Detector dynode voltage.*
Z GRAD	*Axial gradient current (amp).*
C OFFSET	*Equal and opposite DC voltages applied to the upper and lower C's.*

BIBLIOGRAPHY

L. W. Alvarez and F. Block, Phys. Rev. 57, 111, (1940).

E. R. Andrew, Nuclear Magnetic Resonance (Cambridge Univ. Press, Cambridge, 1956).

H. S. Boyne and P. A. Franken, Phys. Rev. 123, 242 (1961).

V. E. Bower, Proceedings of the Fourth International Conference on Atomic Physics and Fundamental Constants, 1971, (In press).

C. N. Burrous, A. J. Lieber, and V. T. Zaviantseff, Rev. Sci. Instr. 38, 1477 (1967).

S. Chandrasekar, Plasma Physics (University of Chicago Press, 1960).

R. V. Churchill, Complex Variables and Applications (McGraw-Hill, New York, 1960).

D. N. Craig, J. I. Hoffman, C. A. Law, and W. J. Hamer, J. Res. Nat. Bur. Stand., (U.S.), 64A, 381 (1960).

W. C. Dickenson, Phys. Rev., 81, 717 (1951).

H. E. Duckworth, Mass Spectroscopy, (Cambridge University Press, Cambridge, 1958).

H. E. Duckworth, et al., Proceedings of the Third International Conference on Atomic Masses, R. C. Barber, Ed. (University of Manitoba Press, Winnipeg), p. 702 (1968).

E. Fermi, Nuclear Physics (University of Chicago Press, Chicago 1950).

D. O. Fystrom, Phys. Rev. Letters, 21, 1469 (1970).

A. Garren, et al., Proceedings 2nd International Conference Peaceful Uses of Energy, vol. 31, p. 65 (1958).

J. R. Gilleland, Ph.D. Thesis, The University of Michigan, 1969 (unpublished).

J. R. Gilleland and A. Rich, Phys. Rev. A5, 38 (1972).

G. W. Goodrich and W. C. Wiley, Rev. Sci. Inst. 32, 846 (1961).

H. Gubler, et al., in Proceedings of the International Conference on Precision Measurement and Fundamental Constants, Nat. Bur. Std. (U.S. GPO, Washington, D. C., 1971).

L. Heroux and H. E. Hinteregger, Rev. Sci. Inst., 31, 280 (1960).

J. D. Jackson, Classical Electrodynamics (John Wiley and Sons, New York, 1962), Chapter 12.

G. Liebmann, Proc. Phys. Soc., B62, 213 (1927).

J. L. Luxon, A. Rich, and J. C. Wesley, submitted to Phys. Rev. Letters, and G. W. Ford and V. L. Telegdi, submitted to Phys. Rev. Letters.

J. L. Luxon and A. Rich, Proceedings of the International Conference on Precision Measurement and Fundamental Constants, Natl. Bur. Std. (U. S. GPO, Washington, D. C., 1971).

J. L. Luxon and A. Rich, submitted to Phys. Rev. Letters.

B. A. Mamyrin and A. A. Frantsuzov, Zh. Eksp. Teor. F. 2, 48, 416 (1965) (Soviet Physics-JETP 21 274 (1965).

B. A. Mamyrin and A. A. Frantsuzov, Proceedings of the Third International Conference on Atomic Masses, R. C. Barber, Ed. (University of Manitoba Press, Winnipeg) 427 (1968).

B. A. Mamyrin, N. N. Arujev, and S. A. Alekseenko, Proceedings of the Fourth International Conference on Atomic Masses and Fundamental Constants, 1971 (in press).

B. A. Mamyrin, N. N. Arujev, and S. A. Alekseenko, Reports of the A. F. Ioffe Physico-Technical Institute, Nos. 373 and 374, Leningrad (1971).

G. Marinenko and J. K. Taylor, Anal. Chem. 40, 1645 (1968).

J. B. Marion and H. Winkler, Phys. Rev. 156, 1062 (1967).

T. G. Northrop, The Adiabatic Motion of Charged Particles, (John Wiley and Sons, New York, 1963) Chapter 3.

J. H. Parker and R. W. Warren, Rev. Sci. Instr. 33, 948 (1962).

B. W. Petley, and K. Morris, Nature, 213, 586 (1967).

B. W. Petley, and K. Morris, Proceedings of the Third International Conference on Atomic Masses, R. C. Barber Ed. (University of Manitoba Press, Winnipeg) 461, (1968).

B. W. Petley and K. Morris, in Proceedings of the Fourth International Conference on Atomic Masses and Fundamental Constants, 1971 (in press).

B. W. Petley and K. Morris, (1972) Private communication.

J. H. Sanders and K. C. Turberfield, Proc. Roy. Soc. A272, 79 (1963).

J. A. Simpson, Rev. Sci. Inst. 32, 1283 (1961).

L. G. Smith, Phys. Rev. C4, 22 (1971).

H. Sommer, H. A. Thomas, and J. A. Hipple, Phys. Rev. 82, 697 (1961).

K. R. Spangenberg, Vacuum Tubes (McGraw-Hill, New York, 1948).

C. M. Stevens and P. E. Moreland, Proceedings of the Third International Conference on Atomic Masses, R. C. Barber, Ed. (University of Manitoba Press, Winnipeg) 673 (1968).

B. N. Taylor, W. H. Parker, and D. N. Langenberg, Rev. Mod. Phys. 41, 375 (1969).

K. R. Trigger, Bull. Amer. Phys. Soc. II 1, 220 (1956).

A. H. Wapstra, Proceedings of the Third International Conference on Atomic Masses, R. C. Barber, Ed. (University of Manitoba Press, Winnipeg) 842, (1968).

A. H. Wapstra, Proceedings of the International Conference on Precision Measurement and Fundamental Constants, Nat. Bureau of Standards, (U. S. GPO, Washington, D. C., 1971).

A. H. Wapstra and N. G. Gove, Nuclear Data Tables, (1971).

J. C. Wesley, Ph.D. Thesis, The University of Michigan, 1970 (unpublished).

J. C. Wesley and A. Rich, Phys. Rev. A4, 1341, (1971).